TÉCNICO LISBOA

Study of a solar photovoltaic system towards the development of an energy management algorithm

André Palminha Franco da Cruz

Thesis to obtain the Master of Science Degree in

Engineering Physics

Supervisor(s): Prof. Dr. Carlos Augusto Santos Silva

Prof. Dr. Luís Filipe Moreira Mendes

Examination Committee

Chairperson: Prof. Dr. Maria Joana Patrício Gonçalves Sá

Supervisor: Prof. Dr. Carlos Augusto Santos Silva

Member of the Committee: Prof. Dr. Horácio João Matos Fernandes

October 2017

ACKNOWLEDGMENT

First of all, I would like to express my gratitude to the supervisor of this work Prof. Carlos Silva for his restless support and availability, for the motivation, enthusiasm, patience and share of ideas that, without which, the conclusion of thesis would never have been be possible. In fact, it was really fulfilling to work with him, especially because there was not a distant professor-student working relationship but, instead, a close colleague-colleague one.

Second, but not least, I would thank especially to my co-supervisor Prof. Luís Filipe Mendes, for his permanent availability and effort to enlighten all my doubts. His help in the solar radiation part of this work was indispensable.

I would like to manifest my deepest gratitude to Grupo de Previsão Numérica do IST, for gently giving me hourly radiation on horizontal surface and temperature data, without which, this work would never be possible. To LNEG, as well, in particular to Maria João Carvalho, for giving me hourly radiation data on a horizontal and tilted sufaces. Also, to Cláudia Pinto, for letting me use PV production data from the FCUL system. Without their help, I would have never been able to access data to test the models.

To my friends and colleagues from IST, especially to Ana Luísa Casimiro and António Ornelas, for their help and monitoring, which eased my work and to make me feel that we were on the "same boat". Also, to Miguel Machado, for his availability and help with the data acquisition and respective treatment.

During the time I was working on this thesis, I carried out an internship (PEJAME 17 and 18 program) at the Electricity Museum. All my fellow colleagues and friends accompanied my work and were a permanent source of inspiration, motivation and ideas. A very special thanks to all of them.

To my family, I would also like to express my deepest gratitude, for all the support, patience and mostly for giving me the tools to become what I am today, without which, I would never be able to bring to closure this stage of my life.

Finally, to my girlfriend, Catarina Oliveira, for her endless support, patience, affection and intellectual stimulation. All the conversations and discussions with her kept my mind fresh and inspired enough to finish this work and to maintain the momentum. Thank you very much.

RESUMO

Há uma maior consciencialização para os problemas ligados à poluição e ao excesso de consumo de energia. Acompanhando os novos avanços tecnológicos e científicos, existem novas soluções energéticas eficientes e não poluentes, que apresentam melhor rendimento e poupança para o consumidor, de uma forma acessível e confortável.

No presente trabalho, propõe-se uma ferramenta de gestão de energia para um sistema doméstico com produção fotovoltaica. A radiação incidente num painel é modelada usando os modelos Isotropic Sky, HDKR e Perez. A produção fotovoltaica usa o modelo dos 3 parâmetros (3P). Os modelos Perez e 3P apresentam os resultados concordantes com os dados experimentais e são utilizados num algoritmo de programação linear de gestão energética, em MATLAB. Um processo de otimização do custo de energia (em €) foi simulado para uma casa com um sistema fotovoltaico integrado, termoacumulador e sistema de baterias, conhecendo os perfis de consumo de energia dos ocupantes.

Os resultados são avaliados considerando uma otimização horária e diária, o estado de carga inicial nas baterias e a influência do efeito sazonal e do tipo de dia (dia da semana ou dia de folga) no consumo energético. A abordagem diária apresenta maiores poupanças do que a horária. O estado inicial de carga das baterias não influencia o resultado final da otimização, mas apenas a alocação de energia ao longo do dia. Partindo dos resultados da abordagem diária, é possível concluir que as poupanças absolutas (em €) dependem da estação e do tipo de dia, enquanto as poupanças relativas (€/kWh) não.

Palavras-chave: Gestão Energética, Modelos de Radiação Incidente, Fotovoltaico, Programação Linear, Simulação.

ABSTRACT

There is increasing awareness to problems related to pollution and excess energy consumption. Accompanying the new technological and scientific advances, there are new energy-efficient and non-polluting solutions that present greater savings and energetic optimization to the consumer, in an accessible and comfortable way.

In the present work, an energy management tool applicable to a domestic system with photovoltaic production is proposed. The incident radiation on a panel is modeled using the Isotropic Sky, HDKR and Perez models. The modeling of photovoltaic production uses the 3-parameter model (3P). The Perez and the 3P models present according results with experimental data and are assembled in a toolbox used in a MATLAB linear programming energy management algorithm. An energy cost (in €) optimization process was simulated for a household with an integrated photovoltaic system, a thermal accumulator and a batteries system, knowing the energy consumption profiles of the occupants.

The results are evaluated considering an hourly and daily optimization, different initial state of charge in the batteries system and seasonal and type of day (weekday or day off) influence in the energetic consumption behavior. The daily optimization approach presents better savings than the hourly one. The initial state of charge of the batteries does not influence the optimization final result, but only the allocation of energy throughout the day. From the type of day approach results, it is possible to conclude that the absolute savings (in €) depend on the season and type of day, while the relative savings (in €/kWh) do not.

Keywords: Energy Management, Incident Radiation Modeling, Photovoltaic, Linear Programming, Simmulation.

TABLE OF CONTENTS

LIST OF FIGURES

LIST OF GRAPHICS

LIST OF TABLES

LIST OF ABBREVIATIONS

AC	Alternate Current
ADSM	Active Demand Side Management
DC	Direct Current
DHW	Domestic Hot Water
DL	Decreto-Lei
DSM	Demand Side Management
EIA	Energy Information Administration
EMA	Estação Meteorológica Automática
EU	European Union
FCUL	Faculdade de Ciências da Universidade de Lisboa
GA	Genetic Algorithms
GPNT	Grupo de Previsão Numérica do Tempo
HDKR	Hay-Davies-Klucher-Reindl
HVAC	Heating, Ventilation and Air Conditioning
IST	Instituto Superior Técnico
LCOE	Levelized Cost Of Electricity
LNEG	Laboratório Nacional de Engenharia Civil
LP	Linear Programming
MPP	Maximum Power Point
MPPT	Maximum Power Point Tracker
NZEB	Net-Zero Energy Buildings
PV	Photovoltaics
RE	Renewable Energy
STC	Standard Test Conditions
UPAC	Unidades de Produção para Auto Consumo
UPP	Unidades de Pequena Produção
USA	United States of America
WRC	World Radiation Center
ZEB	Zero Energy Buildings
3P	3 Parameters

NOMENCLATURE

SOLAR RADIATION MODELS

QUANTITIES

F_{a-b}	View factor (from which a can observe b)	β	Collector's tilt or slope
G	Irradiance	γ	Surface azimuth angle
G_{sc}	Solar constant	γ_s	Solar azimuth angle
G_{on}	Extraterrestrial irradiance on the plane normal to the radiation	δ	Declination of sun rays
H	Daily irradiation	Δ	Brightness
I	Hourly irradiation	ε	Clearness
k_T	Hourly clearness index	θ	Incidence angle
L_{loc}	Local longitude	θ_z	Zenith angle
L_{st}	Standard longitude	ρ_g	Albedo
m_{air}	Air mass coefficient	ϕ	Latitude
n	Day of the year	ω	Sun hour angle
t	Solar time	ω_s	Sunset hour angle
α_s	Solar altitude	ω_{sr}	Sunrise hour angle

SUBSCRIPTS

b	Beam or direct	max	Maximum
cs	Circumsolar	n	Plane normal to the direction of propagation
d	Diffuse	o	Above the Earth's atmosphere
hz	Horizon brightening	$refl$	Reflected
iso	Isotropic	T	Tilted plane

PHOTOVOLTAIC MODELS

QUANTITIES

A	Area	$NOCT$	Normal operation cell temperature
E_g	Energy gap	N_s	Number of cells connected in series

FT_b	Fraction of transmitted beam radiation through optical material relative to normal incidence	P	Power
I	Electric current	V	Voltage
m	Modified ideality factor	α	Temperature coefficient
m'	Ideality factor	η	Efficiency

SUBSCRIPTS

amb	Ambient	oc	Open circuit
c	Cell	s	Generated from the sun
D	Diode	sc	Short circuit
eff	Effective	T	Thermal
max	Maximum	0	Reverse saturation

SUPERSCRIPTS

ref	Reference or standard test conditions

OTHER MODELS

QUANTITIES

DOD	Depth of discharge
DOD_{max}	Maximum depth of discharge
E	Electrical energy generated by the system
F	Fuel expenditures
I	Investment expenditures
M	Operations and maintenance expenditures
Q	Reactive power
$\dot{Q}$	Heat transfer
Q_{pr}	Energy losses of the thermal accumulator to the surroundings in a day
r	Annual effective discount rate
S	Apparent power
SOC	State of charge
U_{loss}	Heat loss coefficient
V_{DHW}	Used volume of domestic hot water
V_{total}	Total volume of water inside the thermal accumulator

SUBSCRIPTS

t	Relative to year t

ENERGY MANAGEMENT ALGORITHM

QUANTITIES

E	Electric energy delivered from a source
E_{AC}	PV system's available electric energy
$E_{available_{batt}}$	Batteries system current available energy
$E_{charge_{batt}}$	Necessary energy to fully charge the batteries system
$E_{heat\,therm}$	Necessary energy to heat the water inside the thermal accumulator
$E_{max_{batt}}$	Batteries system maximum available energy
$E_{other\ devices}$	Other devices current electric energy consumption
F	Objective function
h	Hour
k	Electric grid tariff
$P_{contract}$	Contracted power
$P_{max_{therm}}$	Thermal accumulator's maximum working power

SUBSCRIPTS

A	Hourly case A
B	Hourly case B
$batt$	From the batteries system
C	Daily case C
D	Daily case D
$grid$	From the electric grid
PV	From the PV system

SUBSUBSCRIPTS

$batt$	To the batteries system
$therm$	To the thermal accumulator

1. INTRODUCTION

1.1. MOTIVATION

The demand for energy has been increasing for the last years and will continue to increase. According to the United States Energy Information Administration (EIA), the total world energy consumption will raise by 56% between 2010 and 2040, from 154 million GWh to 240 million GWh. EIA also predicts that the renewable energy (RE) production will increase by 2.5% each year however, fossil fuels will still be responsible for 80% of the energy production in the world by 2040 [1]. The consumption of fossil fuels has negative impacts on the environment, such as global warming or air pollution, but it also has associated political and sociological problems, such as the constant change in price, which is not related to the real extraction cost and availability, but to political and economic speculation and also the fact that it is only available in few regions in the world.

It is necessary to find sustainable and environment friendly solutions to respond to the demand of energy in the world. For example, the European Union (EU) is making an effort towards a more sustainable future with the 2020 climate and energy package, which expects to reduce the greenhouse gas emissions by 20% from 1990 levels, raise the share of EU energy consumption produced from renewable resources to 20% and to improve energy efficiency by 20% [2]. According to the Energy Efficiency Status Report 2012, the residential sector was responsible for 29.71% of the energy consumption in the EU in 2010, therefore it plays an important role in energy efficiency policies and programs [3].

RE technologies are becoming more affordable and with this advent, a new paradigm is arising: the emergence and improvement of electric energy self-production systems and microgrids, which are basically small grids with a well defined boundary, that can be connected or not to the main grid. This solution is now receiving more credibility and is started be thought of as a possible solution for some energy-related problems. Besides the energy generation problem mentioned above, there is also the problem of transporting the energy, which, for larger distances, has tremendous losses. In the United State of America (USA) alone, 1 MW of consumed power costs about 2.2 MW of generation and transmission capacity, which corresponds to more than 50% of losses in the generation and transport processes. Therefore, on-site generation and the implementation of microgrids solve the transport problem, alongside with contributing for more personalized energy services. Microgrids can also be associated to a storage system, such as battery systems [4].

Solar photovoltaic (PV) energy is one of the most implemented and well suited ways of electric energy self-generation for households or service, commercial or industrial buildings from a

renewable source, since it can be easily personalized according to their energetic needs [5], [6]. One of the major concerns regarding these systems, is that the production depends on the availability of the sun's energy which, most of the time, may not match the needs of the consumer, so there is a need of improving their efficiency. A possible way of solving this problem is to implement a management system, such as a toolbox or an algorithm, capable of studying the consumers behavior and that is able to manage the production and the supply of energy according to the consumers needs [7].

1.2. OBJECTIVES

The theme behind this thesis is quite comprehensive. With this work, it is pretended to develop an energy management algorithm for a system with self-production from a PV platform, which can be associated to a battery storage system. The algorithm optimizes the energy supply, taking into account the energetic behaviors and needs of the respective consumer. In order to accomplish that, it will use, as a baseline, typical energetic consumption profiles. The main objective of this work is to prove that more detailed models for production can be used to improve the decision making process of an energy management tool.

It is also important to refer that this work was proposed in the framework of two courses of the Physics Engineering course from Instituto Superior Técnico (IST) in Lisbon: Solar Photovoltaic Energy and Solar Thermal Energy. In the classes of those courses, some models regarding solar radiation geometry, forecast, data analysis, etc. and solar PV panels and solar thermal collectors' production and working principles are addressed. However, there is a lack of experimental infrastructures and tools to test and validate these models, which made the study of these subjects exclusively theoretical. The first aspiration of this thesis was to dimension a PV and solar thermal laboratorial platform for the students to complement the study of these subjects, but due to problems of bureaucratic and practical nature, that was not possible. Despite this, the link between this work and those courses was not broken and, therefore, another objective was proposed: the creation of a solar radiation and PV toolbox. This toolbox will contain a code developed in *Matlab* software language, basically consisting on a set of functions to model incident solar radiation and PV production. This toolbox has two main purposes:

- To be used as a tool for the management algorithm in what regards the optimization of the production, since it models the PV production in a detailed way, taking into account the physics and the main principles regarding solar radiation and PV production;
- To be used by the students of the Solar Photovoltaic Energy and Solar Thermal Energy courses as a tool for testing the models taught in the classes, in order to help their work and complement their academic course.

1.3. CONTRIBUTIONS

In literature, it possible to find several examples on energy management techniques using different types of algorithms, with or without self production, in particular PV generation. There can also be found several examples on how to model and to predict incident radiation and PV production, alongside with significant amount of available worldwide data from solar radiation. Despite this, most of the energy management studies do not use detailed models for PV modeling and production, using in most cases simple stochastic and statistic models, not taking into account the physics of the solar radiation or the PV units. In most cases, this is not taken much into account and the modeling can be deficient due to fact that the tools and devices to measure incident radiation values (pyranometers, pyrheliometers, etc.) are expensive and hard to implement on a regular household. But still, by using improved models for incident radiation and PV production, this would contribute for the development of new and better solutions of energy management, in particular for households.

The other main contribute of this work is the fact that it will allow to create a tool in an accessible software language: *Matlab*. The codes and functions created for this, can be used separately or integrated in an energy management tool, *i.e.*, any student can test the radiation or PV production models taught in classes separately or integrated and any user can use it to manage their own system, by providing the necessary data.

1.4. STRUCTURE OF THE THESIS

This thesis is divided in seven different chapters, on which different subjects regarding the work are described and discussed. The present chapter (Chapter 1), named Introduction, there is a brief introduction to the theme, alongside with an overall view of this work. It is also presented the motivation for the elaboration of this thesis, as well as its main objectives and contributions. Chapter 2 is entitled Literature Review, where it is made a concise review and research from scientific publications on the state of the art in what regards the theme of this work and also on the main concepts necessary to understand its scope. This chapter is divided in four different sections: Solar Energy; Solar Photovoltaic Models; Domestic PV Solutions and Optimization Algorithms. The characteristics and locations of the experimental setups used for data acquisition are described in Chapter 3. Chapter 4 is the one that summarizes the hypothetical household design and features, where the energy management algorithm will be implemented. Also, it specifies the modeling of each characteristic parameter necessary for the implementation of the algorithm. Chapter 5 describes the energy management algorithm, defining its conditions by taking into account the characteristics of the system, the limitations of the models and the behavior of the household's inhabitants. The results are presented in Chapter 6. In Chapter 7, there is a small discussion of the results of this work with some conclusions and suggestions to improve it and for future work.

2. LITERATURE REVIEW

2.1. SOLAR RADIATION

The sun is approximately a black body at an effective temperature of 5777 K, at a mean distance of 1.495 x 10^{11}m from Earth, which emits energy in the form of radiation into space that reaches the Earth's surface afterwards [8]. This energy that powers the sun comes from nuclear fusion reactions, which transform atoms of hydrogen into atoms of helium [9]. At that distance, the sun is limited in the sky by an angle of 32' so, the emitted radiation that reaches the outer atmosphere has a nearly constant intensity. The radiation that reaches the Earth's atmosphere is different from the one that reaches its surface. The first is called extraterrestrial radiation and has a regular behavior and the second is called terrestrial radiation and its behavior is more variable. The extraterrestrial models are detailed in chapter **9.**, in **A.1**. The terrestrial radiation models will be addressed next.

There are two useful definitions: irradiance, which is the intensity of the incident solar radiation as energy per unit of time per unit of surface; irradiation, which is the energy from incident solar radiation per unit of surface, found by integration of irradiance over a given time, usually an hour or a day [8]. In what regards the involved quantities, this thesis will use the nomenclature from Duffie et al. [8], in order to ease the definitions and calculations.

2.1.1. RADIATION LOSSES THROUGHOUT THE ATMOSPHERE – AIR MASS COEFFICENT

As it was described in **2.1**, the total radiation that reaches the outer atmosphere is not the same that reaches the Earth's surface, since some of the radiation is scattered throughout the atmosphere. The effects that originate this loss of energy can be described by the air mass coefficient ratio, which gives the ratio between the mass of atmosphere that beam radiation has to travel through, as if it were at the highest point in the sky (zenith), to the mass of atmosphere that it has to travel for a given zenith angle θ_z, i.e, the angle between the zenithal direction and the direct rays direction [8]. The coefficient of air mass is approximately given by:

$$m_{air} = \frac{1}{cos\,\theta_z} \tag{2.1.1.1}$$

which is only valid for angles between 0^o and 70^o. For angles close to 90^o, there is a more detailed expression [14]:

$$m_{air} = \frac{e^{-0.0001184h}}{\cos\theta_z + 0.5057(96{,}080 - \theta_z)^{-1.634}} \tag{2.1.1.2}$$

where h is the altitude of the given site in meters.

2.1.2. CLEARNESS INDEXES

One of the greatest problems of making predictions for the available amount of radiation that may be harvested by a collector is the unpredictable nature of the frequency of clear and cloudy days in a year, which becomes even harder to forecast for longer periods of time. But, if one is able to determine this frequency distribution, it is possible to know the correlation between the fraction of diffuse radiation and the total radiation for a given period of time. It is possible to define a clearness index as the ratio between the radiation on a horizontal surface to the extraterrestrial radiation for the same period of time [8], [15]. There are three relevant definitions for clearness indexes: monthly average, daily and hourly. Although there are expressions to calculate the monthly average and the daily clearness indexes, these are only relevant when there is only available daily radiation data.

The hourly clearness index k_T corresponds the ratio between hourly radiation on a horizontal surface and hourly extraterrestrial radiation [8] and follows the expression:

$$k_T = \frac{I}{I_o} \tag{2.1.2.1}$$

where I is the experimental terrestrial irradiation on a horizontal surface. The value of I must come from available data from measurements of total solar radiation on a horizontal surface or can come from accurate predictions from a nearby weather forecast station. These measurements usually come from pyranometers, installed in stations nearby the location in study. These are the devices more commonly used for measuring total radiation.

2.1.3. BEAM AND DIFFUSE COMPONENTS OF RADIATION

The estimation of the fractions of diffuse and beam radiation and respective methods is a subject far from being settled and the model's accuracy depends on the access to and processing of a vast amount of collected data. In fact, it is very important to separate these two components, because the models that use data from radiation on a horizontal surface to calculate total radiation on a surface with a different orientation require a separate approach for beam and diffuse radiation. Nevertheless, the models that will be studied are the ones described in Duffie et al. [8].

The basic principle behind these models consists in compare the ratio between the diffuse component and total radiation for a given period and the respective clear index. For hourly data, the model used is described in [8], [16] and is given by:

$$\frac{I_d}{I} = \begin{cases} 1.0 - 0.09k_T, & \text{for } k_T \leq 0.22 \\ 0.9511 - 0.1604k_T + 4.388{k_T}^2 & \text{for } 0.22 < k_T \leq 0.80 \\ -16.638{k_T}^3 + 12.336{k_T}^4, & \\ 0.165 & \text{for } k_T > 0.80 \end{cases} \quad (2.1.3.1)$$

2.1.4. RADIATION ON SLOPPED SURFACES

Generally, solar panels are tilted, with endless possible angles but, as it was said before, most collected data corresponds to radiation on a horizontal surface so, it is necessary to know the beam and the diffuse components of radiation, as it was discussed in **2.1.2**. In what regards the direction of beam radiation, it can be easily calculated from the expressions described in **A.1**. On the other hand, the direction from which a surface receives diffuse radiation is harder to determine, since its distribution over the sky dome depends significantly on the cloudiness or clearness of the atmosphere, which are extremely unpredictable [8].

Experimental data suggests that the diffuse component of solar radiation can be separated into three components: isotropic, which is uniformly distributed over the sky dome; circumsolar, which corresponds to the radiation scattered in the area in the sky around the sun; horizon brightening, which is more concentrated near the horizon [8], [17]. Another important factor to take into account in these models, is the reflectance of the ground or albedo, which is denoted by ρ_g. This factor takes into account the amount of radiation that is reflected by the ground and that reaches the surface [8]. This way, in order to estimate the total radiation reaching the surface, it is necessary to know the beam, diffuse and reflected components of radiation so, may be written as:

$$I_T = I_{T,b} + I_{T,d,iso} + I_{T,d,cs} + I_{T,d,hz} + I_{T,refl} \quad (2.1.4.1)$$

where iso, cs, hz and $refl$ correspond to the isotropic, circumsolar, horizon brightening and reflected components respectively. Now, if we take into account the area of the surface, the sky and the view factor F_{a-b}, which represents the solid angle from which a can observe b, the equation (2.1.4.1) becomes:

$$I_T = I_b R_b + I_{d,iso} F_{c-s} + I_{d,cs} R_b + I_{d,hz} F_{c-hz} + I\rho_g F_{c-g} \quad (2.1.4.2)$$

One of the first models proposed to solve (2.1.4.2) assumes that the diffuse component of radiation is isotropic, which means that the amount of diffuse radiation that is incident on the tilted surface does not depend on its orientation. Therefore, the incident radiation must have three components: beam, isotropic diffuse and diffusely reflected. Since the diffuse component is isotropic, the circumsolar and horizon terms in (2.1.4.2) must vanish and, for a collector of slope β, the view factors become $F_{c-s} = (1 + \cos\beta)/2$ and $F_{c-g} = (1 - \cos\beta)/2$. This model is called the Isotropic Sky model and comes described in Liu et al. [18]. It follows the equation:

$$I_T = I_b R_b + I_d \left(\frac{1+\cos\beta}{2}\right) + I\rho_g \left(\frac{1-\cos\beta}{2}\right) \quad (2.1.4.3)$$

The Isotropic Sky Model is simple and eases calculations, but it does not take into account the circumsolar or the horizon brightening components. A more detailed model that that has had many contributions from different works and that takes into account these components is called the Hay-Davies-Klucher-Reindl model (HDKR) or Anisotropic Sky model [8]. From Davies et al. [19], comes that the diffuse component can be split into the isotropic and circumsolar components and that the horizon brightening one is not taken into account. The diffuse component of radiation on a tilted surface is therefore:

$$I_{d,T} = I_d \left[(1-A_i)\left(\frac{1+\cos\beta}{2}\right) + A_i R_b\right] \quad (2.1.4.4)$$

where $A_i = I_b/I_o$ is the anisotropy index, which is a function of the transmittance of the atmosphere and determines the portion of diffuse that has the same direction as the beam component. From Duffie et al. [21], Klutcher [22] the horizon brightening component is taken into account as a component of diffuse with a geometric correction factor of $1+\sqrt{I_b/I}\sin^3(\beta/2)$, where $\sqrt{I_b/I}$ is a term that takes into account the cloudiness. Combining all of these contributions, the HDKR Model becomes:

$$I_T = (I_b + I_d A_i)R_b + I_d(1-A_i)\left(\frac{1+\cos\beta}{2}\right)\left[1+\sqrt{\frac{I_b}{I}}\sin^3\left(\frac{\beta}{2}\right)\right] + I\rho_g\left(\frac{1-\cos\beta}{2}\right) \quad (2.1.4.5)$$

There is last and more improved model known as the Perez model [22]**,** which settles on a more detailed study of the three diffuse components. The diffuse component on a tilted surface is given by:

$$I_{d,T} = I_d \left[(1-F_1)\left(\frac{1+\cos\beta}{2}\right) + F_1\frac{a}{b} + F_2\sin\beta\right] \quad (2.1.4.6)$$

where F_1 and F_2 correspond to the circumsolar and horizon brightening coefficients, respectively and $a = \max(0, \cos\theta)$ and $b = \max(\cos 85^\circ, \cos\theta_z)$ are terms that take into account the angles of incidence of the cone of circumsolar radiation on the tilted and horizontal surfaces, respectively. In fact, a/b becomes R_b for most hours of the day. F_1 and F_2 depend on θ_z, a parameter called brightness Δ and another called clearness ε that basically describe sky conditions. The brightness Δ is given by the expression:

$$\Delta = m_{air}\frac{I_d}{I_{on}} \tag{2.1.4.7}$$

where m_{air} is the air mass defined in (2.1.1.1) and (2.1.1.2) and I_{on} comes from (A.1.1), but in terms of hourly radiation. The clearness is given by:

$$\varepsilon = \frac{\frac{I_d + I_{b,n}}{I_d} + 5.535 \times 10^{-6}{\theta_z}^3}{1 + 5.535 \times 10^{-6}{\theta_z}^3} \tag{2.1.4.8}$$

where $I_{b,n}$ is the normal incidence beam radiation. ε will not appear directly in F_1 and F_2 expressions, but will be used to determine statistical coefficients that will appear in those expressions. The recommended way of determining those coefficients is described in Table 1 and allows the determination of those coefficients.

Table 1 - Brightness Coefficients for Perez Model (adapted from [22]).

Range of ε	f_{11}	f_{12}	f_{13}	f_{21}	f_{22}	f_{32}
1.000 – 1.065	−0.008	0.588	−0.062	−0.060	0.072	−0.022
1.065 – 1.230	0.130	0.683	−0.151	−0.019	0.066	−0.029
1.230 – 1.500	0.330	0.487	−0.221	0.055	−0.064	−0.026
1.500 – 1.950	0.568	0.187	−0.295	0.109	−0.152	0.014
1.950 – 2.800	0.873	−0.392	−0.362	0.226	−0.462	0.001
2.800 – 4.500	1.132	−1.237	−0.412	0.288	−0.823	0.056
5.500 – 6.200	1.060	−1.600	−0.359	0.264	−1.127	0.131
6.200 – ∞	0.678	−0.327	−0.250	0.156	−1.377	0.251

F_1 and F_2 may be calculated by the equations:

$$F_1 = \max\left[0, \left(f_{11} + f_{12}\Delta + \frac{\pi}{180}\theta_z f_{13}\right)\right] \tag{2.1.4.9}$$

$$F_2 = f_{21} + f_{22}\Delta + \frac{\pi}{180}\theta_z f_{23} \tag{2.1.4.10}$$

which permit the full calculation of the three diffuse components. Adding the beam and ground-reflected components as in (2.1.4.3) and (2.1.4.5), the Perez model may be written as:

$$I_T = I_b R_b + I_d(1 - F_1)\left(\frac{1 + \cos\beta}{2}\right) + I_d F_1 \frac{a}{b} + I_d F_2 \sin\beta + I\rho_g\left(\frac{1 - \cos\beta}{2}\right) \quad (2.1.4.11)$$

2.2. SOLAR PHOTOVOLTAIC MODELS

PV is the technology behind the process of generating direct current (DC) with a given power (measured in Watts - W), from a semiconductor material when it is illuminated by photons. Each PV system is composed by a set of individual elements called PV cells. For as long as there incident light on a PV cell, it generates electrical power [5]. These cells are made of materials that are adequate for the occurrence of the photoelectric effect, in which an incident photon excites an electron from the material, giving it enough energy to escape the influence of the nucleus, thus generating an electrical current. The typical power of a cell is of about 1.5 W, which corresponds to a voltage of about 0.5 V and an electric current of about 3 A. To obtain higher power, cells are connected in series and/or parallel, creating modules, which power can go from 50 to 100 W. These modules can also be connected, creating a PV panel, which power depends on the manufacturing process [23].

2.2.1. TYPES OF PV CELLS

One of the most commonly used material in the manufacturing of PV cells is the monocrystalline silicon, which basically consists on a single continuous silicon crystal layer. It can be intrinsic (with only pure silicon) or doped, to alter its semiconductor properties. It is mainly used in high performance PV cells and these have a high efficiency, between 14.0 and 26.6%. The manufacturing of these cells is more expensive, so their market value is higher [24].

The other material is polycrystalline silicon, which is composed of multiple small silicon crystals, instead of single one. Like monocrystalline silicon, it can be intrinsic or doped. The manufacturing process of these cells is cheaper, so they are the leading technology, having the highest market share. However, their efficiency is lower, ranging between 13.0 and 21.3% [24].

There are other PV technologies in the market with a lower share, like the thin-film solar cell. These are made by depositing one or more thin layers of a PV material in a substrate such as a plastic, a metal or a glass. The cells can have an efficiency between 12.0 and 20.0%, but the modules on the market usually have a value close to 9.0% [25].

2.2.2. THE IDEAL SINGLE DIODE OR 3P MODEL

The solar cells are, in fact, simple devices. Semiconductors have the capacity of absorbing light and transmit some of its energy to electrons and holes. Since there are separated regions (*p*-region and *n*-region) in the cell, there is a well-defined electric field in the junction, so the electrical

current is generated in a preferred direction. Therefore, a PV cell may be approximated by a large scale diode, which efficiently absorbs and converts light energy into electrical energy [5].

In literature, there are several models that attempt to describe the best equivalent circuit for a PV cell and the more parameters the model has, the further from the ideal it is. The most common models depend on the physical nature of the cells and on parameters relative to the characteristics of each panel, which are usually given by the manufacturer, but also depend on the weather conditions (irradiance and temperature), which cannot be obtained immediately and have a more random behavior. So, the characteristic *I(V)* curve of a PV cell is a non-linear equation with multiple parameters that are given by the manufacturers, that are constant and must be computed [26].

The simplest model to describe a PV cell is called the Ideal Single Diode Model or the 3 Parameters Model (3P Model), which consists on a current source connected in parallel to a diode. The model does not take into account internal losses [26] and is represented in Figure 1:

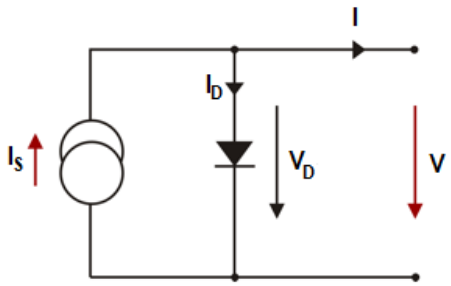

Figure 1 - The Ideal Single Diode or 3P Model [27].

The current source I_s represents the electric current generated and depends on the radiation incident on the cell [23]. It is unidirectional and it is constant for a given value of intensity of the incident irradiance. I_D is the diode current, V_D is the diode voltage, I is the load current and V is the load voltage. From the the Kirchhoff law, I becomes $I = I_s - I_D$ [5], [26]. The diode current I_D is given by the equation:

$$I_D = I_0\left(e^{\frac{V}{mV_T}} - 1\right) \qquad (2.2.2.1)$$

where I_0 is the reverse saturation or leakage current of the diode [5], [23], m is the modified ideality factor, which is a constant parameter [5] and V_T is the thermal voltage which translates the dependence of the diode on the temperature of the cell [5], [26]. V_T is given by $V_T = k\,T_c/q$, where k is the Boltzmann constant ($k = 1.381 \times 10^{-23}$ J/K), T_c is the cell temperature and q is the elementary electron charge ($q = 1.602 \times 10^{-19}$C) [26]. This way, the expression for I [5] becomes:

$$I = I_s - I_0\left(e^{\frac{V}{mV_T}} - 1\right) \tag{2.2.2.2}$$

2.2.3. DETERMINATION OF THE PARAMETERS OF THE 3P MODEL

Considering the 3P model, it is possible to take some conclusions about its parameters if the external circuit is taken into account, in particular, by taking the short circuit or open circuit cases. In the case of a short-circuit, $V = 0$ and $I_D = 0$ so, I becomes:

$$I = I_s = I_{sc} \tag{2.2.3.1}$$

where I_{sc} is called the short circuit current and corresponds to the maximum current on the load which, in fact, corresponds to the current generated by the PV effect. On the other hand, for the open circuit case, the value for the load current immediately becomes $I = 0$ and the value for the respective voltage becomes:

$$V = V_{oc} = mV_T \ln\left(1 + \frac{I_{sc}}{I_0}\right) \tag{2.2.3.2}$$

where V_{oc} corresponds to the open circuit voltage, which is the maximum value of voltage in the electrical contacts of the cell. In a similar way as for I_{sc}, its value is given by the manufacturer for certain conditions of irradiance and temperature and it is also a characteristic value for the cell [23].

It is not possible to determine the parameters of the 3P model without having reference test values. For this, the manufacturers give the data of the characteristic parameters for reference or standard test conditions (STC), which will be denoted with the superscript ref. These conditions are for irradiance $G^{ref} = 1000\ \mathrm{W/m^2}$, ambient temperature $\theta^{ref} = 25^o\mathrm{C}$ and air mass ${m_{air}}^{ref} = 1.5$.

But, the cell does not always work under STC, so it is necessary to convert these parameters to the ones correspondent to a real situation. Taking (2.2.2.2), (2.2.3.1) and (2.2.3.2) and using the characteristic values for reference conditions, it is possible to obtain the following equations:

$$m' = \frac{\left(V_{max}^{ref} - V_{oc}^{ref}\right)}{V_T^{ref} \ln\left(1 - \frac{I_{max}^{ref}}{I_{sc}^{ref}}\right)} \tag{2.2.3.3}$$

$$I_0^{ref} = \frac{I_{sc}^{ref}}{e^{\frac{V_{oc}^{ref}}{m' V_T^{ref}}} - 1} \quad (2.2.3.4)$$

$$I_s^{ref} = I_{sc}^{ref} \quad (2.2.3.5)$$

where m' is the ideality factor, which is $m' = m/N_s$, where N_s is the number of cells connected in series in the module [23]. It is important to refer that m' is a constant, so it remains the same for any conditions of irradiance and temperature [5].

Having determined all reference values, it is now possible to calculate the values for any operating conditions. As it was mentioned in **2.2.2**, I_s depends on the irradiance, in fact, it is proportional to it. So, for any operation conditions, it can be calculated [23] by:

$$I_{sc} = I_{sc}^{ref} \frac{G}{G^{ref}} \quad (2.2.3.6)$$

Another important parameter to calculate is the thermal voltage V_T, which depends on the temperature of the cell T_c, that can be calculated by the expression:

$$T_c = T_{amb} + \left(\frac{NOCT - 20}{0{,}8}\right) G \quad (2.2.3.7)$$

where T_{amb} is the ambient temperature, $NOCT$ is the normal operation cell temperature (in $^{o}\mathrm{C}$), which is given by the manufacturer. The saturation current can also be calculated using reference and temperature related parameters:

$$I_0 = I_0^{ref} \left(\frac{T_c}{T_c^{ref}}\right)^3 e^{\frac{q}{m'}\left(\frac{E_g^{ref}}{kT_c^{ref}} - \frac{E_g}{kT_c}\right)} \quad (2.2.3.8)$$

where $E_g = E_g^{ref}\left[1 - C\left(T_c - T_c^{ref}\right)\right]$, where $E_g^{ref} = 1.121\ \mathrm{eV}$ is the energy gap of silicon for reference conditions and $C = 0.0002677$ is a constant [5].

2.2.4. MAXIMUM POWER POINT AND MAXIMUM POWER POINT TRACKERS

The output DC power of the module depends on the output voltage (V) and output current (I) by the Joule law: $P = VI$. Therefore, the maximum power of the module will be:

$$P_{max} = V_{max} I_{max} \quad (2.2.4.1)$$

where V_{max} and I_{max} correspond to the voltage and current correspondent to the maximum power point (MPP), as it is presented in Figure 2. The efficiency η of the module is directly related to this parameter and can be calculated by:

$$\eta = \frac{P_{max}}{AG} \tag{2.2.4.2}$$

where A is the area of the panel or the module. In the case of PV applications, especially in systems isolated from the grid or connected directly to loads, P_{max} is the most important parameter to be taken into account, since the highest efficiency is achieved in MPP conditions [23].

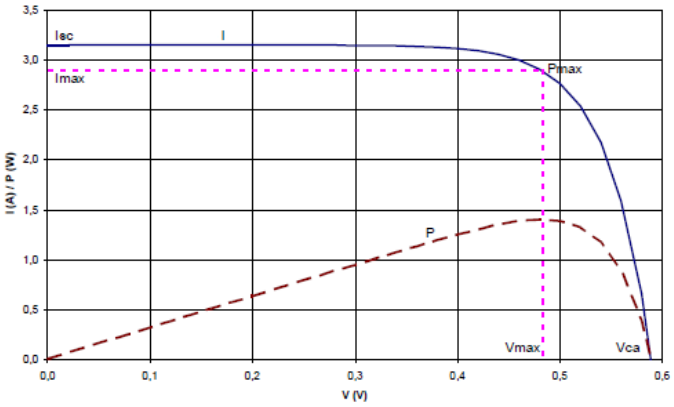

Figure 2 – Simulation of an I-V (blue) and respective P-V curve (brown) for a typical silicon PV cell, under STC. The MPP is marked in pink (adapted from [23]).

It is therefore necessary for the modules to work at maximum power, but the MPP might change with the conditions of temperature and irradiance. To achieve this, the PV modules and panels are equipped with an electronic system called maximum power point tracker (MPPT) that adjusts the output voltage, in order for the module to always work at the MPP. The fact that each PV system is equipped with this, makes it necessary to calculate effectively the maximum power [23]. Taking (2.2.2.2) and (2.2.4.1), P becomes:

$$P = V\left[I_{sc} - \left(I_0\left(e^{\frac{V}{m'V_T}} - 1\right)\right)\right] \tag{2.2.4.3}$$

To determine P_{max} is therefore necessary to solve $dP/dV = 0$. The solution is therefore:

$$e^{\frac{V_{max}}{m'V_T}} = \frac{\left(\frac{I_{sc}}{I_0} + 1\right)}{\left(1 + \frac{V_{max}}{m'V_T}\right)} \tag{2.2.4.4}$$

which can be solved numerically [5].

2.2.5. TEMPERATURE EFFECT

The temperature has a crucial role in the performance of the PV cells, since it changes the properties of its constituents. The output power of the cell decreases with the increase of the temperature. In particular, V_{oc} decreases significantly and I_{sc} increases slightly with temperature. The real values for the two parameters [5] are given respectively by:

$$V_{oc}^{real} = V_{oc}\left(1 + \propto_{V_{oc}} (T_c - \theta^{ref})\right) \quad (2.2.5.1)$$

$$I_{sc}^{real} = I_{sc}\left(1 + \propto_{I_{sc}} (T_c - \theta^{ref})\right) \quad (2.2.5.2)$$

where $\propto_{V_{oc}}$ (negative and given in $\mathrm{V}/\,^{\mathrm{o}}\mathrm{C}$) and $\propto_{I_{sc}}$ (positive and given in given in $\mathrm{A}/\,^{\mathrm{o}}\mathrm{C}$) are the open circuit voltage and short circuit current temperature coefficients, respectively. The values from (2.2.5.1) and (2.2.5.2) can be used to calculate the remaining parameters of the 3P model, as described before.

2.2.6. RADIATION ABSORPTION IN PHOTOVOLTAIC CELLS: ANGLE OF INCIDENCE AND DIRT EFFECTS

One of the components of the PV modules is the cover of glass. For any optical material, the reflectance and transmittance of radiation depends on the angle of incidence. Therefore, for any PV module, the absorbed radiation will be necessarily dependent on its angle of incidence. For a clean surface, the relative transmittance, which represents the fraction of radiation transmitted through the optical material when compared with normal incidence, is based on the Fresnel law and given [8], [28] by:

$$FT_B(\theta) = 1 - b_0\left(\frac{1}{\cos\theta} - 1\right) \quad (2.2.6.1)$$

where b_0 is a characteristic parameter for each type of PV module, which can be determined empirically. If its value is not known, it is possible to use a general value of $b_0 = 0.07$.

The previous expression is simple and has some limitations, since it is not adequate for incidence angles of $\theta > 80^o$ and it does not take into account the dirt on the surface of the panel, such as dust. For a real situation, dust and other kinds of dirt will be present and this will decrease the transmittance and will change the shape of the curve described by (2.2.7.1). The expression that takes into account the whole range of θ and the effects of dirt [5] is given by:

$$FT_B(\theta) = 1 - \frac{\exp\left(-\frac{\cos\theta}{a_r}\right) - \exp\left(-\frac{1}{a_r}\right)}{1 - \exp\left(-\frac{1}{a_r}\right)} \quad (2.2.6.2)$$

where a_r is a parameter associated with the level of dirtiness of the panel, as shown in Table 2. (2.2.6.1) and (2.2.6.2) however, are only valid fordirect and circumsolar radiation, since these are the components with a well-defined angle of incidence. It is important to note that $FT_B(0^o) = 1$, so (2.2.6.2) does not include the effect of dirt on the relative normal transmittance, but only angular losses relative to normal incidence. So, it is also necessary to determine the degree of dirtiness of the surface, which is given by $T_{B_{dirt}}(0^o)/T_{B_{clean}}(0^o)$ and shown in Table 2:

Table 2 – Recommended values for the parameters of the angular loss expressions [5].

Dirtiness degree	$T_{B_{dirt}}(0^o)/T_{B_{clean}}(0^o)$	a_r
Clean	1	0.17
Low	0.98	0.20
Medium	0.97	0.21
High	0.92	0.27

The effective beam or circumsolar diffuse component of radiation reaching the solar cells of a PV module is [5] therefore:

$$G_{eff} = G\ \frac{T_{B_{dirt}}(0^o)}{T_{B_{clean}}(0^o)} FT_B(\theta) \qquad (2.2.6.3)$$

2.3. DOMESTIC PV SOLUTIONS

The main purpose of having a PV or other renewable system installed in a household is to enable self-production, energy cost reduction or even energetic independence and to generate clean and sustainable energy. There are several possible solutions to improve the efficiency of PV system and the combination with other technologies may lead to significant savings and higher efficiency.

2.3.1. PV SYSTEM WITH BATTERIES

A solar PV system installed in a household will generate electricity during the sunshine hours and that often corresponds to periods when the occupants are not at home. For regular PV systems without electric storage, the energy surplus can be sold to the grid. However, the exportation price of the electricity may fluctuate significantly, which can be disadvantageous to the consumer. In fact, due to these fluctuations, export prices might be significantly lower than import prices and occupants are incentivized to promote self-consumption and to avoid exporting which, in some cases, might not be the desired solution [29].

A possible solution to this problem is the introduction of batteries to the PV system. This allows the system to store energy instead of exporting it to the grid. At the start, it is more advantageous to have this system, but it is also necessary to find out if it is economically viable. Also, the manufacturing of these have an associated environmental cost, which is important to take into account, especially when the main purpose is to use an "environmental-friendly" energy solution.

If a PV system with batteries is well dimensioned, it is possible for the batteries system to replace the MPPT, since the output voltage can be regulated and fixed in order to meet the MPP.

There are two types of batteries used in association with PV system: Lithium-ion and Lead-acid. Each of these have advantages and disadvantages [30], which are summarized in Table 3:

Table 3 – Advantages and disadvantages of each type of batteries used associated with PV systems (adapted from [30]**)**.

Lithium-ion	**Lead-acid**
More expensive	Less expensive
Increasingly common in domestic grid-connected solar PV storage systems	Often used for off-grid systems where more storage is required
Lighter and smaller	Heavier and larger
Require integrated controller to manage charge and discharge	Requires a constant charging and discharging routine
More efficient	Less efficient
Can discharge more stored energy	Discharges less stored energy
Longer expected lifetime	Shorter expected lifetime

2.3.2. ZERO ENERGY BUILDINGS

Zero Energy Buildings (ZEB) or Net-Zero Energy Buildings (NZEB) are a new type of solution for future residential or commercial buildings. Their most important feature is the fact that they have reduced energy needs through great efficiency gains and so, its energetic needs may be suppressed by renewable energy sources, such as PV for electricity and solar thermal for heating or for domestic hot water (DHW). The core of the ZEB concept is the thought that buildings may satisfy their energetic demand from low-cost, locally-available, nonpolluting renewable sources [31]. These types of buildings can be classified according to the RE type and location regarding the building. There are many possible RE supply options, which depend on the location of the building and the resources available there [32].

ZEB can be connected to the grid (electric grid, domestic hot water grid), since by definition, it produces as much or more energy that it uses annually. Also, the connection to grid may be necessary to meet the buildings' needs when the energy production is not sufficient to supply the demand. Also, in cases of high market penetrations, the grid may not need the excess energy, so it is advisable to associate it with a storage system. Off-grid systems are possible, but need to be equipped with systems with improved storage and on-site generation capabilities. Regarding the usage of fuel, when the ZEB needs to import energy, it may use energy that results from fossil sources. So, the ZEB the rate of renewability may be given by the balance between the consumption of energy from fossil fuels and the exportation to the grid of energy from renewable sources [32].

2.4. OPTIMIZATION ALGORITHMS

In literature, there can be found several optimization algorithms applied to energy management problems, but there are few examples on energy management of households and, therefore, there are even fewer examples on energy management of households with generation.

2.4.1. MATHEMATICAL OPTIMIZATION METHODS

It is frequent to have problems that need optimization and there are mathematical tools to solve them. Three of the most important mathematical methods to solve optimization problems are: linear programming, dynamic programming and genetic algorithms.

Linear programing basically assumes that all the functions associated with the problem are linear and, with some given restrictions tries to find the optimal solution by maximizing or minimizing an objective function. This method will be detailed in **2.4.2**.

Dynamic programming is a set of mathematical tools which, when applied to decision or management problems, pretends to determine the best decision and solution combinations, though a systematic sequence of related decisions and processes [33]. In this type of programming, there is generated a set of possible solutions for a stage or state and, afterwards, the algorithm selects the one that matches the best the solution of the problem. This can be used in non-linear problems, but requires a large computing power [34].

A genetic algorithm (GA) is a computational program that mimics nature's processes of natural selection and genetic mutation in order to find the best solutions, within a set of possible solutions, for problems with seemingly random or stochastic characteristics. In the same way as breeding can lead to a virtually infinite number of genetic combinations, due to the complexity of the genetic heritage of an organism, GAs can be used to solve problems with a complex and stochastic nature [4]. Due to their versatility, GAs are widely used as tools of numerical optimization in different application fields, including energy management [35]. GA programming is similar to dynamic programming, but requires less computing power, since it uses a selection process to discard the

worst solutions and to find in less computations the optimal solution, by crossing the previous solutions to find a new one closer to the desired outcome.

In literature it is possible to find examples of each of these methods applied to energy management problems. Dynamic programming and GA are used for more complex problems that involve more decision variables, models and equipment, for example heating, ventilation and air conditioning (HVAC) systems [36] or in cases where each electric or electronic device is discriminated [37]. For simple cases, for instance where the production and consumption profiles are fixed, linear programming is sufficient to perform an optimization.

2.4.2. LINEAR PROGRAMMING

Linear programming (LP) is an optimization methodology in which all the mathematical functions associated with a problem are linear, *i.e.* which input variables are proportional to the output variables. LP also assumes that all variables may take fraction values. The word programming refers to planning, *i.e.* the preparation of the tasks and objectives to achieve the best outcome possible. To successfully formulate and solve a problem using LP, it is necessary to take into account the following stages:

- Comprehend and define well the problem;
- Define the variables of the problem, which are called the decision variables, *i.e.* which decision must be taken (taking into account the respective units);
- Define the restrictions of the problem in terms of the decision variables;
- Enounce the objective function as a function of the decision variables, *i.e.* the function that is pretended to optimize (minimize or maximize).

LP comprises a distinctive mathematical formulation. The decision variables $x_1, x_2, \dots, x_n$ satisfy a system of linear equations or inequations, which translate the restrictions of the problem:

$$\sum_{k=1}^{n} a_{ik}x_k + b_i \geq 0\,, \qquad x_k \geq 0, \qquad i = 1,2,\dots,m \;\wedge\; k = 1,2,\dots,n \tag{2.4.2.1}$$

where a_{ik} are constant coefficients, x_k are the decision variables (which are necessary nonnegative for LP problems), b_i are constant coefficients, n is the number of decision variables and m are the number of constraints. The objective function, being a function of the decision variables, takes the form:

$$F(x_1, x_2, \dots, x_n) = c_1x_1 + c_2x_2 + \cdots + c_kx_k + \cdots + c_nx_n \tag{2.4.2.2}$$

where c_k are constant coefficients that weight the contribution of each variable for the LP problem solution [38].

In most practical engineering cases, the problems are non-linear, which complicates the optimization method. Nevertheless, it is possible to apply the LP methods to a problem with non-linear variables. In that case, it is necessary to linearize the non-linear terms by using Taylor series expansions [38]:

$$F(x,y,\dots) = F(x_0,y_0,\dots) + \frac{1}{1!}\left((x-x_0)\frac{\partial}{\partial x} + (y-y_0)\frac{\partial}{\partial y} + \cdots\right)F(x_0,y_0,\dots) + \frac{1}{2!}\left((x-x_0)^2\frac{\partial^2}{\partial x^2} + (y-y_0)^2\frac{\partial^2}{\partial y^2} + \cdots\right)F(x_0,y_0,\dots) + \cdots \quad (2.4.2.3)$$

where x and y are the decision variables (the previous notation was not used to ease the representation of the function) of the problem and $(x_0, y_0, \dots)$ represents the point where the series is evaluated. In most cases, it is enough to replace the non-linear function by the first order Taylor series. However, there are limitations for the LP method, in particular, the degree of nonlinearity of the problem. In fact, higher the degrees of nonlinearity reduce the adequacy and efficiency of the LP method [38].

In literature, there can be found several examples of LP method applied to energy management problems. Dragićević et al. (2009) used a LP model to optimize an industrial steam-condensing system. By using this, it was possible to minimize the total costs for energy used and the net costs in steam-condensing systems [38]. Üçtuğ et al. (2012) used a LP method to maximize the energy savings of a hypothetical household in Turkey, while optimizing the allocation of the necessary budget for each solution [39]. Youn et al. (2009), used a LP method that determined the optimal operation of energy storage unit and the optimal initial storage energy level for a small power producing energy facility operating in parallel with the power grid. The model takes into account the possibility of buying and selling energy to the grid. To model the electrical load, a modified Gaussian distribution was used and for the on-site generation and the electrical power grid, a binomial distribution was used [40]. Conejo et. al (2010) used an optimization model to adjust the hourly load level of a given consumer in response to hourly electricity prices. The objective of the model was to maximize the effectiveness of the consumer, focusing on a minimum daily energy-consumption level and to achieve adequate maximum and minimum hourly load levels, by creating ramping limits on these. The price uncertainty was also taken into account for the modeling. The variables of decision, in this case, were the energy consumption and the hourly load level. At each hour, it was known the price of the energy and the consumption in the previous hour [41].

3. RADIATION AND PV PRODUCTION DATA ACQUISITION – EXPERIMENTAL SETUPS AND LOCATION

The optimization methods developed for this work, focused on two separate models: estimation the intensity of the incident radiation on the panels' surface from collected or forecast data and the production and performance of the PV system under certain working conditions (irradiance, temperature, orientation, etc.).

Due to limitations in experimental setup, the data for each of the validations came from different sources. The models that estimate the intensity of the incident radiation on the panels' surface were tested by using data gently given by the Laboratório Nacional de Engenharia e Geologia (LNEG) and the model that estimates the production and performance of the panels for a given value of incident irradiation was evaluated by using data from Faculdade de Ciências da Universidade de Lisboa (FCUL) and from the Grupo de Previsão Numérica do Tempo (GPNT) from Instituto Superior Técnico (IST).

3.1. LNEG

LNEG is located in Alfragide, Amadora, a place situated approximately 5 km from Lisbon. The latitude of the local is $\phi = 38^o46'25''$ N, the standard longitude is $L_{st} = 0^o$ and the local longitude is $L_{loc} = 9^o10'9''$W.

The system used a pyrheliometer to measure direct radiation; a set of three pyranometers, in order to measure the radiation in the plane of the collector, diffuse and on the horizontal plane, respectively and a sensor to measure ambient temperature. The pyrheliometer and the pyranometers were orientated with a variable β according to the season (Table 9) and a fixed azimuth of $\gamma = 0^o$. It is also important to refer that there are no relevant shadowing effects and the ground is mainly concreted darkened from the usage and natural degradation.

3.2. FCUL

The system to validate the 3P model is located in FCUL, in the campus of the Universidade de Lisboa in Campo Grande, a place close to the center of the city of Lisbon. It is mounted on the roofs of three different buildings, which are marked in yellow in Figure 3. The latitude of the local is $\phi = 38^o42'54''$ N, the standard longitude is $L_{st} = 0^o$ and the local longitude is $L_{loc} = -9^o9'23''$W.

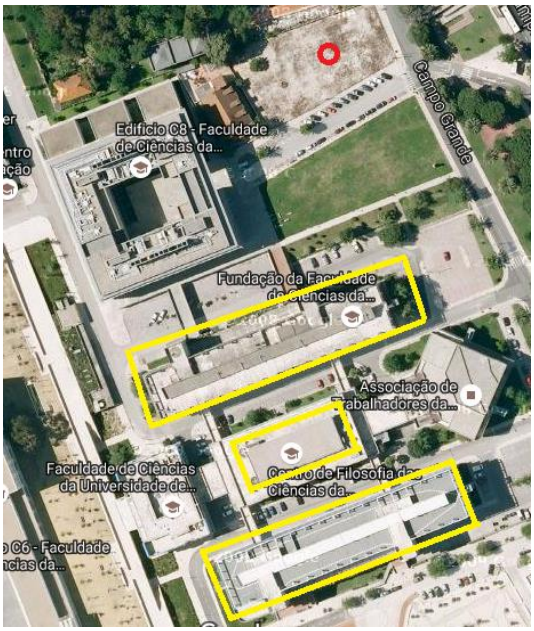

Figure 3 – Satellite view from the system's site. The rooftops on which the PV modules are mounted are marked in yellow and the site of the meteorological station is marked in red (adapted from Google Maps).

The system is composed by 3 rows in parallel with 23 PV modules each that are all connected to a MPP tracker which, in turn, is connected to an inverter. The whole system is directly connected to the electrical grid and has no associated batteries, which makes possible the usage of the MPP-Tracker. The panels are all oriented in the same way, with an azimuth of $\gamma = 0^o$ and a tilt of $\beta = 30^o$.

The total 69 photovoltaic modules are of polycrystalline silicon and their model is *Conergy PH Series 245P*, which has a maximum power of 245 W. The characteristic parameters for STC given by the manufacturers are stated in Table 4.

The system is not equipped with a temperature sensor, therefore it is not possible to get values for the ambient temperature and for the temperature of the cell directly from the system. On the other hand, there is a meteorological station equipped with a set of pyranometers with the tilt correspondent to the tilt of the panels. This way, it is possible to measure the total irradiance incident on the panels, so it is not necessary to recur to the models described in **2.1**. This enables the evaluation of the models described in **2.2** in the most rigorous way as possible, which is the main purpose of the usage of this system.

The system is equipped with a device to measure the total voltage and the total current of the 69 modules on the DC side of the system, *i.e.*, before the inverter transforms the current into AC. Therefore, it is not necessary to know the specifications of the inverter. This data is acquired in periods of 15 minutes, which is averaged for each hour to facilitate comparison with the simulation.

Table 4 - Relevant characteristic parameters for the *Conergy PH Series 245P* photovoltaic module model.

Conergy PH Series 245P	
Maximum power (P_{max})	245 W
Module efficiency	14.90%
Maximum power voltage (V_{max})	29.92 V
Maximum power current (I_{max})	8.20 A
Open circuit voltage (V_{oc})	37.98 V
Short circuit current (I_{sc})	8.62 A
NOCT	43±2 ºC
Temperature derate coefficient of V_{oc}	-0.34%/ºC
Temperature derate coefficient of I_{sc}	0.05%/ºC
N_s	60
Module dimensions (L x W x H)	1 652 x 994 x 40 mm

3.3. GRUPO DE PREVISÃO NUMÉRICA DO TEMPO (GPNT)

The Grupo de Previsão Numérica do Tempo is a group from IST which works in the area of modeling and forecasts of high resolution. It is responsible for the meteo|Técnico online platform, which gives a free and specialized service of meteorological predictions for continental Portugal. It is also in charge of a meteorological station called Estação Meteorológica Automática (EMA), which measures, for each minute, the local values of temperature, humidity, atmospheric pressure, wind speed and direction, precipitation and total solar radiation on a horizontal surface. EMA is located on the rooftop of the Southern Tower of IST and that corresponds to a latitude of $\phi = 38^o 44' 10''$ N, a standard longitude of $L_{st} = 0^o$ and a local longitude of $L_{loc} = -9^o 8' 17''$W.

The only data used from this group was of temperature, since it was the only quantity that was not measured by the FCUL system. The GPNT did not have available the specifications for the temperature sensor, but it was assumed to be an ordinary digital thermometer.

4. CASE STUDY: DESIGN AND MODEL OF A HOUSEHOLD'S ENERGETIC CONSUMPTION AND PRODUCTION

The development of the energy management algorithm has the main goal of creating a tool that can be implemented in an ordinary household with PV production to optimize the energy usage. Due to the limitations of the experimental setup, it will not be tested in a real household but, instead, the household's electricity consumption profiles and hypothetical system will be modeled and simulated by the algorithm.

The algorithm will simulate and predict the electric energy production from the PV system using the models described in **2.1** and **2.2** and tested in **6**, which will later be assembled in a toolbox of functions. However, as was described in **2.1**, the respective set of equations only estimates the incident radiation on a tilted surface (the PV panels are usually tilted) from radiation data on a horizontal surface, which is the standard data collecting practice of a meteorological station or of any other solar radiation data acquisition center. Therefore, these models are not adequate to make a forecast. In order to achieve an acceptable forecast, it is necessary to have web access to incident radiation on a horizontal surface predictions (from a trustworthy metheorological forecast tool) or sufficient collected data, both for a location as near as possible to the system or for a location with a similar average climate profile. This data can be converted into incident radiation forecasts on the actual PV system by using the models described in **2.1**.

4.1. SYSTEM DESIGN

A system as close as possible to a regular household will be idealized and all its components will be chosen as if it were for a real situation and to satisfy the needs of the occupants as better as possible. The system will be connected to the grid and will have an associated batteries bank storage system. The electricity comes from three different sources: the electric grid, the PV production system and/or the batteries bank. The loads of the system will be divided as being fixed or variable. The fixed loads will not be discriminated, but their consumption profiles will be assumed as a baseline for the consumption profiles. The variable loads will basically consist on a thermal accumulator, which provides DHW to the users and is the focus of the optimization process and the batteries (as to be charged). Therefore, the system needs to have the following main components:

- Electric energy sources - electrical grid, PV panels array and batteries system;
- Inverter;
- Fixed loads - indiscriminate;
- Variable load - thermal accumulator;
- Electrical energy storage system, which serves as an electric energy source and as variable load - batteries bank.

Taking this setup into account, a possible scheme of the system is presented in Figure 4.

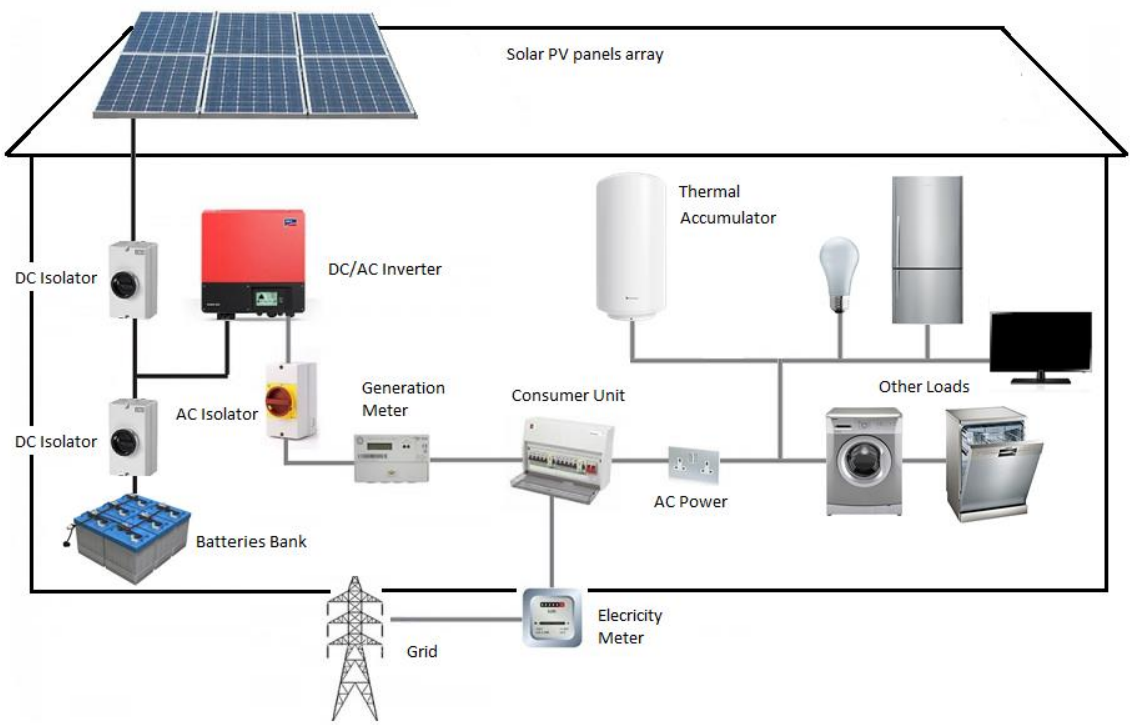

Figure 4 - Scheme of the possible configuration of the PV system, inverter and loads.

The system follows the PV Array / Batteries Bank → Inverter → Loads ← Grid configuration but, as it is possible to observe in Figure 4, there are other components like smart meters, isolators and a consumer unit present. These components are required for the system to operate normally, but their modeling is out of the scope of this work, since their influence in the electricity production and consumption is negligible.

All the components of the system, with the exception of the PV array, will be installed inside the household, which will be assumed to have a mean temperature of $25^{o}C$. Therefore, for the modelling of the important components, the temperature effects will only be considered for the PV array system. Also, since it is out of the scope of this work, the humidity effects will be neglected.

As it was mentioned before, the system is connected to the grid, so there will be a contract with an electricity distribution company, which establishes the cost of electricity. Also, the electric energy produced on the PV system will have an associated cost. This will be addressed in **4.8**.

4.2. INCIDENT RADIATION MODELING

For the radiation modeling, a toolbox with a set of code functions was created. The functions in this toolbox are based on the equations from **2.1** and are written in Matlab software language.

In **9**, it is possible to find a table with the toolbox functions and the respective input and output quantities. The algorithm uses these functions to calculate all the daily (δ, ω_s and ω_{sr}) and hourly (ω, θ, θ_z, γ_s, R_b, G_{on}, G_o, I_o, m, k_t and I_d) parameters individually. The inputs are basically the ones that regard the location (ϕ, L_{st}, L_{loc} and ρ), the ones that regard the orientation of the panels (β and γ) and the hourly irradiation data for a horizontal surface (I), which, in order to be more reliable, needs to correspond to the system's location or as close as possible. The main outputs for each hourly iteration are the three irradiation values of I_T calculated by using the Isotropic Sky, HDKR and Perez models, respectively, and the three correspondent mean irradiance values of G, which can afterwards be used as inputs in the PV production estimation models.

The algorithm is set to make estimations that can have a daily basis or can make calculations throughout an entire year, if the accordingly inputs are given. It can be used for any location and PV/solar thermal panel system. In Figure 5, there is a scheme that shows the steps that the algorithm follows, with the given inputs and outputs.

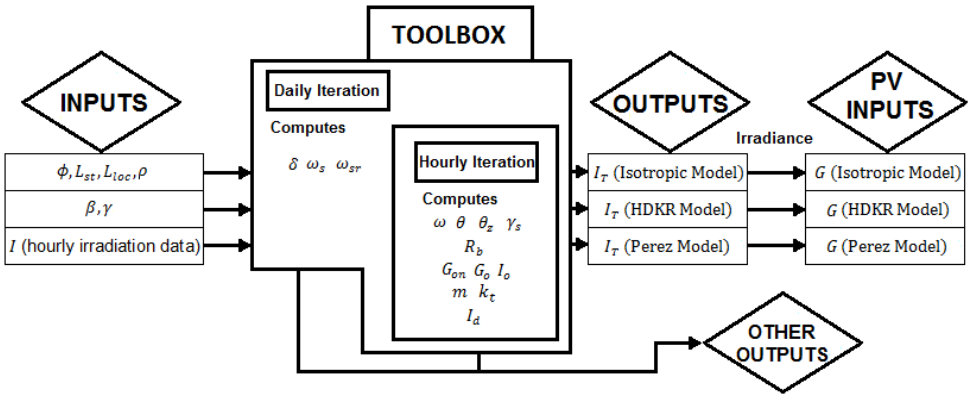

Figure 5 - Scheme of the algorithm for radiation on a tilted surface estimation.

4.3. PV PRODUCTION MODELING

The algorithm for PV production is based on the 3P model, described in **2.2**. It was developed differently, not relying on a toolbox of functions. Instead, the algorithm used one single function called *threep_pv*, that was also written in Matlab software language and which mainly objective was to calculate the power delivered by the modules under certain working conditions. To determine the performance of the PV system, this function uses, as inputs, values referent to weather conditions, which are data for the hourly incident irradiance (G) and the ambient temperature (T) for a year. As it was said before, the hourly values for G can also be obtained by using the algorithm described in **4.2**. The electrical characteristics of the panels of the PV system for STC are also used as an input, such as ${P_{max}}^{ref}$, ${V_{max}}^{ref}$, ${I_{max}}^{ref}$, ${I_0}^{ref}$, ${I_{sc}}^{ref}$, ${V_{oc}}^{ref}$, $NOCT^{ref}$, which is the coefficient that translates the variation of P_{max} with the temperature of the cell (in

%/K) [5]. Also, the generic physical characteristics of the panels are used as input parameters, which are N_s, $length_{panel}$ and $width_{panel}$.

The algorithm can be used for any PV system, by using the adequate weather conditions data and by using the respective specifications for the panels. For each hourly iteration, the algorithm computes the values of T_{cell}, V_T, I_{sc}, V_{oc}, I_0 and m' and subsequently calculates the expression for V as a function of I. Then, it solves the equation for P_{max} ($dP/dV = 0$) by intersecting the two sides of the equation and then computes the values for V_{max}, I_{max} and P_{max}. In Figure 6, there is a scheme which demonstrates the steps that this algorithm follows, with the respective inputs and outputs.

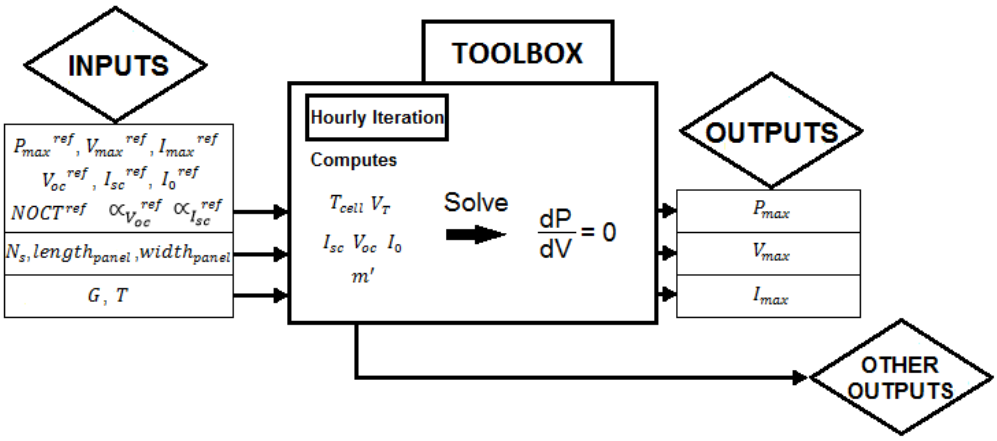

Figure 6 – Scheme of the algorithm for the PV panel performance estimation, using the 3P model.

4.4. INVERTER MODELING

The PV panels produces DC, but most devices at households use alternate current (AC). Therefore, it is necessary for any PV system connected to a grid or off-grid to have a device that converts DC into AC: an inverter. The inverter needs to impose an AC voltage of 230 V, which is the one required in a household. The equation that relates the generated DC power with the AC power delivered to the grid is:

$$\eta_{inv} V_{DC} I_{DC} = V_{AC} I_{AC} \cos\varphi \qquad (4.4.1)$$

where η_{inv} is the efficiency of the inverter, which can be considered as a constant parameter, since it remains significantly constant for a wide range of loads' power input and $\cos\varphi$ is called the power factor, which relates the real power P (in W) with the reactive power Q (in VAR), which is basically due to the opposition of the circuit elements to a change in the current or voltage (as it happens in AC), which in turn comes from its inductance or capacitance. P and Q can be related by the power factor, which is given by $\cos\varphi = P/S$, where S is the apparent power (in VA), which

is given by $S = \sqrt{P^2 + Q^2}$. However, for real cases, if there is generation, the power factor usually is above 0,90 for an inverter accordingly sized. This way, it can be assumed that, without large margin of error, $Q \ll P$ while the system is operating, from which comes $\cos\varphi \simeq 1$. For the rest of the cases, it can be assumed that $\cos\varphi \simeq 0$ [43]. Taking (4.4.1) and $\cos\varphi \simeq 1$, the AC power P_{AC} delivered to the grid by an inverter while the PV is generating is given [23] by:

$$P_{AC} \simeq \eta_{inv} P_{DC} \tag{4.4.2}$$

4.5. THERMAL ACCUMULATOR MODELING

Before the optimization process takes place, it is necessary to model the temperature and the energetic balance of the thermal accumulator.

4.5.1. ENERGY BALANCE

The energy balance of the thermal accumulator will consider two different cases: when the water is being heated and when the thermal accumulator is losing energy to its surroundings. The equation that describes the first case is [44]:

$$\dot{Q}_{heat}(t) = \frac{c_{p_{water}}\, \rho_{water}\, V_{DHW}(t)\, \left(T_{DHW} - T(t)\right)}{\eta_{heat} \times 1000 \times 3600} \tag{4.5.1.1}$$

where $\dot{Q}_{Heat}(t)$ represents the heat transferred to the thermal accumulator in kW for a given hour t, $c_{p_{water}} = 4181.3\ \mathrm{J\,kg^{-1}K^{-1}}$ the isobaric specific heat of water per unit of mass, $\rho_{water} = 997\ \mathrm{kg\,m^{-3}}$ the density of water, $V_{DHW}(t)$ the demanded volume of DHW for a given t in $\mathrm{m^3}$, T_{DHW} the demanded temperature of DHW in $^{\mathrm{o}}\mathrm{C}$, $T(t)$ the temperature of the water during a given t and η_{heat} the thermal accumulator efficiency at heating water. On the other hand, the equation that describes the second case is [44]:

$$\dot{Q}_{loss}(t) = U_{loss}\, \frac{T(t) - T_{amb}}{1000} \tag{4.5.1.2}$$

where $\dot{Q}_{loss}(t)$ represents the thermal accumulator heat losses to the surroundings in kW for a given hour t, $U_{loss}$the heat loss coefficient in $\mathrm{W\ ^{o}C^{-1}}$ and T_{amb} is the ambient temperature of the surroundings.

For the chosen thermal accumulator, the heat loss coefficient may not be specified in the product data sheet so, it is necessary to find a reference value. The thermal dispersion Q_{pr} is a parameter that gives the heat losses of the thermal accumulator in kWh in a 24h period of time and, for a typical thermal accumulator with a water volume of $V \leq 200\ \mathrm{l}$. According to the Portuguese legislation [45], it has to be less than:

$$Q_{pr}[\text{kWh/24h}] \leq \frac{(21 + 10.33\, V^{0,4}) \times 24}{1000} \qquad (4.5.1.3)$$

Taking Q_{pr}, a major for the heat loss coefficient U_{loss} can be obtained by:

$$U_{loss} \leq \frac{P_{loss}}{\Delta T} \qquad (4.5.1.4)$$

where $P_{loss} = Q_{pr}/24\text{h}$ is the loss power in W and $\Delta T = T_{DHW} - T_{amb}$. Taking reference values, it is possible to get that $\dot{Q}_{loss} \ll \dot{Q}_{Heat}$, which is as expected, since thermal accumulators are designed to have low energy losses. This way, $\dot{Q}_{loss}$ will only be significant when the water is not heating ($\dot{Q}_{Heat}$, = 0, $T(t) = T_{DHW}$), which also corresponds to higher difference between the DHW and the environment temperatures.

4.5.2. TEMPERATURE BALANCE

The temperature of the water inside the thermal accumulator may vary due to: heat transfer or loss and/or DHW consumption and subsequent replacement of the lost volume with an equivalent amount of water from the grid. In the first case, $T(t)$ may be calculated by inverting (4.5.1.1) and (4.5.1.2). In the second case, $T(t)$ may be calculated by making an average between the replaced water from the grid and the remaining water inside the thermal accumulator:

$$T(t) = \frac{V_{DHW}(t-1)\, T_{grid} + \left(V_{total} - V_{DHW}(t-1)\right)\, T(t-1)}{V_{total}} \qquad (4.5.2.1)$$

where V_{total} represents the total volume of water inside the thermal accumulator and T_{grid} the temperature of the water from the grid, which will be assumed to be $T_{grid} = 20^{o}\text{C}$.

It is important to refer that the models described in **4.5.1** and **4.5.2** are simple thermal models and do not consider effects like the stratification of the temperature inside the thermal accumulator.

4.6. BATTERY SYSTEM MODELING

The batteries system will be used as both source and load so, the discharge and charge of the batteries were modeled.

4.6.1. BATTERY DISCHARGE

The battery storage capacity (in Ah) translates the yield of the battery at a given discharge rate that would drain out the battery over a specified period of time and at a given temperature. Usually manufacturers specify this for a temperature of 25^{o}C and a period of 20h, which is denoted by $\text{C}/20$. In this case, a battery with $220\ \text{Ah}$ capacity would deliver constant current of $11\ \text{A}$ for 20

hours. This capacity is connected to the discharge rate: a faster discharge of battery results in a lower Ah capacity and slower discharge translates in a higher Ah capacity [5].

The lifetime of a battery depends on many factors related to its maintenance and the ambient conditions on which it is working, but one of the main factors is how the discharge occurs. The available currently energy state is given by the state of charge (SOC) of the battery, which translates, in terms of a percentage, the charge of the battery. The depth of discharge (DOD) is the complement of SOC and gives, also in terms of a percentage, the capacity of the battery used in terms of the total capacity. The deeper the discharge, the higher is the DOD and the lower will be number of available cycles of the battery and thus the lifetime of the battery. A deep discharge cycle is defined as any discharge over 80% of the capacity and a short discharge cycle is defined as a discharge up to 20% of the capacity.

To increase the lifetime of the battery while having it working at the expected conditions, it is necessary to define a maximum depth of discharge (DOD_{max}). Therefore, the maximum available capacity at any instant [5] is given by:

$$C_{av_{max}} = C_{nominal}(C/20, 25^{\circ}\mathrm{C}) \times DOD_{max} \tag{4.6.1.1}$$

and the available energy, at any instant t, in kWh, is given by:

$$E_{av}(t) = \left(SOC(t) - (1 - DOD_{max})\right) \times C_{av_{max}} \times V_{batt} \times \eta_{inv} \tag{4.6.1.2}$$

4.6.2. BATTERY CHARGE

The charging process of the battery is the inverse of the discharging process. The equations that describe the usable capacity and the usable energy are like (4.6.1.1) and (4.6.1.2), but have an additional term that was neglected for the discharge, the charging efficiency of the battery η_{charge}. The necessary energy to charge the battery, at a given instant is:

$$E_{charge}(t) = \frac{\left(SOC(t) - (1 - DOD_{max})\right) \times C_{av_{max}} \times V_{batt}}{\eta_{inv} \times \eta_{charge}} \tag{4.6.2.1}$$

4.7. EQUIPMENT CHOICE AND SPECIFICATIONS

The choice of each equipment is a crucial part for the modeling. In this section, it will be specified the chosen models for the PV modules, inverter, thermal accumulator and batteries, as well as the respective system configuration.

4.7.1. PV MODULES

For simplicity purposes, the chosen PV modules for the system installed in the household were the same as the ones installed in FCUL, *i.e.*, the polycrystalline silicon *Conergy PH Series 245P* model. The characteristic parameters given by the manufacturers for STC are presented in Table 4. It was chosen an array of 6 panels connected in series which makes, for STC, an installed total of $I_{max\,total} = 8.20$ A, $V_{max\,total} = 179.52$ V and $P_{max\,total} = 1472.06$ W.

To match the data for irradiation on a horizontal surface, the location of the household will be assumed to be the same as EMA's. This corresponds to a latitude of $\phi = 38^o 44' 10''$ N, a standard longitude of $L_{st} = 0^o$ and a local longitude of $L_{loc} = -9^o 8' 17''$W. For optimization purposes, the modules will be facing south ($\gamma = 0^o$) and will have a tilt equal to the latitude ($\beta = 38{,}74^o$).

4.7.2. INVERTER

Table 5 - Relevant characteristic parameters for the *Sunny Boy 1.5* PV inverter model

Sunny Boy 1.5	
Input (DC)	
Max. DC power (at $\cos\varphi = 1$)	1600 W
Max. input voltage (V_{max})	600 V
MPP voltage range	160 V to 500 V
Rated input voltage	360 V
Min. input voltage / initial input voltage	50 V / 80 V
Max. input current (I_{max})	10 A
Max. input current per string	10 A
Output (AC)	
Rated power (at 230 V, 50 Hz)	1500 W
Max. output current	7 A
Power factor at rated power	1
Efficiency	
Max. efficiency / European weighted efficiency	97.2 % / 96.1 %

For this system, the inverter *Sunny Boy 1.5* was chosen, since it is an adequate inverter for small PV systems, like in a regular household. This is a simple inverter, with some convenience

features, like easy installation, easy integration into the home network and wireless operation, small size and adequate characteristic parameters for the set of PV modules.

The characteristic parameters of the inverter are summarized in Table 5. The inverter is adequate to the PV system, since $I_{max\,total} < I_{max}$, $\text{Min. input voltage} < V_{max\,total} < V_{max}$, $V_{max\,total} \in \text{MPP Voltage Range}$ and $P_{max\,total} < P_{max}$. It is important to refer that, for this assessment, it was assumed that the maximum values for these parameters do not change significantly with temperature, since Lisbon has a mild climate.

4.7.3. THERMAL ACCUMULATOR

For the thermal accumulator, the chosen model was the *Vulcano NaturaAqua ES 120*. It is a class C thermal accumulator, with an adequate size for a family of 3 or 4 members. It is relatively small and easy to install. It was also chosen because it is compatible with solar thermal systems, thus being an alternative of electric backup. In what regards the scope of this work, this model has the following important characteristic parameters, which are described in Table 6.

Taking the total volume of water of the thermal accumulator of $V = 120\,\text{l}$ and (4.5.1.3) and assuming $T_{DHW} = 60^{\text{o}}\text{C}$ and $T_{amb} = 25^{\text{o}}\text{C}$, it is possible to obtain an average maximum power loss in W of $P_{loss} = 91.11\,\text{W}$. The heat loss coefficient can be obtained by using (4.5.1.4), from which comes $U_{loss} \leq 2.60\,\text{W}/\,^{\text{o}}\text{C}$. It will be assumed that the chosen thermal accumulator respects the legislation and, since it is not possible to obtain an exact value for P_{loss} or U_{loss}, the value obtained in (4.5.1.4) will be assumed as a reference value for U_{loss}. Also, as it was said before, $\dot{Q}_{loss}$ is usually small when compared with $\dot{Q}_{heat}$, which legitimizes this assumption.

Table 6 – Relevant characteristic parameters for the *Vulcano NaturaAqua ES 80* thermal accumulator model.

Vulcano NaturaAqua ES 120	
Total volume (V_{tot})	120 l
Power consumption (P)	2 kW
Water heating efficiency (η_{heat})	1

4.7.4. BATTERIES SYSTEM

The batteries bank was dimensioned taking into account the installed power of the PV system and the specifications of the inverter. The voltage in the battery bank needs to match the input voltage of the inverter. For a maximum value of AC power between 1200 and $2400\,\text{W}$, the recommended input voltage of the inverter is of $24\,\text{V}$. A set of 6 lead-acid batteries of the *Autosil*

I452008 model were chosen. These batteries are used in alternative energy systems. The specifications of the batteries are assembled in Table 7:

Table 7 - Relevant characteristic parameters for the *Autosil I452008* lead-acid battery model.

Autosil I452008	
Nominal capacity at C/20, $25^{o}\mathrm{C}$	105 Ah
Voltage (V)	12 V

The 6 batteries will be connected in 2 rows in parallel with 3 batteries in series each, making a total capacity of $315\ \mathrm{Ah}$ and an exit voltage of $24\ \mathrm{V}$. For efficiency purposes and to increase the expected lifetime of the batteries, the maximum depth of discharge will be set to $DOD_{max} = 60\%$. For lead-acid batteries, the charging efficiency of the batteries, η_{charge}, will be assumed to be $\eta_{charge} = 91\%$ [46].

4.8. ELECTRIC GRID TARIFFS AND EQUIVALENT COST OF ELECTRICITY FOR SELF-GENERATING SOURCES

The parameter that will be subject to the optimization process of the energy management algorithm is the cost of electricity so, it will minimize the cost of the electricity used to power the thermal accumulator and to charge the batteries.

The price of electricity in a household depends whether it comes from the grid or from a self-production source. The tariffs associated with electric energy from the grid are established by the distribution company and can vary depending on the contract. On the other hand, the on-site generation itself does not have associated a tariff, but it is possible to associate an equivalent cost to it, which is called levelized cost of electricity (LCOE). This relates the investment and maintenance costs of the equipment to the total energy produced by the equipment.

4.8.1. GRID TARIFF CHOICE

Since the case study household is connected to the grid, it is necessary to establish the tariffs of the electricity. It will therefore be assumed that the household has an electricity contract with EDP Comercial, with a contracted power of $3.45\ \mathrm{kVA}$ and a bi-horary daily cycle for winter and summer tariff option. A table with the hours and respective prices per kWh for the chosen tariff option is presented in Figure 7:

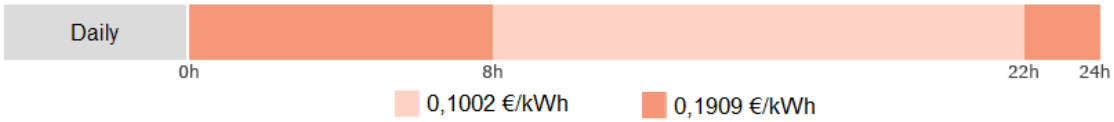

Figure 7 - Daily tariff for a bi-horary daily cycle for Winter and Summer (adapted from [47]).

4.8.2. LEVELIZED COST OF ELECTRICITY

The levelized cost of electricity (LCOE) is an economic calculation of the average total cost to build and operate a power-generating asset over its lifetime divided by the total energy produced by it during that period. It represents the value for which an equal-valued fixed revenue delivered over the lifetime of the asset's generating period would permit the return of the investment *i.e.*, the project to break even. For an electric energy generating system, the LCOE in €/kWh is given by [48]:

$$LCOE = \frac{\sum_{t=1}^{n} \frac{I_t + M_t + F_t}{(1+r)^t}}{\sum_{t=1}^{n} \frac{E_t}{(1+r)^t}} \quad (4.8.1.1)$$

where I_t are the investment expenditures with the equipment in the year t, M_t the operations and maintenance expenditures with the equipment in the year t, F_t are the fuel expenditures with the equipment, E_t the electrical energy generated by the system during the year t in kWh, r the annual effective discount rate, which expresses the amount of interest paid as a percentage of the balance at the end of the period of a year and n the expected lifetime of the system.

In the case of PV, the investment expenditures I_t parameter is not immediate to calculate. In literature, it is possible to find some empirical expressions that calculate the PV installation price per kWp for a given year. It is possible to get that PV price halves every four years. These curves depend on the year and on the nominal power and the expression the price for PV installation p in €/kWp for a given time y (in years since 1/1/2009) is given [49] by:

$$p(y) = a2^{-by}\left(1 + \frac{c}{N}\right) \quad (4.8.1.2)$$

where $a = 3370$, $b = 0.26$ and $c = 0.57$ are fitting parameters and N is the total nominal power. To obtain the value of I_t, it is necessary to divide p by the lifetime of the equipment n.

4.8.3. PV SYSTEM LCOE

For the calculations of the LCOE associated to the PV system, it was assumed that the system would last in acceptable working conditions for about 25 years, which is the current mean performance duration period warrantied by the manufacturers, thus having $n = 25$. The interest

rate was assumed to be $r = 0{,}03$, which is common value for commercial/domestic investments in this kind of technology [49].

For the total investment costs, I was calculated by using (4.8.1.2) and assuming $y = 7$ (correspondent to 2016) and $N = 1.472\ \mathrm{kW_p}$, thus being obtained $p = 1324.05\ €/\mathrm{kW_p}$ and, by dividing it by the expected lifetime of the equipment n, it was possible to get $I_t = 52.96\ €/\mathrm{kWp}$. The maintenance and operation costs were assumed to correspond to 1.5% of the total investment costs per year, which is assumed to be a fixed value. Therefore, $M_t = 19.86\ €/\mathrm{kW_p}$. Finally, F_t was set to be $0\ €/\mathrm{kW_p}$, since the PV system does not consume any fuel.

In what regards E_t, it was assumed that in the case of Portugal, in particular in the center region, the number of hours in a year in which the system operates at the peak power is of about 1500 h/year [23], thus having $E_t = 2208\ \mathrm{kWh}$.

From (4.8.1.1), it comes that, for the PV system, $LCOE = 0.0330\ €/\mathrm{kWh}$.

4.8.4. BATTERIES SYSTEM LCOE

The batteries system also has an associated LCOE. For a lead-acid battery, the number of cycles during its lifetime for a DOD of 60%, is of about 2500 [50], as it is possible get from **Error! eference source not found.**. Since the batteries were dimensioned to satisfy the demand of energy by the thermal accumulator, it will be assumed that they will perform 1 cycle per day, which means that the batteries system will last for about 7 years *i.e.*, $n = 7$. The interest rate was assumed to be the same as for the PV system *i.e.*, $r = 0.03$.

The investment costs were assumed to be the sum of the batteries cost with the installation and maintenance costs. The costs of each battery was assumed to be of $150\ \$$, which corresponds to about $140\ €$ and this cost was also assumed to correspond to 20% of all investment costs [51]. Taking this into account the obtained value for the total investment costs was of $I + M = 8400€$, which gives $I_t + M_t = 1200\ €$. F_t was set to be $0\ €/\mathrm{kW_p}$, since the batteries system does not consume any fuel.

Taking the value of DOD for the system and the maximum available energy of the batteries, the estimated value for the energy delivered for a day is of $9.07\ \mathrm{kWh}$, which for a year corresponds to $E_t = 3311.3\ \mathrm{kWh}$.

From (4.8.1.1), it comes that, for the batteries system, $LCOE = 0.3624\ €/\mathrm{kWh}$, which is close to the one in [50].

4.9. INHABITANTS' DEMANDS AND CONSUMPTION PROFILES

The study of the behavior in what regards electrical consumption is a crucial part towards the development of an energy managing algorithm. In literature, it is possible to find several examples of works on modeling the general electricity consumption behaviors at households, regardless of the method or site of this electricity generation. Despite this, there is a lack of information and study on how these behaviors change in presence of domestic generation. There are some studies that attempt to model the impact of PV electricity generation on household electricity consumption behaviors, which are more adequate than the less specific models [7].

It is important to refer that there are deterministic approaches that use regression and correlation methods, in order to simulate consumers' direct response to a certain stimuli or decision making stage that might change the demand behavior [52] and there are stochastic approaches that use random functions of time and are less based on the deterministic and stimuli-response characteristics of human behavior [7]. There are also other more invasive strategies which implement a set of deliberate household actions, in order to achieve a certain management goal (*e.g.* minimization of the costs, maximization of the comfort) [53].

Despite this, the consumption profiles of the household, respective modeling, prediction and intense study are out of the scope of this work. For this work, there will be used fixed base energy consumption profiles as an energetic consumption baseline for a typical family. The algorithm will not implement an active and invasive energy saving strategy, but will make sure that electric energy distribution is successful. For this, it is necessary to know the demand and supply at a given time and to optimize energy allocation, to avoid the easy solution of increasing the production when the demand also increases which, in most cases, is far from being the optimal solution [54].

4.9.1. INHABITANTS' CHARACTERISTICS AND BEHAVIORS

The household in study will be considered as being inhabited by a family of four people: a couple of adults and two baby kids. On weekdays, the couple is working and the kids are at school from the end of morning until afternoon and the household is occupied during the early morning, evening and night. There are essentially three load peaks:

- Night – Off-peak of heavy loads, correspondent to washing or dishwashing machines. This peak occurs during the night because of the bi-horary tariff option.
- Early morning – The family wakes up, takes breakfast and the adults take a bath before going to work.
- Evening – The family arrives home, dinners, watches TV, etc., the kids take a bath.

These peaks can be considered as being the main ones for a regular day, but there can be fluctuations. For instance, the family might have a housemaid going to the house in some of

days of the week during the afternoon and it might be possible to observe peaks correspondent to ironing or vacuum cleaning. Also, the family energetic behaviors may change throughout the year and even during a week. The energy consumption is different in winter and in summer and in a weekday and a weekend day. Consequently, to define the energy profiles, two different approaches will be considered: seasonal and type of day related. In **4.9.4**, the typical chosen profiles are presented.

4.9.2. SEASONAL APPROACH

In what regards the seasonal features, it was considered a typical profile for summer and for winter. There are significant differences in the energy habits as the season, since many seasonal factors directly condition the usage of energy. For example, in winter, the days are shorter and there is not so much daylight available, which may lead to an increase in the usage of electric lighting; also, the air is colder and this might lead to a rise in the usage of electric air or water heaters; finally, since the weather is rainier or snowier, people tend to spend more time at home and, therefore, there is an increase in the electric energy consumption. On the other hand, in summer the opposite is verified and people tend to use less electric lighting and to spend more time outside but, nevertheless, since the ambient air is hotter, there can also occur an increase of the usage of air conditioners.

This is a simplistic approach, since it does not consider the mild seasons. To be possible to formulate this, it was assumed that:

- For the days between January 1st (inclusive) and April 15th (inclusive) and from October 16th (inclusive) to December 31st (inclusive), the profiles correspond to a typical Winter one;
- For the days between April 16th (inclusive) and October 15th (inclusive), the profiles correspond to a typical summer one.

4.9.3. TYPE OF DAY APPROACH

The type of day is also important to consider, since the energetic habits are quite different in work day or in a day off. For example, in a work day, people tend to be outside from the middle of the morning until the beginning of evening and people also wake up and go to bed early. Taking this into account, weekdays usually follow certain strict patterns, intimately related to the day's schedule. In days like weekends or holidays, there is less conditioning and, for instance, people tend to wake up and go to bed later or spend more time at home. To express this, it will be assumed that:

- For the days corresponding to $n = 4 + (i - 1) \times 7$ (Saturdays), $n = 5 + (i - 1) \times 7$ (Sundays), where i is an arbitrary integer and for the January 1st, April 18th, 20th and 25th, May 1st, June 10th and 19th, August 15th, October 5th, November 1st, December

1st, 8th and 25th (Portuguese holidays), the profiles correspond to a typical day off one and will be denoted as weekend days;

- For the remaining days, the profiles correspond to a typical work day and will be denoted as a week day.

It is important to note that these considerations were made for the year of 2014, for which corresponds the data for irradiance on a horizontal surface and ambient temperature.

4.9.4. BASELINE PROFILE CHOICE

Four profiles were chosen considering what was discussed in **4.9.2** and **4.9.3**. These correspond to a typical Summer weekday, Summer weekend day, Winter weekday and Winter weekend day and are represented in Graphic 1, Graphic 2, Graphic 3 and Graphic 4, respectively.It was assumed that these profiles did not include DHW, which demand will be specified in **4.9.5**.

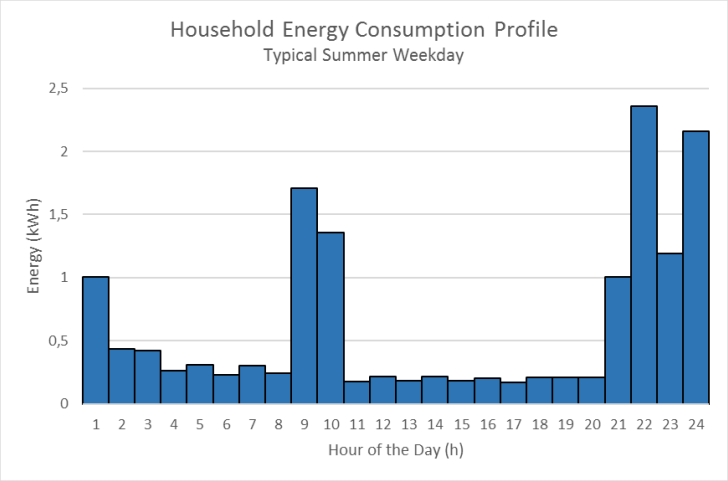

Graphic 1 – Typical Summer weekday energetic consumption profile for a family of two adults and two baby kids.

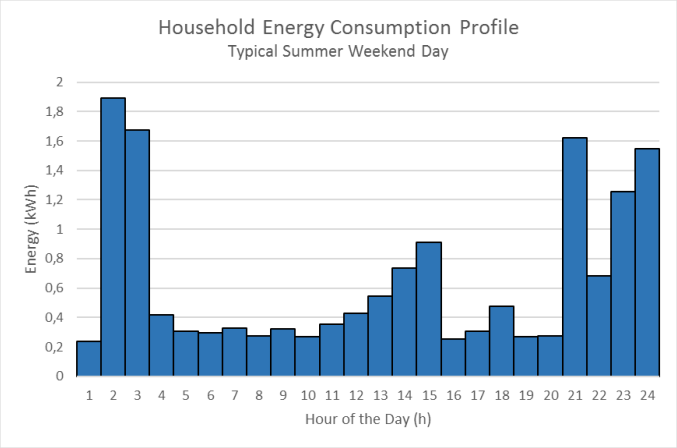

Graphic 2 - Typical Summer weekend day energetic consumption profile for a family of two adults and two baby kids.

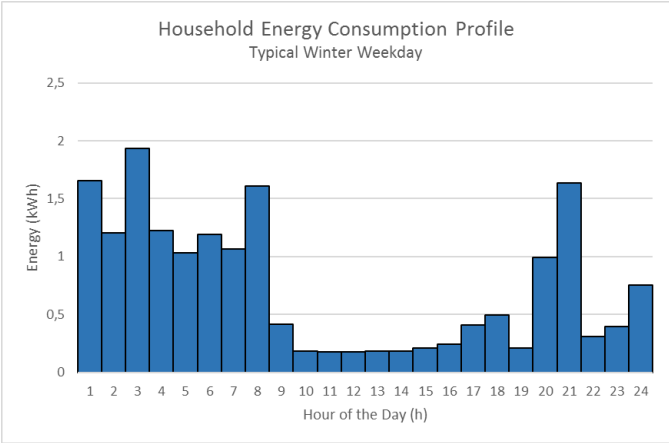

Graphic 3 - Typical Winter weekday energetic consumption profile for a family of two adults and two baby kids.

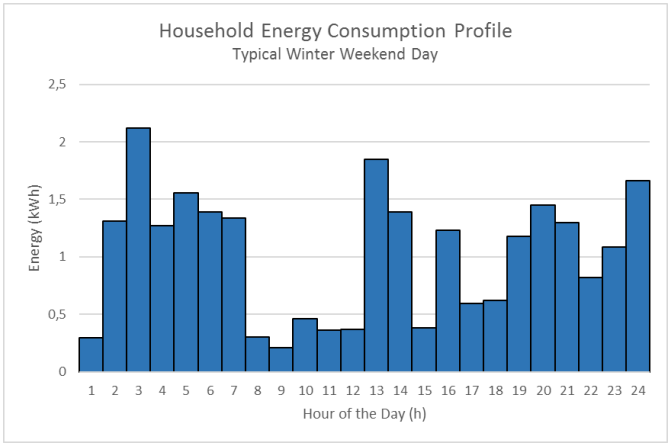

Graphic 4 - Typical Winter weekend day energetic consumption profile for a family of two adults and two baby kids.

4.9.5. DOMESTIC HOT WATER DEMAND

As it was mentioned in **4.9.1**, it was assumed that, in a regular day, the adults take a bath in the morning and the children in the evening. Each of the users take a single bath every day and this occurs on fixed periods of one hour. The demands for DHW volume and temperature and the hours of the baths were assembled in Table 8.

Table 8 – Users' DHW demand parameters choice according to their characteristics.

Domestic Hot Water Demand				
Users	V_{DHW}	$Total\,V_{DHW}$	T_{DHW}	**Demand Hours**
Children	$40\ l$	$80\ l$	$60\ ^{o}C$	20h-21h
Adults	$40\ l$	$80\ l$	$60\ ^{o}C$	7h-8h (Weekdays) 9h-10h (Days off)

5. LINEAR PROGRAMMING ENERGY MANAGEMENT OPTIMIZATION ALGORITHM

In this chapter, there is a description of the optimization algorithm and the different approaches towards the management of energy consumption in the household described in **4**. The algorithm was developed from scratch for this work and is based on the linear programming method. The algorithm was implement using the *Matlab* software language.

The consumption profiles are assumed as a baseline and since the algorithm does not intend to model the household occupants' behavior, the optimization process will minimize the cost of energy *i.e.*, it will search for the less expensive solution that addresses the needs of the users. For this, two approaches were considered: hourly and daily, with two different cases each. The hourly optimization finds, for each hour, the optimal solution for charging the thermal accumulator and the batteries system and has a more detailed analysis on the energy balance for each equipment. The daily optimization searches for an optimal daily solution, considering the restrictions of each hour, but having a less detailed energy balance analysis. This approach has an important advantage, since it enables the allocation of the energy for the hours demanded by the users.

Each case has an associated objective function, but all will use the same nomenclature. The decision variables E_g and E_{PV} correspond to the energy usage (in kWh) to power the thermal accumulator and/or the battery system from the grid and the PV system, respectively, and E_b to the energy usage (in kWh) to power the thermal accumulator from the batteries system, during a given hour; k is the grid tariff (in $€/\mathrm{kWh}$) for the respective hour; $LCOE_{PV}$ and $LCOE_b$ are the $LCOE$ (in $€/\mathrm{kWh}$) for the PV and batteries system, respectively. The energy consumption profiles presented in Graphic 1, Graphic 2, Graphic 3 and Graphic 4 and the contracted power impose a limit on E_g. The available PV energy production estimation conditions E_{PV}. And, finally, the present SOC of the battery set a limit to E_{batt} and, also, to the fraction of E_g and E_{PV} used to power the batteries. The values for E_g, E_{PV} and E_b must take into account the characteristics of the thermal accumulator and the batteries system and the respective state of temperature/charge.

5.1. FIRST APPROACH – HOURLY OPTIMIZATION

The hourly optimization approach finds the minimum solution for the cost objective function for each hour, finding 24 combinations of optimal solutions. From $h = 1$ to $h = 24$, the algorithm tries to find the less expensive solution to charge the thermal accumulator and the batteries system, considering the restrictions for each source. The steps the algorithm takes for each hour are the following:

(1) Checks the state of the thermal accumulator and the batteries;

(2) Choses the amount of energy for the thermal accumulator and for the batteries by:
    a. taking into account the restrictions for each source and the state and characteristics of the thermal accumulator and the batteries system,
    b. considering the heat losses in the thermal accumulator,
    c. minimizing the cost,
    d. maximizing the temperature increase and charge of the equipment;
(3) Calculates the current temperature of the water inside the thermal accumulator and the new state of charge of the batteries, which will be used as an input to the step (1) of the next hour.

Although the models that calculate the state of the thermal accumulator and the batteries are non-linear, they can be used in the hourly optimization, since the optimization itself does not depend on them, but only the initial and the final state.

The batteries system works as a source and as a load, so the charge of the thermal accumulator and the batteries are dependent on each other. For a deeper insight and simplification of the problem, two cases were considered: one that makes first the optimization for the thermal accumulator and secondly to the batteries and another one that does the reverse.

5.1.1. HOURLY ALGORITHM - A (THERMAL ACCUMULATOR AND BATTERIES OPTIMIZATION)

For the case A, the objective function for the hourly optimization of the thermal accumulator is:

$$F_{A_{therm}}\left(E_{grid_{therm}}(h), E_{PV_{therm}}(h), E_{batt_{therm}}(h), h\right) = \\ = k(h)E_{grid_{therm}}(h) + LCOE_{PV}E_{PV_{therm}}(h) + LCOE_{batt}E_{batt_{therm}}(h) \quad (5.1.1.1)$$

The bound constraints on the decision variables are:

$$0 \leq E_{grid_{therm}}(h) \leq P_{contract} \times 1\,hour - E_{other\ devices}(h) \quad (5.1.1.2)$$

$$0 \leq E_{PV_{therm}}(h) \leq E_{AC}(h) \quad (5.1.1.3)$$

$$0 \leq E_{batt_{therm}}(h) \leq E_{available_{batt}}(h) \quad (5.1.1.4)$$

where $P_{contract} = 3.45$ kVA, $E_{other\ devices}$ is the energy (in kWh) used by the other devices that comes from the baseline profiles, E_{AC} is the available energy from the PV system and $E_{available_{batt}}$ is the currently available energy on the battery, considering its SOC.

Finally, the equality constraints are:

$$E_{grid_{therm}}(h) + E_{PV_{therm}}(h) + E_{batt_{therm}}(h) = \\ = \min \begin{Bmatrix} P_{contract} \times 1\ hour - E_{other\ devices}(h) + E_{AC}(h) + E_{available_{batt}}(h) \\ E_{heat_{therm}}(h) \\ P_{max_{therm}} \times 1\ hour \end{Bmatrix} \quad (5.1.1.5)$$

where $E_{heat_{therm}}$ is the necessary energy (in kWh) to heat the water inside the thermal accumulator until it reaches the $60\ ^{o}\text{C}$ and $P_{max_{therm}} = 2\ \text{kW}$ is the maximum working power of the thermal accumulator.

After optimizing the energy usage of the thermal accumulator, the algorithm does the same to the batteries system. The respective objective function is:

$$F_{A_{batt}}\left(E_{grid_{batt}}(h), E_{PV_{batt}}(h), h\right) = k(h)E_{grid_{batt}}(h) + LCOE_{PV}E_{PV_{batt}}(h) \quad (5.1.1.6)$$

The bound constraints on the decision variables are:

$$0 \leq E_{grid_{batt}}(h) \leq P_{contract} \times 1\ hour - E_{other\ devices}(h) - E_{grid_{therm}}(h) \quad (5.1.1.7)$$

$$0 \leq E_{PV_{batt}}(h) \leq E_{AC}(h) - E_{PV_{therm}}(h) \quad (5.1.1.8)$$

The equality constraints are:

$$E_{grid_{batt}}(h) + E_{PV_{batt}}(h) \\ = \min \begin{Bmatrix} P_{contract} \times 1\ hour - E_{other\ devices}(h) - \\ -E_{grid_{therm}}(h) + E_{AC}(h) - E_{PV_{therm}}(h) \\ E_{charge_{batt}}(h) \\ E_{max_{batt}} \end{Bmatrix} \quad (5.1.1.9)$$

where $E_{charge_{batt}}(h)$ is the necessary energy (in kWh) to charge the batteries and $E_{max_{batt}}$ is the batteries' maximum input of energy (in kWh) which, by considering the characteristics of the batteries, was assumed to be $E_{max_{batt}} = 3 \times 105\ \text{Ah} \times 2 \times 12\ \text{V} \times 10^{-3} = 7.56\ \text{kWh}$.

5.1.2. HOURLY ALGORITHM - B (BATTERIES AND THERMAL ACCUMULATOR OPTIMIZATION)

This case is like the one described in **5.1.1**, but instead of optimizing first the thermal accumulator, it does it to the batteries system. The objective functions remain the same: (5.1.1.6) for the batteries system and (5.1.1.1) for the thermal accumulator. The difference is in the constraints.

For the batteries system, the bound constraints are:

$$0 \leq E_{grid_{batt}}(h) \leq P_{contract} \times 1\ hour - E_{other\ devices}(h) \quad (5.1.2.1)$$

$$0 \leq E_{PV_{batt}}(h) \leq E_{AC}(h) \quad (5.1.2.2)$$

and the equality constraints are:

$$E_{grid_{batt}}(h) + E_{PV_{batt}}(h) = \min \begin{Bmatrix} P_{contract} \times 1\ hour - E_{other\ devices}(h) + E_{AC}(h) \\ E_{charge_{batt}}(h) \\ E_{max_{batt}} \end{Bmatrix} \quad (5.1.2.3)$$

In the case of the thermal accumulator, the bound constraints on the decision variables are given by:

$$0 \leq E_{grid_{therm}}(h) \leq P_{contract} \times 1\ hour - E_{other\ devices}(h) - E_{grid_{batt}}(h) \quad (5.1.2.4)$$

$$0 \leq E_{PV_{therm}}(h) \leq E_{AC}(h) - E_{PV_{batt}}(h) \quad (5.1.2.5)$$

$$0 \leq E_{batt_{therm}}(h) \leq E_{available_{batt}}(h) \quad (5.1.2.6)$$

The equality constraints for the thermal accumulator are:

$$E_{grid_{therm}}(h) + E_{PV_{therm}}(h) + E_{batt_{therm}}(h) = \min \begin{Bmatrix} P_{contract} \times 1\ hour - E_{other\ devices}(h) - E_{grid_{batt}}(h) + \\ + E_{AC}(h) - E_{PV_{batt}}(h) + E_{available_{batt}}(h) \\ E_{heat_{therm}}(h) \\ P_{max_{therm}} \times 1\ hour \end{Bmatrix} \quad (5.1.2.7)$$

5.2. SECOND APPROACH – DAILY OPTIMIZATION

The daily optimization is a different approach than the one described in **5.1**, since it evaluates the whole day, finding the best overall solution and not the individual solution for each hour. With this approach, instead of having an objective function for each hour, there is only one objective function, with $24 \times 5 = 120$ decision variables. The objective function consists of the combination of (5.1.1.1) and (5.1.1.6) for all the hours:

$$F = \sum_{h=1}^{24} \Big[k(h) \left(E_{grid_{therm}}(h) + E_{grid_{batt}}(h) \right) + LCOE_{PV} \left(E_{PV_{therm}}(h) + E_{PV_{batt}}(h) \right) + LCOE_{batt} E_{batt_{therm}}(h) \Big] \quad (5.2.1)$$

The algorithm does not take hourly steps, but instead follows the next ones only once for each day:

(1) Checks the state of the thermal accumulator and the batteries system at the beginning of the day;
(2) Choses the amount energy for the thermal accumulator and for the batteries for the entire day by:

a. taking into account the energy restrictions for each source and the state and characteristics of the thermal accumulator and the batteries system,
b. guaranteeing the desired T_{DHW} for the users at the chosen hours,
c. minimizing the cost,
d. maximizing the charge of the batteries system;

(3) Calculates the state of the thermal accumulator and the batteries system at the end of the day, to be used as inputs for the following day.

This approach has some significant limitations and some advantages when compared to the hourly one. With this approach, it is not possible to use in a detailed way the models for the thermal accumulator and for the batteries but, instead, the initial state is calculated at the beginning of the day, being determined the correspondent available energies and the necessary energy to charge each of the equipment. These will be used as fixed constraints for the optimization process and therefore, the physical detail of the problem is lost. On the other hand, with this approach, the process takes into account the whole day and not the individual hours, which is closer to the ideal solution. This way, the daily approach flaws in the physical detail, but permits to have a more realistic insight of the problem.

One other factor was taken into account for this approach, which is the usage of the battery. The $LCOE_{batt}$ corresponds to the highest energy cost and since the algorithm searches for the lowest cost solution, it is much likely that that the batteries system will never be used as an energy source. Therefore, two algorithms were created: one that seeks the lowest cost solution regularly and another one that imposes the usage of the battery, in order to assess if the mandatory usage of batteries is still compensatory when compared to the case of a household without self-production.

5.2.1. DAILY ALGORITHM - C (NO BATTERY USAGE RESTRICTION)

For this case, the objective function is (5.2.1). The bound constraints are:

$$0 \leq E_{grid_{therm}}(h) \leq P_{contract} \times 1\ hour - E_{other\ devices}(h) \quad (5.2.1.1)$$

$$0 \leq E_{grid_{batt}}(h) \leq P_{contract} \times 1\ hour - E_{other\ devices}(h) \quad (5.2.1.2)$$

$$0 \leq E_{PV_{therm}}(h) \leq E_{AC}(h) \quad (5.2.1.3)$$

$$0 \leq E_{PV_{batt}}(h) \leq E_{AC}(h) \quad (5.2.1.4)$$

$$0 \leq E_{batt_{therm}}(h) \leq E_{available_{batt}} \quad (5.2.1.5)$$

where, $E_{available_{batt}}$ is the available energy of the batteries system calculated at the beginning of the day. These constraints are necessary for the linear programming optimization, but most of the time are redundant. The inequality and equality constraints, which will be defined next, in some cases overlap the bound constraints.

For this case, the inequality constraints are:

$$E_{grid_{therm}}(h) + E_{grid_{batt}}(h) \leq P_{contract} \times 1\,hour - E_{other\ devices}(h) \quad (5.2.1.6)$$

$$E_{PV_{therm}}(h) + E_{PV_{batt}}(h) \leq E_{AC}(h) \quad (5.2.1.7)$$

$$E_{grid_{therm}}(h) + E_{PV_{therm}}(h) + E_{batt_{therm}}(h) \leq P_{max_{therm}} \times 1\,hour \quad (5.2.1.8)$$

$$\sum_{h=1}^{24} E_{batt_{therm}}(h) \leq E_{available_{batt}} \quad (5.2.1.9)$$

It is possible to conclude that (5.2.1.6) makes (5.2.1.1) and (5.2.1.2) redundant except for the limit case when $E_{grid_{therm}}(h) = P_{contract} \times 1\,hour - E_{other\ devices}(h)$ and $E_{grid_{batt}}(h) = 0$ or $E_{grid_{therm}}(h) = 0$ and $E_{grid_{batt}}(h) = P_{contract} \times 1\,hour - E_{other\ devices}(h)$. The same can be concluded for (5.2.1.7) and (5.2.1.3) and (5.1.2.4) when $E_{PV_{therm}}(h) = E_{AC}(h)$ and $E_{PV_{batt}}(h) = 0$ or $E_{PV_{therm}}(h) = 0$ and $E_{PV_{batt}}(h) = E_{AC}(h)$ and for (5.2.1.9) and (5.2.1.5) when $E_{batt_{therm}}(h) = E_{available_{batt}}$ for a given hour and $E_{batt_{therm}}(h) = 0$ for the remaining hours.

The equality constraints are given by:

$$\sum_{h=1}^{7}\left[E_{grid_{therm}}(h) + E_{PV_{therm}}(h) + E_{batt_{therm}}(h)\right] + \\ + \sum_{h=22}^{24}\left[E_{grid_{therm}}(h) + E_{PV_{therm}}(h) + E_{batt_{therm}}(h)\right] \\ = E_{heat_{therm}} \quad (5.2.1.10)$$

$$\sum_{h=9}^{20}\left[E_{grid_{therm}}(h) + E_{PV_{therm}}(h) + E_{batt_{therm}}(h)\right] = E_{heat_{therm}} \quad (5.2.1.11)$$

$$\sum_{h=1}^{24}\left[E_{grid_{batt}}(h) + E_{PV_{batt}}(h)\right] - \sum_{h=1}^{7} E_{batt_{therm}}(h) - \sum_{h=9}^{20} E_{batt_{therm}}(h) - \\ - \sum_{h=22}^{24} E_{batt_{therm}}(h) = E_{charge_{batt}} \quad (5.2.1.12)$$

where $E_{heat_{therm}} = 3.72$ kWh is the necessary heat in to charge the thermal accumulator from $T = 33.3$°C to T_{DHW}. The value for $T = 33.3$°C comes from (4.5.2.1) by taking $V_{DHW} = 80\,l$. $E_{charge_{batt}}$ is the necessary energy (in kWh) to charge the batteries at the beginning of the day obtained from (4.6.2.1), taking into account the SOC also at the beginning of the day. (5.2.1.10) represent the necessary heat transfer to thermal accumulator for it to have $T = T_{DHW}$ at $h = 8$ and (5.2.1.11) for the same at $h = 21$. At $h = 8$ and $h = 21$, the thermal accumulator is being used by

the occupants and, therefore, the energy transferred to the thermal accumulator is null ($E_{grid_{therm}}(h = 8, 21) = 0, E_{PV_{therm}}(h = 8, 21) = 0$ and $E_{batt_{therm}}(h = 8, 21) = 0$).

5.2.2. DAILY ALGORITHM - D (BATTERY USAGE RESTRICTION)

Case D for the daily algorithm approach is quite similar to case C, described in **5.2.1**. This algorithm has the same objective function, bound, inequality and equality constraints as the one for case C, being the only difference an additional equality constraint:

$$\sum_{h=1}^{7} E_{batt_{therm}}(h) + \sum_{h=9}^{20} E_{batt_{therm}}(h) + \sum_{h=22}^{24} E_{batt_{therm}}(h) = E_{available_{batt}} \qquad (5.2.2.1)$$

This constraint forces the system to discharge the batteries once a day taking into account the SOC at the beginning of the day and DOD_{max}.

6. RESULTS

This chapter is dedicated to the presentation and analysis of results. The first subchapter regards the tests and evaluation of the radiation models described in **4.2**, using data from LNEG. It has two subsections for the hourly and daily evaluation. The second one refers to the tests and evaluation of the PV production models, described in **4.3** and using data from FCUL and from GPNT. The respective subchapters refer to two different cases. The last subchapter is dedicated to the presentation and analysis of the results from the energy management algorithm presented in **5**, with three different approaches for this analysis.

6.1. INCIDENT RADIATION MODELS EVALUATION (ISOTROPIC SKY, HDKR AND PEREZ)

6.1.1. HOURLY

The models of incident radiation were tested using the experimental setup located in LNEG, as it was described in **3.1**. The acquired data was referent to two days of each month of the year of 2015. For some days, the acquisition rates were of $2\ \mathrm{min}$ and of $30\ \mathrm{s}$ and, since the models that are being validated are hourly, it was necessary to make an hourly average in both cases. The days and respective rates were assembled in Table 9.

Table 9 – Days for the acquired data and acquisition respective rates.

Rate	Day (n)
$2\ \mathrm{min}$	2, 26, 48, 57, 71, 89, 91, 105, 138, 139, 153, 166
$30\ \mathrm{s}$	200, 206, 216, 226, 260, 262, 281, 294, 310, 311, 337, 355

For the validation, the inputs of the algorithm corresponded to the conditions of the experimental setup. Immediately, the taken values for the location coordinates were $\phi = 38{,}77^o$, $L_{st} = 0^o$ and $L_{loc} = -9{,}18^o$. As it was mentioned before, the values for β changed throughout the year and $\gamma = 0^o$. The values of β are summarized in Table 10.

Table 10 – Values for $\boldsymbol{\beta}$ of the pyrheliometer and the set of pyranometers for different periods of the year.

Period (n)	β
$[2\,,57] \wedge [310\,,355]$	45^o
$[71\,,91] \wedge [260\,,294]$	40^o

$[105, 226]$	35^o

The value for the reflectivity of the ground (ρ) was harder to obtain, but it was assumed to be $\rho_g = 0.2$. This value was not determined in a rigorous way, but assuming a value within a certain range. Lopes [55] studied the effects of urban heat islands in the city of Lisbon and, in particular, used a range of values for the reflectivity of the ground and the surroundings to study this effect. The ground and the surroundings of urban areas tend to be composed by certain characteristic materials, thus for asphalt the reflectivity is situated in the range $0.05 - 0.20$, for concrete is situated between $0.10 - 0.35$ [55]. So, the assumed value for ρ was reached by taking into account the characteristics of these materials, since the concrete from the ground is darkened due to the usage.

For the hourly validation, four different days: $n =$ 105, 206, 281, 355 were chosen as representative of each season and are presented in Graphic 5, Graphic 6, Graphic 7 and Graphic 8, respectively. The four graphics present the hour irradiation curve as a function of the period of one hour (for example, the irradiation corresponding to 10h corresponds to the total irradiation value for the period from 9h to 10h). From the five presented curves in each graphic, three correspond to the models predictions and two to measurements: in blue, red and green, it is represented the predictions from the Isotropic Sky, HDKR and Perez models, respectively, and in yellow and grey, it is represented the data for hourly irradiation on a horizontal and on a tilted surface from LNEG, respectively. For the calculations regarding the three models, it was used as the input I, the hourly irradiation on a horizontal surface. The calculations from the models were afterwards compared with the measurements of the hourly irradiation on a tilted surface.

The experimental error of the hourly irradiation value for each day was obtained by using propagation of uncertainty. For the models used previously, the experimental input parameters are the ones that regard the location (Φ, L_{st} and L_{loc}), the orientation of the panel (β and γ), the hourly irradiation on a horizontal surface (I) and the reflectance of the ground (ρ_g). The parameters that regard the location and the orientation of the panels were assumed to have a negligible error, since they were given directly by LNEG and were not based in data acquisition. Therefore, the parameters that contributed mostly for the uncertainty of the measurements were I and ρ_g. Due to the lack of information of the equipment used to measure these values (pyranometers and pyrheliometers), it was not possible to obtain an exact value for the uncertainty in the measurement of I. Therefore, taking into account the characteristics of standard pyranometers and pyrheliometers, it was assumed a value of 2% for the uncertainty in the measurement of I. On the other hand, the value of ρ_g was not measured, but was assumed within a certain range of values. So, there is not an experimental error associated with this value, but an

uncertainty due to its subjective and less rigorous determination. Consequently, the chosen value for the uncertainty of ρ_g was of 50%.

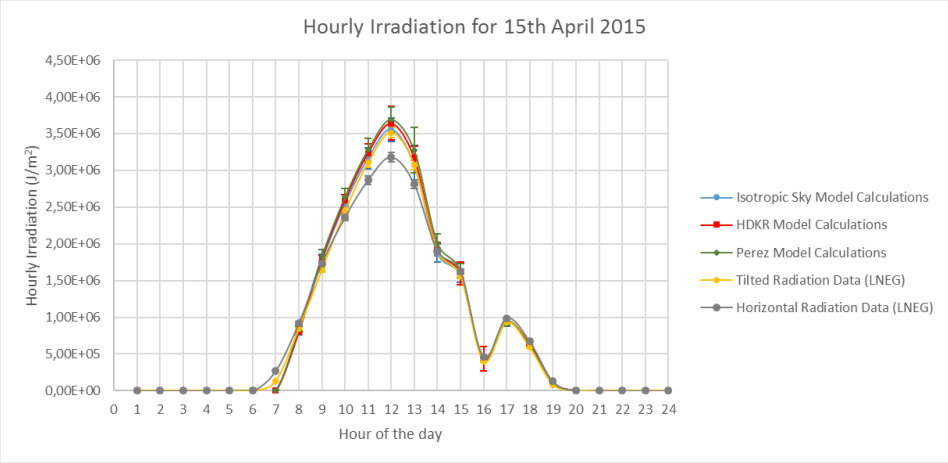

Graphic 5 - Hourly irradiation data and calculations for the 15th of April 2015 (Spring).

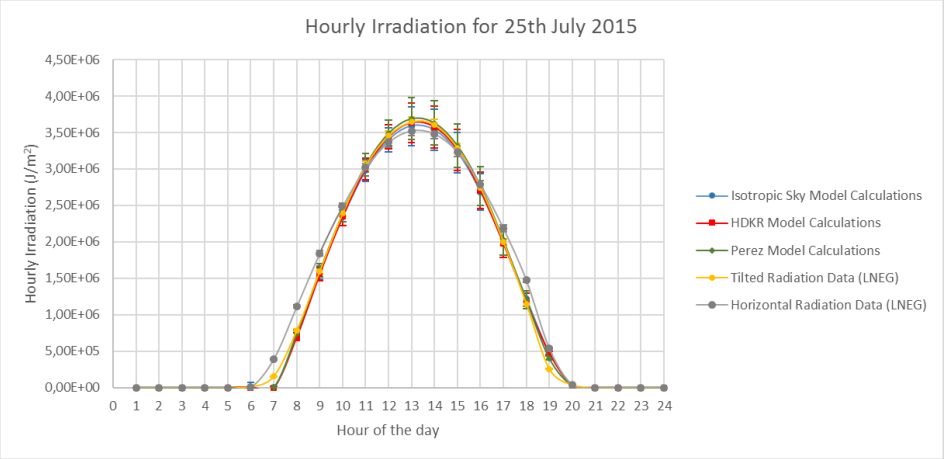

Graphic 6 - Hourly irradiation data and calculations for the 25th July 2015 (Summer).

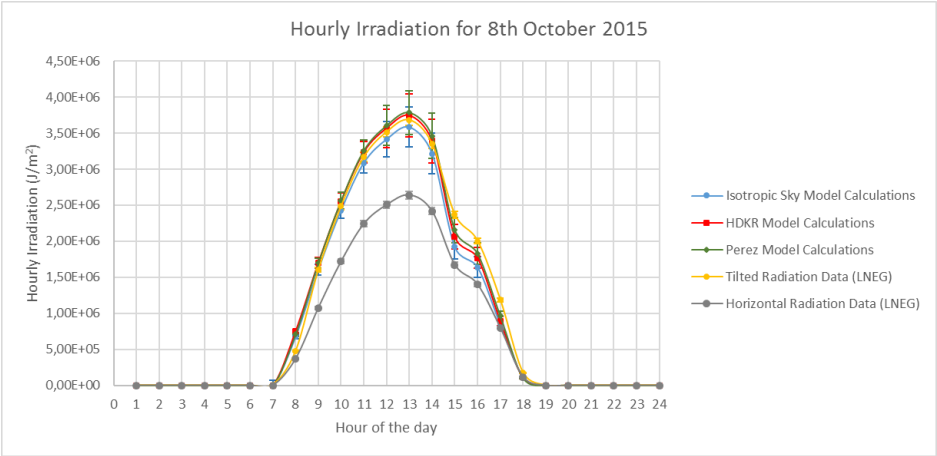

Graphic 7 - Hourly irradiation data and calculations for the 8th October 2015 (Autumn).

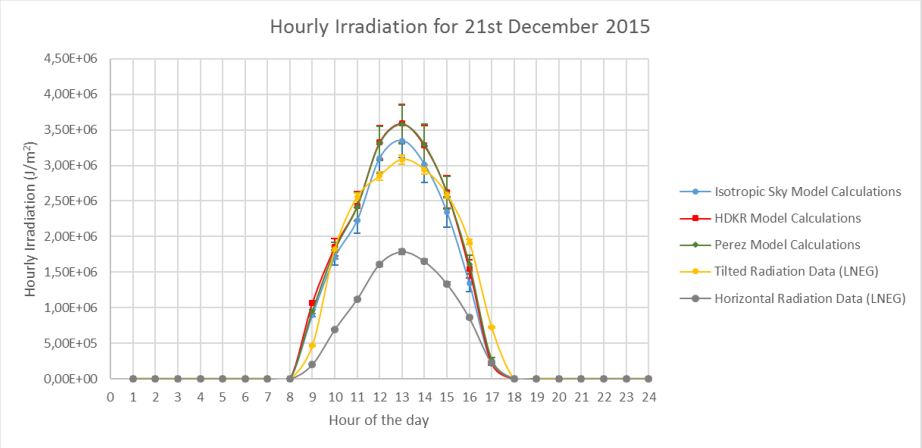

Graphic 8 - Hourly irradiation data and calculations for the 21th December 2015 (Winter).

From Graphic 5, Graphic 6 and Graphic 7, it is possible to observe that the three models are very adequate, since the error bars include the curve that represents the tilted surface radiation data from LNEG for each hour, with exception, in some cases for hours closer to sunrise and sunset, which will be discussed next. By analyzing the three graphics, it seems that the three models are close to the experimental result and it is difficult to distinguish which one is the most accurate. On the other hand, from Graphic 8, it is possible to observe that during the period of 12h to 14h, the HDKR and Perez models error bars do not include the curve for tilted surface, hence overestimating the result. However, for the remaining hours, it seems that these models are closer to the experimental result, with the exception, once again, of the hours closer to sunrise and sunset. Also, Graphic 8 represents a typical Winter day, which can be significantly cloudy, so it has to be treated differently.

As it was said before, for the hours close to sunrise and sunset and giving a special emphasis to Graphic 8, there is significant gap for the periods of 8h-9h and 16h-18h. The values of irradiation for those periods are very low which, in turn, complicate the determination of the diffuse and the beam components. In the hour that includes the sunset and the sunrise, the sun is very low in the sky and that means that θ_z is closer to 90^o and, consequently, from (A.1.2.1), comes that $R_b \rightarrow \infty$. This fact might introduce a significant overestimation of the beam radiation component contribution for the total radiation. The underestimation, in turn, might be due to different reasons. As it was said before, the sun is very close to the horizon and it is more likely to have objects or structures contributing to a shading effect, which can be specially reflected in the detection of beam radiation. Finally, for those hours, the expression that computes I_0, may return a negative or null value, which may not be the case of the value for I. In that case, the algorithm assumes that $I = 0$, and that might lead to an apparently different hour of sunrise or sunset, which can be observed in Graphic 5 and Graphic 6.

Only by observing the graphics, it is not possible to make a quantitative analysis of the error. In Table 11, for each season, it is presented the maximum hourly experimental error for each model.

Table 11 – Maximum hourly experimental error of the Isotropic Sky, HDKR and Perez Models for each season (Spr – spring; Sum – summer; Aut – autumn; Win – winter).

Experimental Error of I_T (%)												
	Isotropic Sky				HDKR				Perez			
Hour	Spr	Sum	Aut	Win	Spr	Sum	Aut	Win	Spr	Sum	Aut	Win
7	29.05	5.77	-	-	71.04	6.08	-	-	30.09	6.10	-	-
8	9.15	7.08	10.19	4.05	9.01	7.50	8.69	3.74	9.32	7.23	8.00	3.85
9	7.72	9.42	11.19	8.74	7.76	7.58	11.08	8.16	7.89	9.59	11.92	8.04
10	9.14	8.97	8.93	8.74	9.18	9.13	8.27	9.78	5.48	9.35	8.16	10.47
11	8.85	8.50	9.35	9.86	8.89	8.62	8.90	9.68	9.18	8.89	9.01	10.30
12	8.99	9.34	8.16	9.74	9.00	9.26	8.41	8.96	9.32	9.42	8.52	9.19
13	9.13	9.24	8.43	7.83	9.12	9.30	8.66	8.07	9.84	9.63	8.81	8.25
14	8.41	8.70	8.94	8.93	8.36	8.79	8.98	9.07	9.17	9.07	9.16	9.33
15	9.10	9.14	9.23	9.14	9.17	9.16	9.00	8.90	9.55	9.61	9.28	9.20
16	9.47	9.47	9.16	9.21	9.49	9.49	8.47	9.14	10.06	9.93	8.34	9.47
17	9.93	9.64	15.09	9.91	9.89	9.64	9.06	11.88	10.47	10.31	13.08	9.96
18	9.84	9.07	42.93	39.26	9.95	9.15	42.89	10.76	10.86	10.46	61.50	11.34
19	7.93	6.80	-	17.51	8.62	6.79	-	17.46	9.90	7.24	-	18.71
20	24.65	97.97	-	-	24.66	97.63	-	-	26.18	95.82	-	-
Mean	9.06	9.12	9.57	9.07	9.35	9.07	9.10	9.11	9.05	9.53	9.56	9.36
Tot.	9.21				9.16				9.38			

As it was expected, for most cases, the error increases for hours closer to sunrise or sunset. For the rest of the hours, the maximum experimental error is typically around 8% or 9%, which is quite satisfactory, which is close to the mean error for each model: 9.21%, 9.16% and 9.38%, respectively. It is also important to refer that the error might be slightly overestimated, since it was not possible to know the specifications of the data acquisition devices and therefore it was necessary to make an overestimation of the acquisition error and, finally, since the value for the reflectance of the ground is difficult to obtain, thus having a large error, which can also be overestimated.

In what regards the exactitude of each model, it was considered to be the deviation that the models have to the measurements of the radiation on a tilted surface. For each season, the exactitude of each model is presented in Table 12.

Table 12 - Exactitude of the Isotropic Sky, HDKR and Perez Models for each season (Spr – spring; Sum – summer; Aut – autumn; Win – winter).

Exactitude of I_T (%)												
	Isotropic Sky				HDKR				Perez			
Hour	Spr	Sum	Aut	Win	Spr	Sum	Aut	Win	Spr	Sum	Aut	Win
7	56.28	54.89	-	-	79.37	14.99	-	-	58.13	58.08	-	-
8	9.28	3.21	89.85	405.22	10.15	6.44	161,62	642.35	10.92	5.35	110.76	420.99
9	5.60	1.85	23.06	68.05	6.52	1.42	33.13	101.45	8.28	1.51	29.59	74.81
10	3.56	2.68	7.92	6.71	5.04	2.15	4.50	11.38	5.61	3.15	4.19	10.71
11	1.69	3.85	9.14	8.09	2.94	2.55	4.99	11.81	3.81	2.34	5.72	10.96
12	1.34	2.39	3.24	2.74	1.76	0.83	2.89	9.04	2.93	2.20	3.37	10.06
13	2.17	1.92	4.05	3.02	1.31	1.25	1.89	7.13	2.33	1.88	2.57	7.36
14	2.45	1.89	8.72	8.68	0.78	1.01	2.32	8.86	1.70	1.75	1.70	8.70
15	2.31	2.42	17.04	11.78	1.17	0.98	9.01	4.40	1.21	1.08	7.38	3.77
16	4.49	3.44	29.72	16.54	3.20	1.15	22.34	8.83	1.52	2.16	18.65	6.86
17	12.19	4.41	50.13	34.28	11.67	2.51	47.54	30.95	11.24	12.40	38.49	25.38
18	12.03	13.54	68.30	23.05	11.14	11.66	68.15	22.75	10.55	54.22	71.24	21.97
19	69.42	65.91	-	62.44	65.59	65.20	-	62.92	51.62	17.09	-	51.87
20	22.72	14.08	-	-	22.62	13.93	-	-	18.04	-	-	-
Mean	3.94	4.28	14.63	10.56	4.00	3.11	14.24	13.80	4.65	5.25	11.61	11.73
Tot.	8.36				8.79				8.31			

By analyzing Table 12, it is possible to check that the deviation has a similar behavior to the experimental error, due to similar reasons. Also, it is possible to conclude that, for the hours further from sunrise and sunset, the mean deviation is included in the maximum error and, in some cases, the error is significantly larger. This might be another indicator that the experimental error is overestimated.

From a seasonal perspective, by analyzing Table 12, it is attainable to conclude that the models make a better estimation for days closer to summer and that for days closer to winter, the deviation is bigger. This might be due to the fact that the models depend on the clearness index k_T. A bigger k_T means that there has not been much attenuation of radiation in the atmosphere, i.e. I is closer to I_0, which makes sense; in summer the clearness index must be higher, since the sky is clearer (therefore, there is less attenuation in atmosphere) and in winter the opposite is verified. This index also determines the fraction of I that is diffuse (I_d) and, when it has a significate weight (such as in winter), the models tend to make estimations with larger error, since they need to

recur to experimental correlations and not simply to solar radiation geometry or the characteristics of the environment. This factor is easily translated by the shape of the curves in the graphics. For instance, the shape of the curves of Graphic 6 is very regular, which means that the sky for that day was clear, as expected. For example, in Graphic 5, near 16h, there is a substantial drop, which might be due to a cloud or fog that obstructed the sun. In Graphic 7 and Graphic 8, there are no noteworthy drops, but the shape is much more irregular that what is observed in Graphic 5, which can translate once again the weather's unpredictable character. On the other hand, by evaluating the radiation on a horizontal surface, it is possible to observe that in summer (Graphic 6), it is really close to the one on a tilted surface, while in winter (Graphic 8) it is significantly smaller.

From an hourly perspective, it is reasonable to conclude that the error increases for lower values of irradiation, i.e. correspondent to hours closer to sunrise or sunset, as it was mentioned before. Despite this, the irradiation values for these periods of the day are considerably small when compared with the rest of the day, so the error is not really relevant. Also, for these hours, the panels will not produce enough useful energy for a household.

Comparing the three models, it is possible to take some conclusions. For hours closer to sunrise (7h-9h), Isotropic Sky model has the best results, while for hours closer to sunset (18h-20h), the Perez model has a lower deviation. For the period of 10h-14h, the HDKR model shows better results. For the remaining hours, Perez model has the best results overall. Finally, in order to evaluate which model is the most adequate, it was made a global average for all values, taking into account the contribution of the radiation of each hour for the global daily radiation. From Table 12, it was possible to get that the Isotropic Sky, the HDKR and the Perez models have a mean exactitude of 8.36%, 8.79% and 8.31%, respectively. Therefore, globally, the Perez model is the one that makes the better estimations. It is important to mention that the models were evaluated only by taking into account data from 24 representative days of the year, thus not forcibly corresponding to the whole year.

6.1.2. DAILY

The daily irradiation (H_T) validation was based on the study of the total irradiation incident on the panel throughout the day and is represented in Graphic 9. H_T was calculated as being $H_T = \sum_{h=1}^{24} I_T(h)$, where h corresponds to an hour. This validation is not as important in terms of direct estimation of the error of the models, but it was made to have a more global overview of the error and the seasonal features. For each day, it was made the sum of the hourly irradiation (I_T) for the whole 24h period for the three predictions - Isotropic Sky (blue), HDKR (red) and Perez (green) models - and for the data from LNEG - horizontal (yellow) and tilted (grey) surface.

The experimental error of the daily irradiation value for each day was obtained by using propagation of uncertainty and then converted to a relative error (in %).

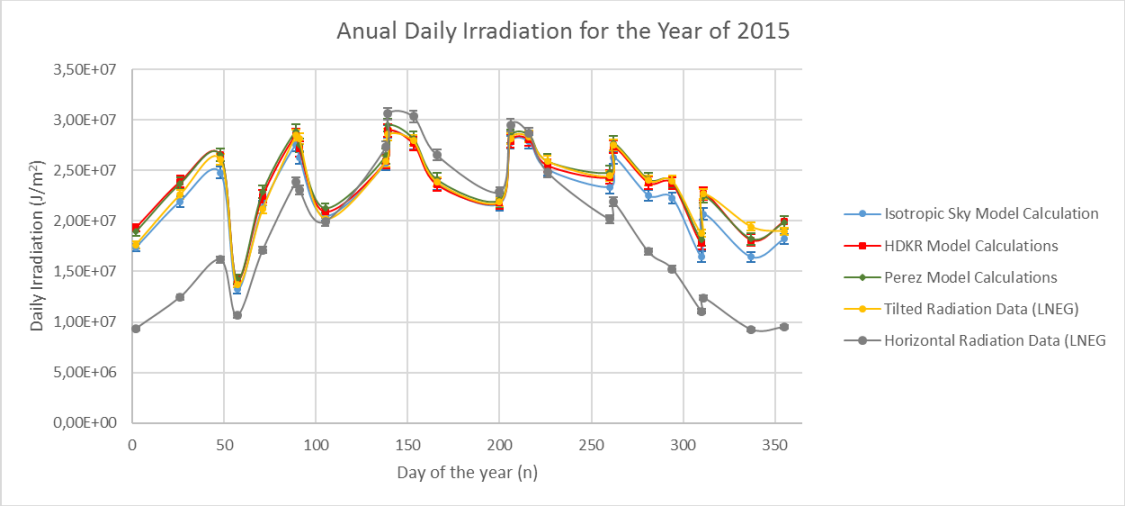

Graphic 9 - Daily irradiation data and calculations for the year of 2015.

By analyzing Graphic 9, it is possible to have a more global overview of the behavior of the irradiation throughout the year. It is possible to observe that the curves obtained from the estimations of the models fit very well for days closer to summer and diverge more for months closer to winter, which is can be realized by taking into account the error bars. In fact, for days closer to summer, the error bars include the experimental data. It is also possible to observe that the HDKR and Perez models slightly overestimate the values for daily irradiation, while for Isotropic Sky model, a slight underestimation is observed. It is also interesting to observe that for Summer, approximately between $n = 150$ and $n = 225$, the total daily irradiation on a horizontal surface surpasses the daily total irradiation on a tilted surface. This confirms that the irradiation incident on a horizontal surface is higher than the one on a tilted surface during summer so, it pays off to have the panel placed horizontally during this season. For months closer to winter, it can also be observed that the total daily irradiation on a horizontal surface is significantly smaller than the daily total irradiation on a tilted surface.

Table 13 - Experimental error of the daily irradiation estimations from the Isotropic Sky, HDKR and Perez models.

Experimental Error of H_T (%)			
Day (n)	**Isotropic Sky**	**HDKR**	**Perez**
2	2.18	2.07	2.14
26	2.44	2.40	2.47
48	2.36	2.31	2.37
57	3.33	3.26	3.32
71	2.80	2.81	2.88

89	2.30	2.28	2.35
91	2.33	2.92	2.39
105	2.05	2.04	2.11
138	2.68	2.72	2.84
139	2.10	2.11	2.18
153	2.32	2.34	2.41
166	2.62	2.64	2.77
200	2.93	2.94	3.09
206	2.33	2.34	2.42
216	2.31	2.32	2.41
226	2.44	2.46	2.55
260	2.71	2.72	2.80
262	2.37	2.39	2.44
281	2.46	3.33	2.50
294	2.38	2.39	2.45
310	3.33	3.33	3.34
311	2.83	2.81	2.89
337	3.16	3.12	3.18
355	2.87	2.90	2.93
Mean	2.57	2.62	2.63

To make a quantitative analysis, the experimental error for each model is presented in Table 13. In it, it is possible to perceive that the experimental error is quite constant throughout the year, being always placed between 2% and 4%, thus not being observed a significant seasonal behavior in terms of experimental error.

Once again, in order to evaluate the deviation of each model, the respective exactitude was calculated. Once again, it corresponded to the deviation of the sum of the hourly values throughout day of each model to the sum of the hourly values throughout the day of the irradiation on a titled surface data. This estimation is assembled in Table 14.

Table 14 - Exactitude of the daily irradiation estimations from the Isotropic Sky, HDKR and Perez models.

Exactitude of H_T (%)			
Day (n)	**Isotropic Sky**	**HDKR**	**Perez**
2	1.55	9.50	7.40
26	3.02	5.61	4.83
48	5.19	1.49	1.51
57	3.03	3.46	3.91

71	1.02	6.02	8.22
89	3.27	0.16	1.53
91	6.62	3.58	2.32
105	1.18	3.31	5.24
138	0.62	0.11	1.97
139	1.02	1.28	3.17
153	0.83	1.03	0.77
166	0.74	1.13	1.05
200	0.83	0.21	0.92
206	1.35	0.91	0.77
216	1.77	0.94	0.75
226	3.24	1.70	0.06
260	4.51	0.48	1.46
262	4.53	0.72	0.57
281	6.21	0.98	0.47
294	7.15	1.20	0.26
310	12.43	5.24	3.28
311	8.79	0.10	0.86
337	15.51	6.94	6.12
355	3.97	5.15	4.69
Mean	4.10	2.55	2.59

By analyzing Table 14, it is possible to take similar conclusions to the ones taken with the analysis made for the hourly data. From a seasonal perspective, it is clear that the deviation is smaller for days closer to summer and is higher for days closer to winter. This is due to the factors mentioned in the hourly analysis of the exactitude of the three models and legitimates the analysis of Graphic 9. In fact, especially for summer, the deviation usually ranges from 0% to 2%, which is smaller than the experimental error for the same period. On the other hand, for days closer to winter, the deviation can be higher than 4%, which is, in some cases, higher than the experimental error.

Comparing the three models, it is possible to conclude that, generally, the Isotropic Sky model is the one that has a larger deviation, having the highest deviation of 15.51% for $n = 337$. On the other hand, the Perez model seems to be the more accurate, usually with deviations between 0% and 2% and with a maximum deviation of 8.22% for $n = 71$. The HDKR model, in turn, appears to be more accurate than the Isotropic Sky and similar to the Perez model. In fact, with this approach, it is possible to get that the Isotropic Sky, the HDKR and the Perez models have a daily mean exactitude of 4.10%, 2.55% and 2.59%, respectively. In fact, by taking these mean values, it possible to see that the deviation of Isotropic Sky model is higher than the experimental error.

With the daily analysis, it is possible to have a clearer overview of the seasonal nature of the exactitude of the three models.

6.2. PV PRODUCTION 3P MODEL EVALUATION

The models for PV production were tested using the experimental setup located in FCUL, as described in **3.2**. The system collected data for every day from January throughout May 2015. For this validation, representative data from two days from different months was chosen from the available one, corresponding to $n = 72$ (13th March) and $n = 132$ (18th May). As it was mentioned before, the data was acquired in periods of 15 minutes and afterwards averaged for each hour. The data from the system includes values of G on the plane of the panels, I_{max} and V_{max} (before the inverter).

It is important to refer that the meteorological station that measured the irradiation is located at a distance of about 70 m, 100 m and 130 m of the three buildings which rooftops have the PV modules, respectively. This way, the values of G were not measured exactly on the site of the PV modules. On the other hand, as it was described in **2.2.7**, the value of G cannot be used directly, but G_{eff} was used instead. As it was not possible to go to system's site and since it belonged to a university and not to a domestic user, it was assumed that the dirtiness degree was low, which corresponds to $T_{B_{dirt}}(0^o)/T_{B_{clean}}(0^o) = 0.98$ and $a_r = 0.20$. However, the data for G is total irradiance for a tilted surface, thus being impossible to discriminate each component and, also, (2.2.7.3) is only applicable to the beam and the circumsolar diffuse components. Since this was the only available data, (2.2.7.3) was applied to the total irradiance G in order to obtain G_{eff}, and the validity of this assumption was afterwards evaluated.

The ambient temperature T was measured in EMA in IST, which is located about 3 km away from the PV system. However, there are not known significant microclimate effects in the city of Lisbon so, the whole city usually has the same ambient temperature. This way, it was assumed that the values measured by EMA corresponded, with a good degree of confidence, to the ones experienced in the PV system's site.

For the validation, the inputs for the algorithm were the characteristic parameters of the PV models in STC, which are described in Table 4 and the hourly values of G_{eff} from FCUL's meteorological station and of T from the measurements of the EMA. The experimental error was calculated by using propagation of uncertainty. Since, it was not possible to get to the specifications of the respective equipment, it was assumed that the error for the irradiance was, once again, of 2% and for the ambient temperature of $0.1^{\mathrm{o}}\mathrm{C}$.

6.2.1. DATA SET 1 (13th MARCH)

For the first evaluation using data from the FCUL system, it possible to observe the effective irradiance on the panels' plane and temperature profiles in Graphic 10 and the experimental and predicted values by the 3P model for I_{max}, V_{max} and P_{max} in Graphic 11, Graphic 12 and Graphic 13, respectively.

By looking at Graphic 10, it is possible to get that the irradiance profile is similar to the one of a clear sky day. Also, the ambient temperature profile is quite regular, with values that range from $11^{o}\mathrm{C}$ to $17^{o}\mathrm{C}$.

By analyzing Graphic 11, it is possible to observe, as it was expected, that the profiles of I_{max} have a shape similar to the irradiation profile. It is also possible to attain that for the hours close to the beginning and the middle of the day, the model overestimates the value for I_{max} and the error does not include the experimental data. On the other hand, by the end of the day, this tendency inverts, being observed an underestimation of the model. Only for the periods of 16h and 17h, the error bars overlap the experimental curve. Also, both curves seem to have different sunset hours.

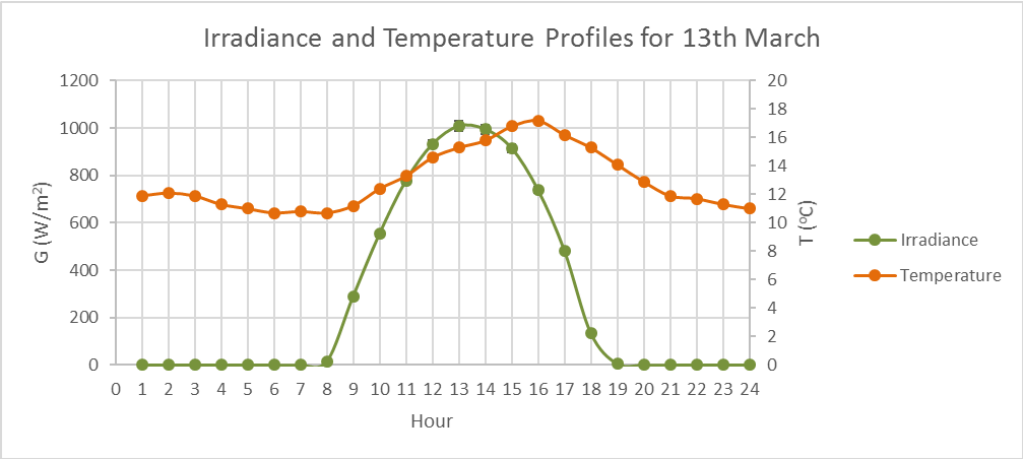

Graphic 10 – Mean hourly irradiance (green) and mean hourly ambient temperature (orange) for the 13th March 2015.

By analyzing Graphic 12, it is possible to observe, as it was expected, that the profiles of V_{max} have a well-defined baseline. However, this baseline presents a slight curvature on the experimental curve, which may be due to a temperature effect on the equipment in the hours of higher irradiance and ambient temperature. Nevertheless, the error bars include the experimental data in the baseline region of the graphic. Also, the model apparently makes an overestimation at the beginning of the day and an underestimation at the end of the day. This underestimation also coincides with the difference between the sunset hours observed in Graphic 11.

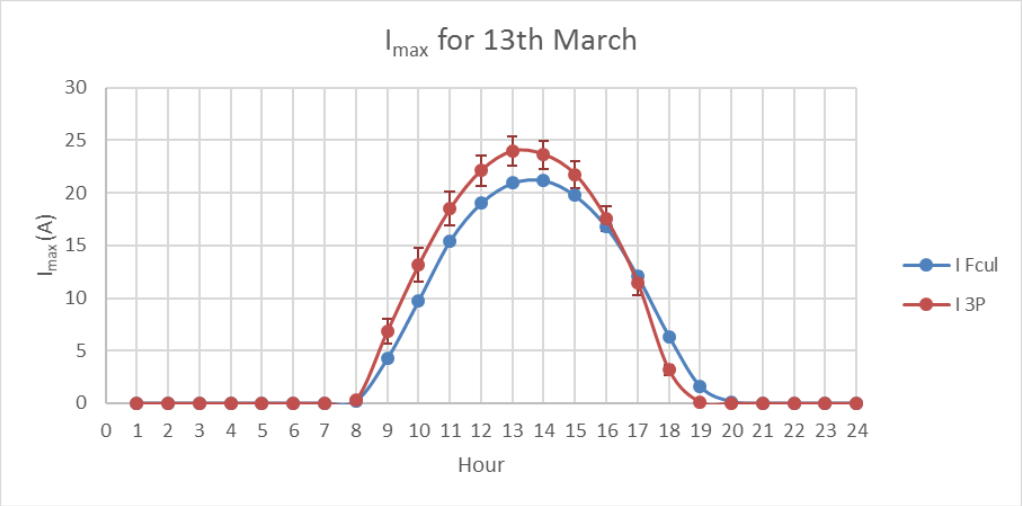

Graphic 11 - $\boldsymbol{I_{max}}$ experimental data (blue) and $\boldsymbol{I_{max}}$ calculations (red) for the 13th March 2015.

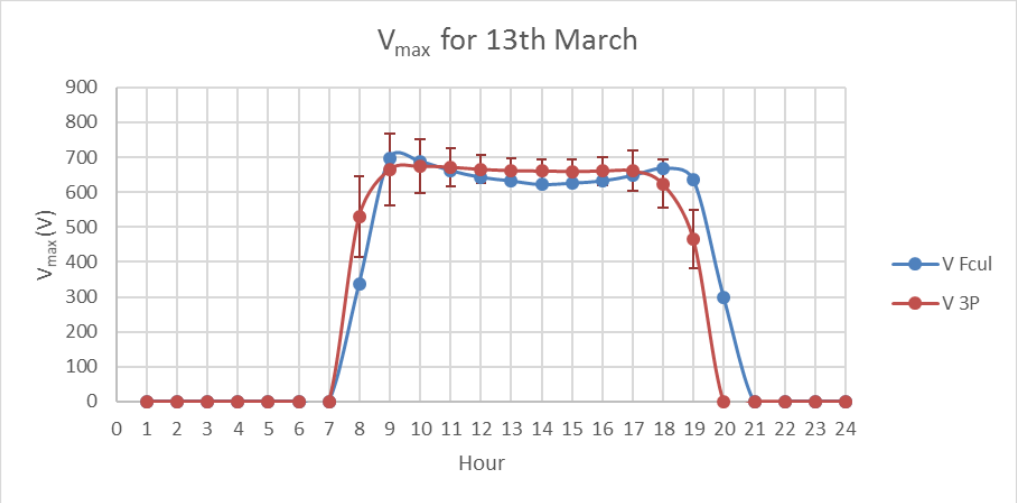

Graphic 12 - $\boldsymbol{V_{max}}$ experimental data (blue) and $\boldsymbol{V_{max}}$ calculations (red) for the 13th March 2015.

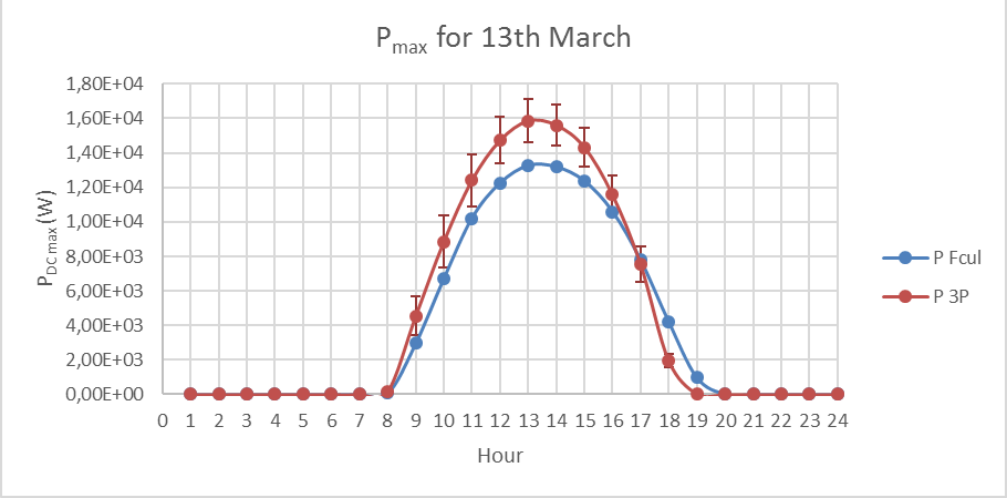

Graphic 13 - $\boldsymbol{P_{max}}$ experimental data (blue) and $\boldsymbol{P_{max}}$ calculations (red) for the 13th March 2015.

By analyzing Graphic 13, it is possible to get that the profiles have a shape similar to the ones of the irradiance in Graphic 10 and to the ones presented in Graphic 11. Nevertheless, it is important to refer that the model overestimates the maximum power output of the system and that the error bars, for most points, do not include the experimental curve. For this day, the mean efficiency of the system was of $\eta = (13.91 \pm 2.15)\%$, which includes the one specified by the manufacturer of $\eta = 14.90\ \%$. This corresponds to a deviation of 6.64%.

A quantitative and more detailed analysis of the experimental error is discriminated in Table 15.

Table 15 - Experimental error of the hourly PV production important parameters using the 3P model for the 13th March 2015.

Experimental error of I_{max}, V_{max} and P_{max} (%)			
Hour (h)	I_{max}	V_{max}	P_{max}
8	36.55	21.94	54.31
9	17.73	15.27	25.10
10	12.17	11.30	17.06
11	8.76	8.19	12.17
12	6.64	6.08	9.10
13	5.80	5.21	7.86
14	5.70	5.10	7.72
15	5.84	5.22	7.92
16	6.89	6.24	9.46
17	9.72	8.70	13.56
18	14.27	11.11	20.31
19	60.22	17.94	97.36
Mean	8.40	9.41	11.85

As it was expected, the error increases for hours closer to sunrise or sunset, since the values of irradiance are significantly low. I_{max} and V_{max} have errors with similar magnitude (although V_{max} being always inferior), except for sunrise and sunset, where there is a greater discrepancy. The error of P_{max} is higher, as it would be expected, since it depends directly on the two previous ones. In a similar way as it was described in **6.1**, the error might be slightly overestimated because, since there was no information about the equipment that measured the irradiance, it was taken the value of 2% as the upper bound of its error. Despite this, the mean error of each of the three parameters appears to be reasonable and, in particular, for values closer to midday.

To assess the deviation of the predictions made by the model to the experimental values, the exactitude was calculated, in a similar way as in **6.1**. For each of the parameters, the deviation is presented in Table 16.

Table 16 - Exactitude of the hourly PV production important parameters using the 3P model for the 13th March 2015.

Exactitude of I_{max}, V_{max} and P_{max} (%)			
Hour (h)	I_{max}	V_{max}	P_{max}
8	66.18	57.41	161.59
9	61.14	4.68	53.60
10	34.75	2.00	32.06
11	19.76	1.48	21.53
12	16.14	3.59	20.30
13	14.33	4.66	19.67
14	11.49	6.29	18.51
15	10.03	5.38	15.95
16	4.52	4.51	9.24
17	5.16	2.08	3.18
18	50.11	6.55	53.37
19	92.24	26.76	94.31
Mean	16.99	9.21	20.37

By looking at Table 16, it is possible to get that, in some way, the exactitude has a similar behavior when compared with the experimental error, since it is higher for hours close to sunrise and sunset and lower for hours close to the middle of the day. In the case of I_{max} and P_{max}, the deviation is higher than the experimental error for most of the hours, which is also true for the mean values. This might indicate that the experimental error of I_{max} is underestimated or the 3P model is not the most adequate. In what regards V_{max}, the opposite is verified, the deviation is lower than the experimental error for most of the hours but, the mean values are close, being the deviation is slightly higher than the experimental error. Despite this, it is important to refer that, for these three parameters, the deviation is always less than the mean deviation for the hours closer to the middle of the day, which are also the most relevant hours in terms of electric energy production of the PV systems.

Taking into account the contribution of each hour for the total daily electric production, it is possible to get a mean value for the exactitude of each parameter. For the 13th of March 2015, I_{max} has a mean exactitude 16.99%, V_{max} of 9.21% and P_{max} of 20.37%.

As mentioned in **6.2**, the values of G_{eff} were calculated by using (2.2.6.3), which is an expression not used for total radiation attenuation, as a correction for the real incident irradiance. Therefore, to assess the legitimacy of the usage of this equation, all the previous calculations for the hourly values of I_{max}, V_{max} and P_{max} were repeated without using this correction. For the same day, it

was obtained a mean exactitude of 21.58% for I_{max}, 9.19% for V_{max} and 25.57% for P_{max}. The deviation of V_{max} with and without the correction are practically the same. The deviation of I_{max} and P_{max} is higher with the correction and therefore, it is possible to conclude that the usage of this correction was more adequate than assuming that there was no attenuation of the radiation.

6.2.2. DATA SET 2 (18th MAY)

The second data set corresponded to the 18th May. The effective irradiance on the panels' plane and temperature profiles are represented in Graphic 14 and the experimental and predicted by the 3P model values for I_{max}, V_{max} and P_{max} in Graphic 15, Graphic 16, Graphic 12 and Graphic 17, respectively.

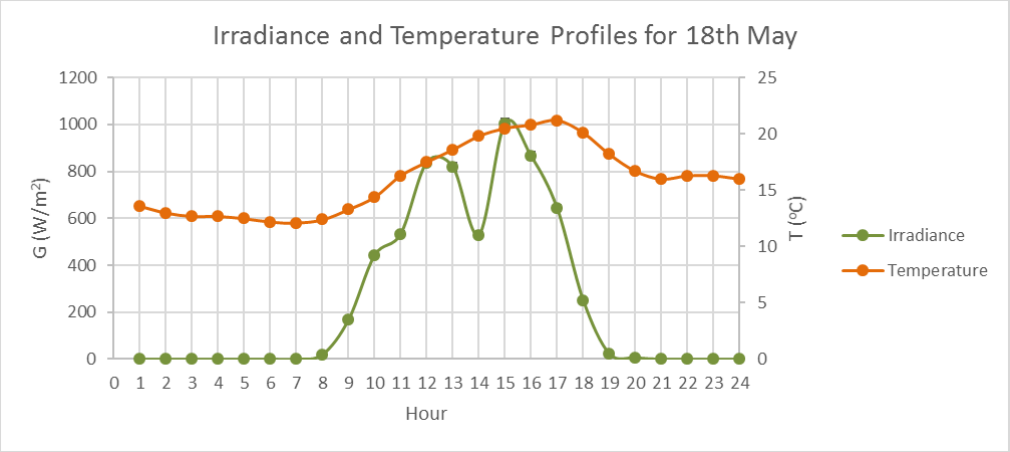

Graphic 14 - Mean hourly irradiance (green) and mean hourly ambient temperature (orange) for the 18th May 2015.

By looking to Graphic 14, it is clear to attain that the irradiance profile does not correspond to the one of a clear sky day. The graphic presents a rough shape and for the period of 14h, there is verified a substantial drop, which could be due to a cloud passing by or due to mist. The temperature profile is also regular with a range of temperatures from $12^{o}C$ to $21^{o}C$.

As it would be expected, the profiles presented in Graphic 15 have a shape similar to the irradiance profile presented in Graphic 14. In this case, the experimental curve and the curve that results from the model's predictions are quite similar, but there is an apparent hourly displacement. This was not this evident for the curves presented in Graphic 11, so it is not likely to be due to an error in the clock calibration. This displacement might be due to the fact that the meteorological station and the PV system are not in the same location (Figure 3). If the drop correspondent to the one observed in Graphic 14 was due to a cloud or mist, then the meteorological station would have detected it at the same time as the PV system, since they are not that far from each other. This way, the drop might be due to some shading effect that had not been taken into account. This could also explain the discrepancy of the values near the sunset. If one ignores the hourly displacement, the model seems to adjust to the experimental curve, at

least in what regards absolute values and respective error bar. For this day, there seems that there was no overestimation.

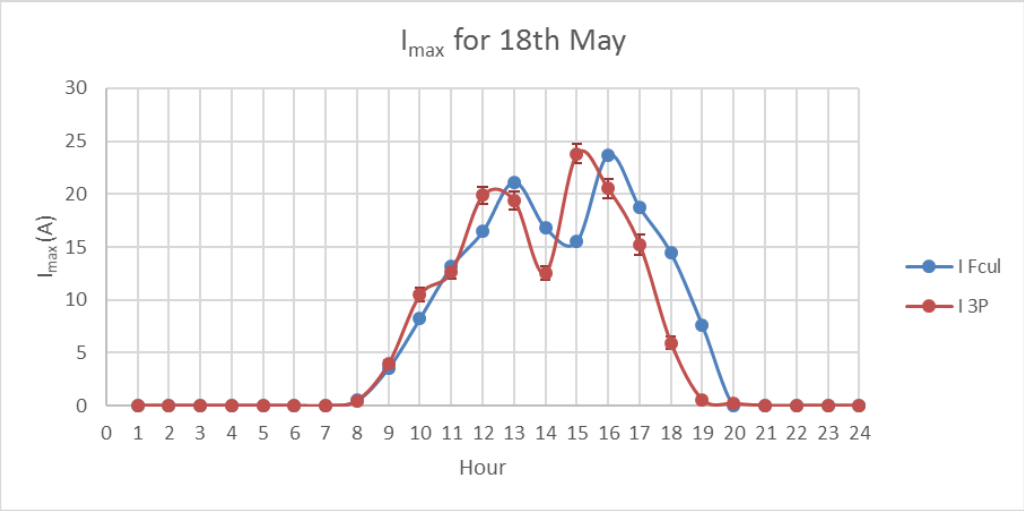

Graphic 15 - $\boldsymbol{I_{max}}$ experimental data (blue) and $\boldsymbol{I_{max}}$ calculations (red) for the 18th May 2015.

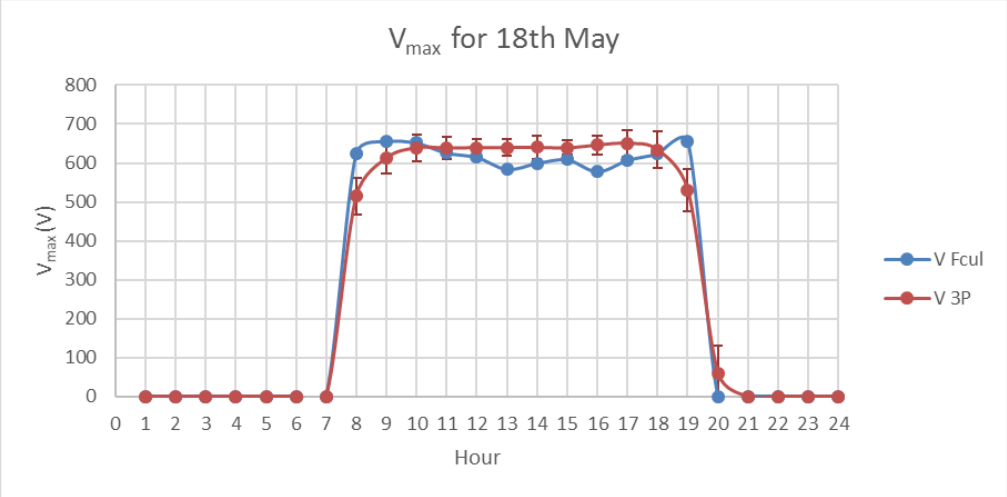

Graphic 16 - $\boldsymbol{V_{max}}$ experimental data (blue) and $\boldsymbol{V_{max}}$ calculations (red) for the 18th May 2015.

In what regards Graphic 16, the same conclusions might be taken as for Graphic 12, with the exception that for some points in the baseline region, the error bars do not include the experimental curve. In the experimental curve, the baseline is also slightly rougher than the one observed in Graphic 12 and the minor peak observable at 15h coincides with the sudden drop in the radiation curve represented in Graphic 14. Once again, since V_{max} does not depend on I_{max}, this might be due to a temperature effect on the system, in particular in the PV cells during the hours of different irradiance levels and ambient temperature.

By analyzing Graphic 17, it is possible to attain that the profiles have a shape similar to the ones of the irradiance in Graphic 14 and the same behavior as the ones presented in Graphic 15. For

this day, the obtained mean efficiency of the system was of $\eta = (13.33 \pm 1.71)\%$, which still includes the one specified by the manufacturer, but has a higher deviation of 10.55% when compared to the test made March 13th.

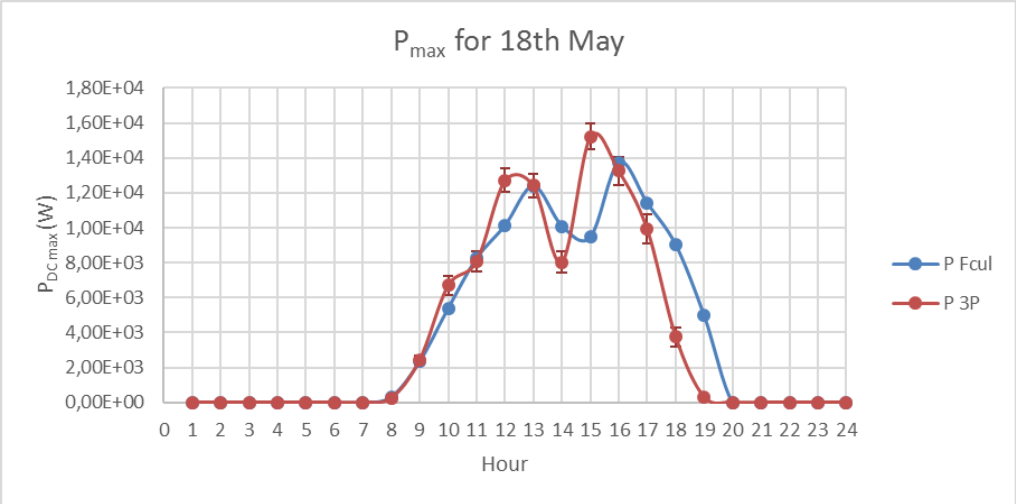

Graphic 17 - P_{max} experimental data (blue) and P_{max} calculations (red) for the 18th May 2015.

In a similar way as it was made in **6.2.1**, the experimental error is discriminated in Table 17 for a quantitative and more detailed analysis of the model and evaluation on of its limitations.

Table 17 - Experimental error of the hourly PV production important parameters using the 3P model for the 18th May 2015.

Experimental error of I_{max}, V_{max} and P_{max} (%)			
Hour (h)	I_{max}	V_{max}	P_{max}
8	12.50	9.25	17.94
9	7.45	6.43	10.32
10	6.02	5.32	8.20
11	5.24	4.59	7.05
12	4.14	3.36	5.38
13	4.22	3.47	5.51
14	5.40	4.80	7.30
15	3.80	2.92	4.84
16	4.65	3.85	6.14
17	6.19	5.21	8.41
18	10.13	7.54	14.22
19	37.96	10.25	59.85
20	-	-	-
Mean	7.00	5.64	10.06

By analyzing Table 17, it is possible to take similar conclusions to the ones taken for By analyzing Graphic 13, it is possible to get that the profiles have a shape similar to the ones of the irradiance in Graphic 10 and to the ones presented in Graphic 11. Nevertheless, it is important to refer that the model overestimates the maximum power output of the system and that the error bars, for most points, do not include the experimental curve. For this day, the mean efficiency of the system was of $\eta = (13.91 \pm 2.15)\%$, which includes the one specified by the manufacturer of $\eta = 14.90\ \%$. This corresponds to a deviation of 6.64%.

A quantitative and more detailed analysis of the experimental error is discriminated in Table 15.

Table 15, since the behavior of the experimental error has the same character. The only major difference is the fact that the absolute value of the error for each of the parameters is significantly smaller than the one for the test of March 13th. This is due to the fact that the month of May is closer to summer, which implies that the values of T and G are higher and, subsequently, the production of the PV module is higher and the experimental has a lower weight. It is also important to refer that the period correspondent to 20h is represented the way it is on the table, since there were available measurements of T and G (which enabled calculations), but not of I_{max} and V_{max}.

The deviation of the predictions made by the models to the experimental measurements was calculated in a similar way as described in **6.2.1** and is presented in Table 18.

Table 18 - Exactitude of the hourly PV production important parameters using the 3P model for the 13th March 2015.

Exactitude of I_{max}, V_{max} and P_{max} (%)			
Hour (h)	I_{max}	V_{max}	P_{max}
8	11.46	17.69	27.12
9	10.59	6.52	3.38
10	26.93	1.94	24.47
11	3.93	2.00	2.02
12	20.84	3.94	25.59
13	8.28	9.49	0.43
14	25.44	6.78	20.39
15	53.49	4.90	61.01
16	13.52	11.75	3.36
17	18.75	7.07	13.00
18	59.00	1.47	58.40
19	92.73	19.04	94.11
20	-	-	-
Mean	24.12	7.33	21.91

By looking at Table 18, it is not possible to take the same conclusions as the ones taken for Table 16. The deviation does not present a regular pattern. This might be due to the fact that the curves from Graphic 15, Graphic 16 and Graphic 17 have a rougher character than the ones presented in Graphic 11, Graphic 12 and Graphic 13.

Comparing the values presented in Table 17 and Table 18, it is possible to get that, for higher deviations the error bars of the predictions clearly do not include the experimental curve. But, it is possible to see that the curves have a very similar shape and amplitude and that they have some hourly displacement, thus for each hour, the deviation is higher. The best way to explain this, is the fact that this displacement might be due to a shadowing effect. In Figure 3, it is possible to observe that the meteorological station is not in the same site as the PV system and, also, that there are buildings, in particular the building southwest to the meteorological station. The shadow of this building might explain the results:

- In the morning, the meteorological station measures higher values of irradiance than the system, hence the model makes an overestimation as observed in Graphic 11 and Graphic 13;
- In the evening, the building overshadows the meteorological station and, therefore, the model makes an underestimation, as it can be also observed in Graphic 11 and Graphic 13;
- In months closer to Summer (like May) the sunset hour angle is higher, and therefore, due to sun's rotation, the shadowing effects on the meteorological station and on the PV system are more pronounced and occur in different hours, which explains the apparent hourly displacement in Graphic 14 and Graphic 16.

Due to the shadowing effect, any detailed numerical analysis may not be sufficiently reliable. Nevertheless, in a similar way as in **6.1.1**, the mean deviations were calculated for the 18th May 2015. The mean deviation obtained for I_{max} was of 24.12%, for V_{max} of 7.33% and for P_{max} of 21.91%. The deviations for I_{max} and for P_{max} are higher for this day, but this does not exactly mean that the results are worse. By observing Graphic 15 and Graphic 17, it is possible to attain that the absolute values from the measurements and from the predictions have the same magnitude, thus this suggests that there was no overestimation and that there was only the displacement due to the shadowing effect. The fact that the mean deviation of V_{max} was lower confirms this hypothesis.

Once again, the calculations for the mean deviations were made for the case with no attenuation and the values obtained were of 24.08% for I_{max}, 6.53% for V_{max} and 22.40% for P_{max}. In this case, I_{max} has a similar deviation, V_{max} a lower one and P_{max} a higher one. It is difficult to take some conclusions based on these values, due to the problem stated above.

6.3. ENERGY MANAGEMENT ALGORITHM TESTS

This subchapter is dedicated to the presentation and analysis of the results from the energy management algorithm presented in **5**. In the next subsubchapters, three different analyzes are presented in order to assess the influence of each approach/parameter choice. The first one concerns the evaluation of the algorithms described in **5.1.1** and **5.1.2**, while the second one the algorithms described in **5.2.1** and **5.2.2**, respectively. This evaluation was made for the same conditions (same day of the year and same initial SOC). In the third one, the hourly and daily algorithms are compared in order to evaluate which one has the best results. The fourth one refers to the influence of the initial SOC in the energy management process, varying this parameter in the same algorithm as chosen before and for the same day. The fifth one concerns the seasonal and type of day – Summer weekday and day off and Winter weekday and day off - influence in the results, for the chosen algorithm with the best results, assuming the same initial SOC.

It will also be assumed, for each of the analyses, that the temperature of the water inside the thermal accumulator at the beginning of the day is $T = 20^{\circ}\mathrm{C}$ *i.e*, the water is at the same temperature as the one from the grid, in opposition to what was considered for the SOC. This assumption is due to the fact that the thermal accumulator is the main load and the system was designed to suppress its energetic needs. In the case of the battery, there were made tests for different initial values of SOC to assess how the system would consider the batteries as a load or as a source.

6.3.1. ALGORITHMS A AND B EVALUATION (HOURLY)

The two hourly - A and B, described in **5.1.1** and **5.1.2**, respectively. - and the two daily - C and D, described in **5.2.1** and **5.2.2**, respectively - codes were tested for the same conditions: 13th June (Summer Weekday) and initial $SOC = 25\%, 75\%$ and 100%, respectively. In Graphic 18 and Graphic 19, there are represented the results for the different algorithms for the chosen day and for a $SOC_i = 75\%$, since it is the condition for which the batteries of the system can be charged and/or discharged.

By looking at Graphic 18, it is possible to get that most of the used energy comes from the grid (yellow and red) and, since the algorithm optimizes the usage at each hour and starts at $h = 1$, most of the energy is allocated at the beginning of the day or immediately after the usage of the thermal accumulator. Since the algorithm optimizes firstly the thermal accumulator and only afterwards the batteries system, it is possible to get that the system only charges the batteries (red) after the thermal accumulator is optimized. Also, it is possible to get that little PV energy is used to charge the batteries (blue) and the thermal accumulator (green), which might indicate that this type of energy is misused or underused. The peak of PV production is during the 11h-15h period and, in this case, the system only uses it during the 8h-10h period, thus not taking advantage of the peak of production. Also, the blue bars are inexistent in this case, which

indicates that the batteries are fully charged during the most intense sunshine hours. Finally, the energy used from the batteries to the thermal accumulator (brown), being the one with the highest $LCOE$, is very small and is only used as a backup. With this algorithm, the thermal accumulator always works at the maximum power of $2\,\mathrm{kW}$ (except when the water reaches the DHW temperature) and when the grid or PV limits are bellow this value, the system uses the batteries system.

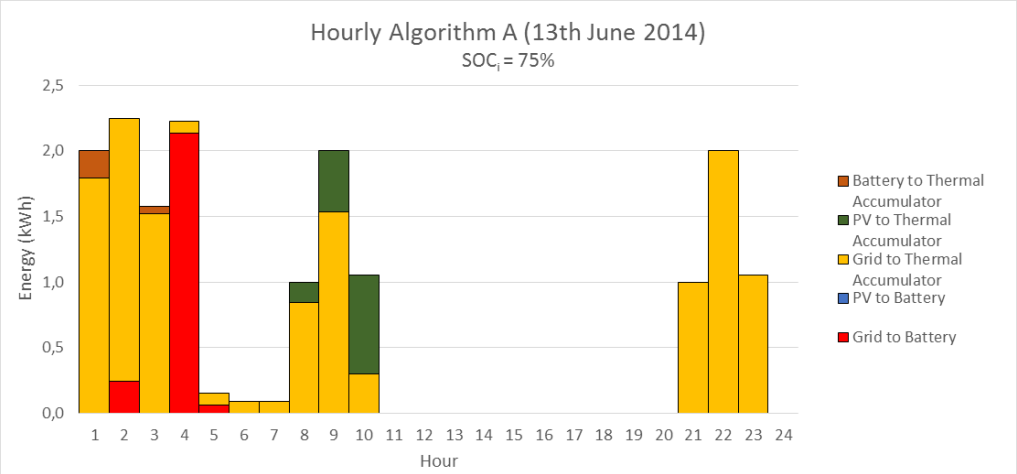

Graphic 18 – Hourly algorithm A results for the 13th June 2014 and $\boldsymbol{SOC_i = 75\%}$.

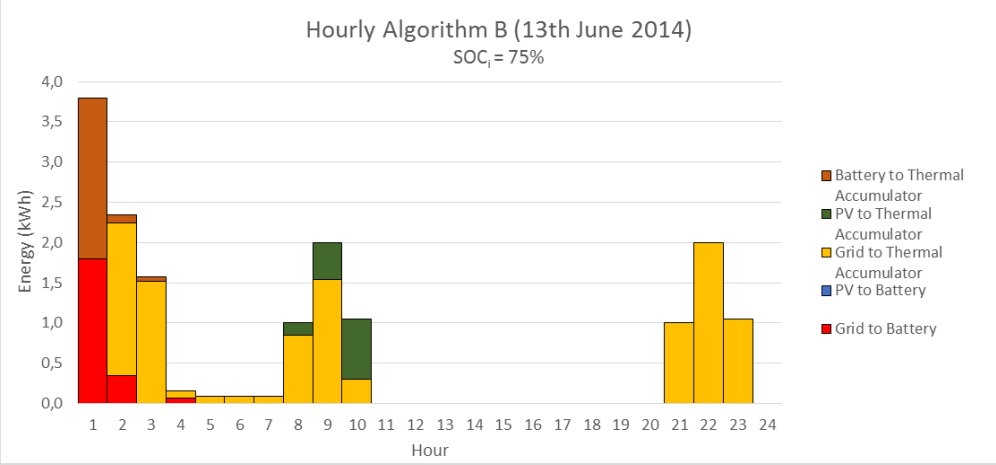

Graphic 19 - Hourly algorithm B results for the 13th June 2014 and $\boldsymbol{SOC_i = 75\%}$.

The results from the hourly algorithm B presented in Graphic 19 are quite similar to the ones presented in Graphic 18. The main difference is that the algorithm charges the batteries first and only afterwards transfers energy to the thermal accumulator. But, by doing this, it is possible to get that in $h = 1$, the batteries are charged in the first optimization (batteries optimization) and are discharged in the second one (thermal accumulator optimization). By firstly powering the batteries, the available energy increases, which is afterwards used by the second optimization, where the algorithm has more available energy in the batteries to power the thermal accumulator.

This is not a satisfactory result, because the optimization process is divided in two steps. The best solution would certainly be to bypass the batteries and to charge the thermal accumulator directly from the grid. This would increase the efficiency of the process and decrease the associated energy cost. The rest of the conclusions are the same as those for the previous case.

6.3.2. ALGORITHMS C AND D EVALUATION (DAILY)

The two daily algorithms - C and D, described in **5.2.1** and **5.2.2**, respectively - were tested for the same conditions as in **6.3.1**: 13th June (Summer Weekday) and initial $SOC = 40\%, 75\%$ and 100%, respectively. In Graphic 20 and Graphic 21, there are represented the results for the different algorithms for the chosen day and for $SOC_i = 75\%$.

Graphic 20 represents the daily algorithm C results and, by looking at it, it is possible to attain that the shape of graphic is quite different than Graphic 18 and Graphic 19. The energy is distributed throughout all day and the algorithm seems to maximize the usage of the PV energy (as it is possible to notice in the blue and green vertical bars). From $h = 9$ to $h = 19$, the system uses PV energy (with the lowest $LCOE$) to power the thermal accumulator (in green) for the DWH demand period of $h = 20$. But, since it is also necessary to deliver energy to thermal accumulator for the DWH demand period of $h = 8$, the system recurs to the grid (yellow), because it is the available source with the lowest $LCOE$ during the period of the night ($h = 1$ to $h = 7$ and $h = 23$ to $h = 24$). Besides, the system does not power the thermal accumulator in the hours it is being used. Also, $SOC_i = 75\%$, so the battery is charged using the excess PV power (green), which is sufficient as the system does not recur to the grid to charge the batteries (red). Finally, the energy from the batteries system has the highest $LCOE$, so it is only used as backup when the available energy from the grid and from the PV system is not enough. Since it was not used, it is possible to conclude that the grid and PV system energy were sufficient to power the thermal accumulator.

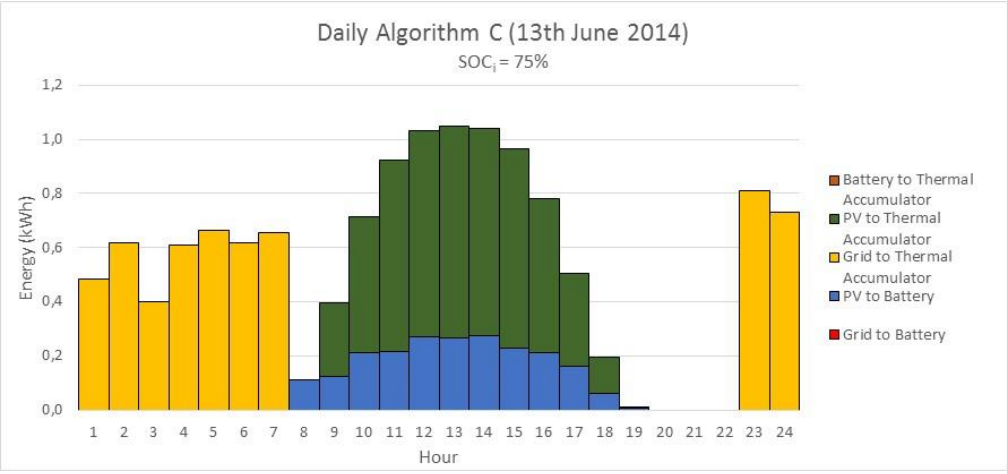

Graphic 20 - Daily algorithm C results for the 13th June 2014 and $SOC_i = 75\%$.

Graphic 21 corresponds to the results from the daily algorithm D and has a shape similar to that of the one in Graphic 20. The difference comes to the fact that, for this algorithm, the system is forced to use the batteries. For the green, blue and yellow curves, the same conclusions can be drawn. The shape of the curve is very similar, but the absolute values differ because of the forced usage of the batteries. In this figure, it is likewise possible to observe the brown (discharging) and red (charging) bars. Since the SOC_i is the same as before, the batteries can be used as a source but also as a load and, due to the restriction of the forced usage of the batteries, the PV production is not enough to charge the batteries throughout the day. Since this is a forced condition and the most expensive one, the algorithm distributes this usage, being this higher in the hours where there is no PV energy available and vice-versa, *i.e.*, the system tries to maximize the charge of the batteries and minimize their usage during the sunlight hours.

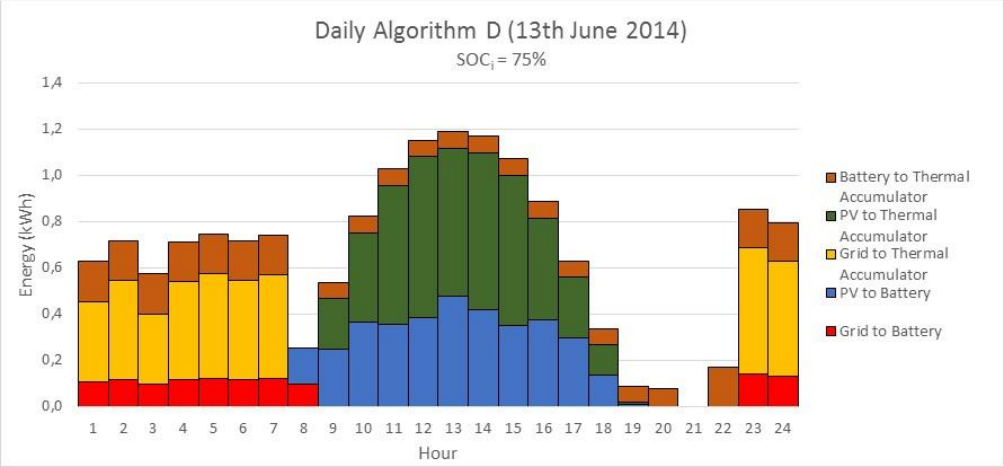

Graphic 21 - Daily algorithm D results for the 13th June 2014 and $\boldsymbol{SOC_i = 75\%}$.

6.3.3. DAILY AND HOURLY ALGORITHMS COMPARISON

By the previous graphical analysis, it seems that the results for the hourly algorithms are not satisfactory, since the optimization loses the scope of the whole day. It makes immediate optimizations for an hourly objective, considering only the cost for that hour and reaching to a solution that does not necessarily correspond to the best solution. On the other hand, the daily algorithms present a more balanced allocation of the energy and a more profitable use of the PV energy. Despite this, they rely on a less detailed model for the energy balance of the thermal accumulator and the batteries system.

The graphical analysis is not sufficient to assess which algorithm has the best performance overall so, a quantitative analysis was made, which is presented in Table 19. In this table, there are assembled the results for $SOC_i = 75\%$, which graphical analysis was made in **6.3.1** and **6.3.2** and also for $SOC_i = 40\%$ and 100%.

By comparing the two hourly algorithms, they are quite similar when it comes to G-B, PV-B and PV-T. The only difference corresponds to whether the system uses the batteries or the grid to power the thermal accumulator, which results from differences discussed above. Also, it is important to observe that the two algorithms present the same results for a $SOC_i = 100\%$, since the batteries do not need to be charged and it is indifferent to optimize firstly the batteries and the thermal accumulator. In what regards the percentage of PV used, it is possible to get that only 25% was used, which is due to the fact that the hourly optimization is practically finished before sunrise. For the saving, it can be observed that algorithm A has always positive savings, being the highest for the case where the batteries are discharged at the beginning of the day. On the other hand, algorithm B presents negative savings (additional cost in the electric bill), except for the case where the batteries are fully charged at the beginning of the day. This is due to fact that, at the beginning of the day, the batteries are charged from the grid and are immediately afterwards used to charge the thermal accumulator, as discussed above.

Table 19 – Comparison of the four different algorithms for 13th June with $\boldsymbol{SOC_i = 40\%}$, $\boldsymbol{75\%}$ and $\boldsymbol{100\%}$. G-B: grid to batteries; PV-B: PV to batteries; G-T: gird to thermal accumulator; PV-T: PV to thermal accumulator; B-T: batteries to thermal accumulator (representing the total energy consumption in $\mathbf{kWh}$). $\boldsymbol{S_t}$: total daily savings (in €); $\boldsymbol{S}$: daily savings per $\mathbf{kWh}$ used (in €/$\mathbf{kWh}$).

Different Algorithm Comparison for 13th June									
Algorithm	$\boldsymbol{SOC_i}$	**G-B**	**PV-B**	**G-T**	**PV-T**	**B-T**	$\boldsymbol{PV_{used}}(\%)$	$\boldsymbol{S_t}(€)$	$\boldsymbol{S}(€/\mathbf{kWh})$
A (Hourly)	40%	5.4	0	12.4	1.4	0.2	25	0.1463	0.0925
	75%	2.4	0	12.4	1.4	0.3	25	0.1332	0.0817
	100%	0.3	0	12.4	1.4	0.3	25	0.1332	0.0817
B (Hourly)	40%	5.1	0	9.2	1.4	3.1	25	-0.6136	-0.1370
	75%	2.2	0	10.5	1.4	2.2	25	-0.3622	-0.1029
	100%	0.3	0	12.4	1.4	0.3	25	0.1332	0.0817
C (Daily)	40%	2.4	2.7	5.6	5.6	0	100	1.2910	0.1562
	75%	0	2.1	5.6	5.6	0	88.8	1.2083	0.1566
	100%	0	0	5.6	5.6	0	62.9	0.8811	0.1579
D (Daily)	40%	2.4	2.7	5.6	5.6	0	100	1.2910	0.1562
	75%	1.2	3.6	3.9	4.7	2.6	100	0.7112	0.0656
	100%	0.8	3.6	2.1	4.6	4.4	100	0.2545	0.0201

In what regards the daily algorithms, it is conceivable to conclude that both are quite similar, except for when it comes to the usage and charge of the batteries. In fact, the two present the same results when the batteries has a $SOC_i = 40\%$, since the only difference between the two is the fact that D forces the system to use the batteries. It is also interesting to perceive that C never

uses the batteries to charge the thermal accumulator, even when they are fully charged at the beginning of the day. This is due to the fact that the algorithm finds recurrently a less expensive solution for all hours. The percentage of PV used is quite high in both of them, being of 100% in all the cases for D. This does not necessarily mean that the algorithm D presents best results. It can also mean that C is the best one but the system is oversized. It is necessary to compare the savings. By comparing the two of them, it is possible to get that C leads to significantly higher savings.

Comparing the two approaches, it is clear that the daily approach presents better results than the hourly approach – higher savings and higher percentage of PV energy used. It is also possible to conclude that, for the daily approach, the forced usage of the battery (D) is not the ideal solution and that, the grid and the PV system are enough to suppress the energetic needs of the thermal accumulator.

Also, in the case of C, for $SOC_i = 75\%$ and 100%, there is spare PV energy, so it is possible to also sell it to the grid, which can even increase the energetic savings. The sell is also possible for A and B, but since it was not modeled, it is not possible to conclude if it would improve significantly the hourly results.

Since the C algorithm presents the best overall results, it was chosen to be used for the next optimization tests and comparisons.

6.3.4. TESTS FOR DIFFERENT SOC_i

The next part of the analysis concerned the different values of SOC_i. For this part, it was chosen the Daily Algorithm C, with data from 13th June 2014 and the values for $SOC_i = 40\%, 75\%$ and 100%, which are represented in Graphic 22, Graphic 20 and in Graphic 23, respectively. This analysis is more qualitative than quantitative, and was made to evaluate how the algorithm behaved for different SOC_i.

In what regards the daily algorithms, it is conceivable to conclude that both are quite similar, except for when it comes to the usage and charge of the batteries. In fact, the two present the same results when the batteries has a $SOC_i = 40\%$, since the only difference between the two is the fact that D forces the system to use the batteries. It is also interesting to perceive that C never uses the batteries to charge the thermal accumulator, even when they are fully charged at the beginning of the day. This is due to the fact that the algorithm finds recurrently a less expensive solution for all hours. The percentage of PV used is quite high in both of them, being of 100% in all the cases for D. This does not necessarily mean that the algorithm D presents best results. It can also mean that C is the best one but the system is oversized. It is necessary to compare the savings. By comparing the two of them, it is possible to get that C leads to significantly higher savings.

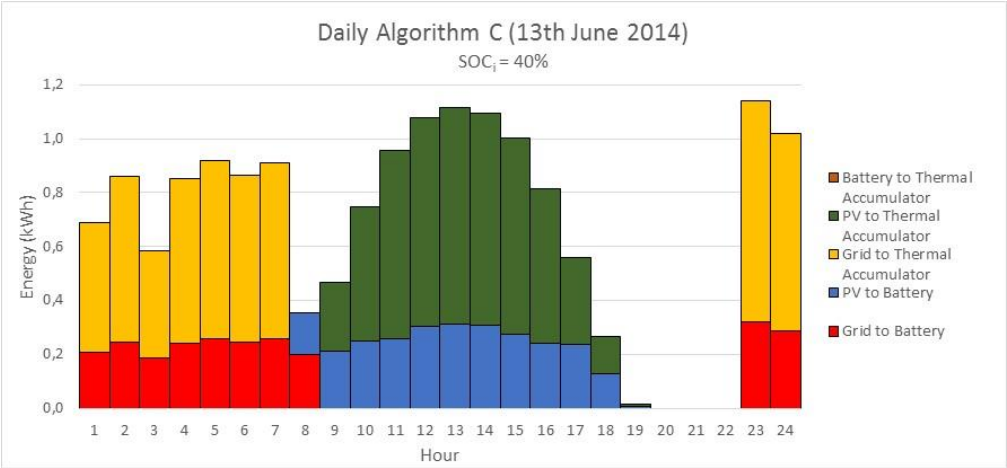

Graphic 22 - Daily algorithm C results for the 13th June 2014 and $\boldsymbol{SOC_i = 40\%}$.

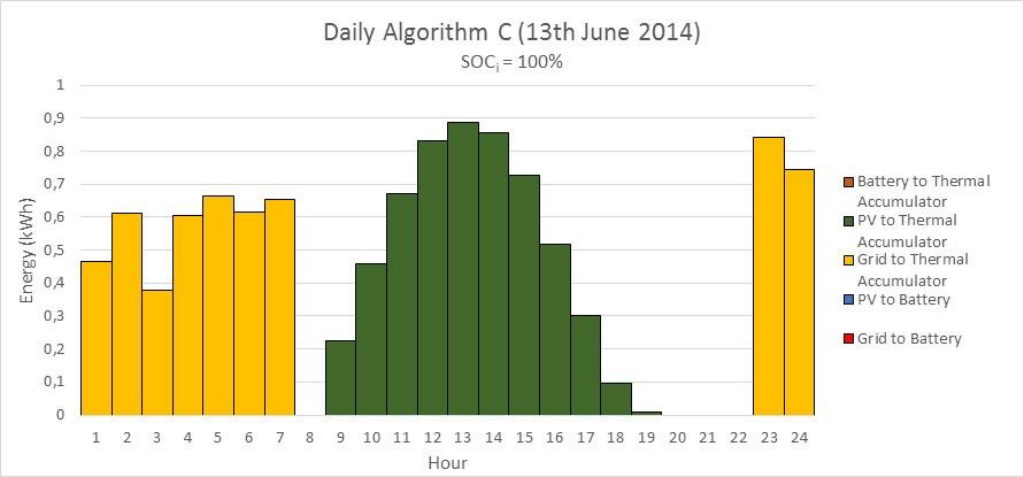

Graphic 23 - Daily algorithm C results for the 13th June 2014 and $\boldsymbol{SOC_i = 100\%}$.

Graphic 23 is also similar to Graphic 20 and to Graphic 22. The main difference is the fact that no energy was used to charge up the batteries, which also makes sense, since the batteries were fully charged at the beginning of the day. Also, this case corresponds to lower use of PV energy, which is due to the fact that the PV production was more than enough to suppress the energetic needs of the thermal accumulator.

It is also important to refer that in all of the three cases, the savings were quite comparable, regardless of the usage of the batteries, (Table 19).

6.3.5. TESTS FOR DIFFERENT DAYS

The last part of the analysis of the energy management algorithm regards the study of the results for different types of day and seasons of the year, as described in **4.9.2** and **4.9.3** and which graphics are presented in **4.9.4**. Once again, it was chosen the Daily Algorithm C and for the year of 2014 the chosen days were 13th and 14th June, and 3rd and 13th December, which

represented a typical summer weekday and day off and winter weekday and day off, respectively. This days are correspondingly presented in Graphic 20, Graphic 24, Graphic 25 and Graphic 26 and the respective graphics are Graphic 1, Graphic 2, Graphic 3 and Graphic 4. The considered value for SOC_i was of 75%.

Graphic 24 is almost equal to Graphic 20, but with two differences. The first one can be related to the fact that the DHW demand hour corresponds to $h = 10$, instead of $h = 8$, which can be easily observed in the graphic, since for that hour, no energy was used to power the thermal accumulator. This restriction forced the system to use the PV energy in a different way and to use all the available PV energy at that energy to charge the batteries, which reduced the amount of energy used in the next hours. The other difference corresponds to the fact that there is a residual use of grid energy to power the batteries, which might be due what was mentioned before, to the different profile for that day or the different of the irradiance and temperature outline.

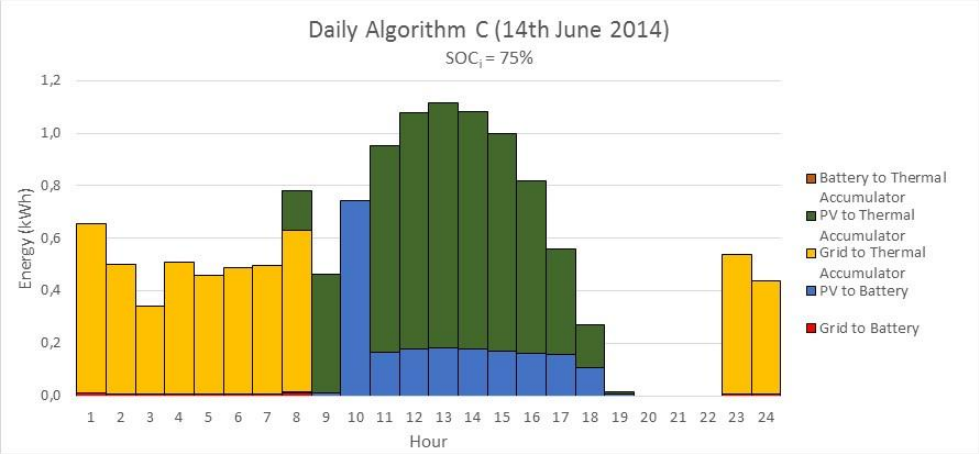

Graphic 24 - Daily algorithm C results for the 14th June 2014 and $\boldsymbol{SOC_i = 75\%}$.

In Graphic 25, it is possible to observe the results for a typical winter weekday. This profile also seems to maximize the usage of PV energy, but has quite different absolute values. The observed differences in the energy from the grid are due to the different profile for a typical winter day, as described in **4.9.4** and to the different temperature and irradiation profile. In this case, it is interesting to observe that all of the PV energy was used to power the thermal accumulator and that it also necessary to recur to the grid as a backup.

In what regards the daily algorithms, it is conceivable to conclude that both are quite similar, except for when it comes to the usage and charge of the batteries. In fact, the two present the same results when the batteries has a $SOC_i = 40\%$, since the only difference between the two is the fact that D forces the system to use the batteries. It is also interesting to perceive that C never uses the batteries to charge the thermal accumulator, even when they are fully charged at the beginning of the day. This is due to the fact that the algorithm finds recurrently a less expensive solution for all hours. The percentage of PV used is quite high in both of them, being of 100% in

all the cases for D. This does not necessarily mean that the algorithm D presents best results. It can also mean that C is the best one but the system is oversized. It is necessary to compare the savings. By comparing the two of them, it is possible to get that C leads to significantly higher savings.

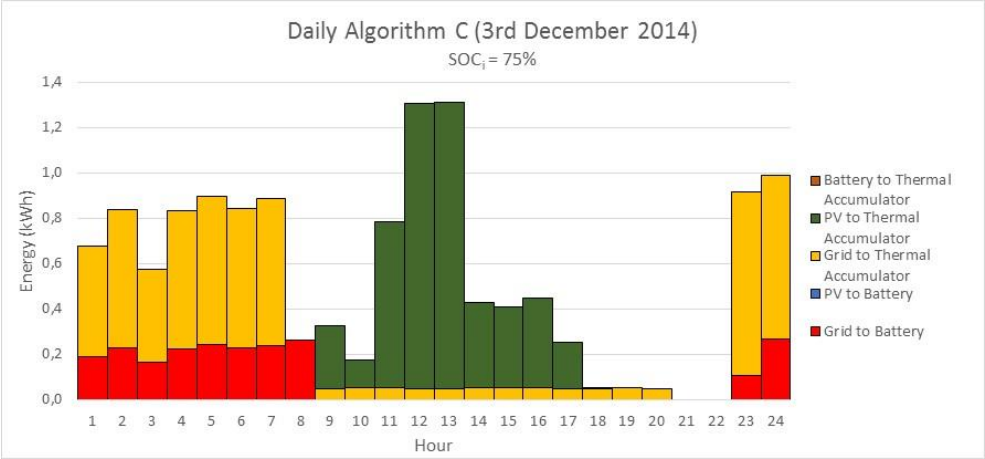

Graphic 25 - Daily algorithm C results for the 3rd December 2014 and $\boldsymbol{SOC_i = 75\%}$.

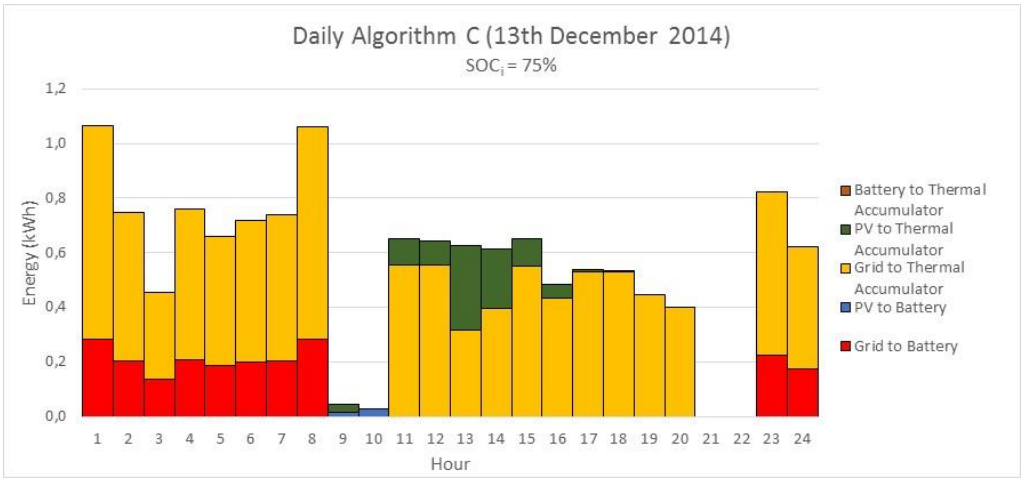

Graphic 26 - Daily algorithm C results for the 13th December 2014 and $\boldsymbol{SOC_i = 75\%}$.

For a more objective analysis and to evaluate the variation of the savings with the season, the numerical results are assembled in Table 20.

By observing Table 20, it is possible to prove that the main difference between the seasons lies in the usage of PV energy, which is due to different seasonal sunshine hours availability. For that fact, the total savings are significantly higher in summer, but the daily savings per kWh are really close. On the other hand, the differences between weekdays and days off are not relevant in Summer and in Winter are only due to the different irradiation profiles. Also, the fact that only 88,9% of the PV energy was used in a summer weekday supports the idea that the system could

be oversized, as it was discussed in **6.3.3**. But, in fact, for the other three days, the system used 100% of PV energy, so the previous assumption was not necessarily correct.

Table 20 - Comparison of the four different algorithms for typical Summer and Winter weekdays and days off with $\boldsymbol{SOC_i = 75\%}$. G-B: grid to batteries; PV-B: PV to batteries; G-T: gird to thermal accumulator; PV-T: PV to thermal accumulator; B-T: batteries to thermal accumulator (representing the total energy consumption in $\mathbf{kWh}$). $\boldsymbol{S_t}$: total daily savings (in €); $\boldsymbol{S}$: daily savings per $\mathbf{kWh}$ used (in €/$\mathbf{kWh}$).

Different Season Comparison									
Season	$\boldsymbol{Day}$	**G-B**	**PV-B**	**G-T**	**PV-T**	**B-T**	$\boldsymbol{PV_{used}}(\%)$	$\boldsymbol{S_t}(€)$	$\boldsymbol{S}(€/\mathbf{kWh})$
Summer	Week	0	2.1	5.6	5.6	0	88.9	1.2083	0.1566
	Off	0.1	2.1	5	6.2	0	100	1.2882	0.1562
Winter	Week	2.1	0	6.2	5	0	100	0.7893	0.1579
	Off	2.1	0	10.3	0.9	0	100	0.1496	0.1579

7. CONCLUSIONS

The Isotropic Sky, HDKR and Perez models are adequate to convert the values for hourly irradiation on a horizontal surface to any tilted surface. Despite this, the one that presented best results was the Perez model, which was expected, since it is the most detailed one. The HDKR model, despite being more detailed than the Isotropic Sky one, presents the highest deviation. But, the HDKR model presents the lowest deviation for the hours of higher irradiation intensity.

From the daily analysis, it was possible to confirm that there is a higher deviation in months closer to winter and a lower for months closer to summer. For this case, the HDKR model presented the best results and the Isotropic Sky the worst. Despite this, the deviations were significantly lower than the ones in the case of the hourly models. This was expected, since the daily analysis does not take into account the daily irradiation profile, but only total values. It was also possible to confirm that for months closer to summer, it pays off to have the panels oriented on the horizontal.

For the 3P model, the results were not so satisfactory. Recurring to local irradiance data, it was not necessary to recur to the radiation models. For the predictions of I_{max}, V_{max} and P_{max}, the deviation is considerably high but, the predictions of the 3P model have a similar shape to the experimental data. However, the presented apparent hour displacement can explain the high deviation. The experimental setup was not the ideal. As it possible to get from Figure 3, there are three rows of panels are placed approximately $30\ \mathrm{m}$ apart and the meteorological station is placed about $100\ \mathrm{m}$ from the furthest row. This is not reason enough for the results to have local variations, but it is important in what regard shading effects. On the left of the system, there is a building close enough to cast a shadow and this can be noticed for the panels and for the meteorological station in different hours. Also, the temperature data was used for a location about $3\ \mathrm{km}$ from the experimental setup site. It was assumed that there were not considerable microclimate effects in the city of Lisbon. For the irradiance input, it was also used a model that predicted its attenuation taking into account the characteristic and dirt conditions of the panel, which were not possible to get rigorously. This could also affect the intensity discrepancy. These results were compared to the predictions that did not consider this factor, presented a lower deviation, which proved that this was an adequate consideration. The fact that the internal resistances were neglected could also be in the root of the problem. The implementation of a more complex more model, such as the 5P, which is similar to the 3P model but considers two internal resistances, one in parallel and another in series, could lead to better results.

For the optimization algorithms, in the hourly approach, the charging a discharging cycles were considered independent, so it is possible for the algorithm to predict the charge and discharge of batteries in the same hour, which is problematic. The optimization was made hourly, so the scope of the whole day was lost. It was not possible to optimize simultaneously the thermal accumulator and the batteries system, hence the two developed algorithms. Algorithm A presented positive

savings, while B presented negative savings. Also, both algorithms presented only a 25% use of the PV energy, which was not desirable. Both hourly algorithms missed the scope and were not adequate.

The daily approach permitted a wider overview of the whole day but, since the thermal accumulator and the batteries models were non-linear, it was not possible to have a detailed analysis of the energy balance. Algorithm C presented significantly higher savings when compared to the hourly ones, but it never used the batteries system as an energy source. Algorithm D presented also significantly higher savings comparing to hourly ones, but since it forced the usage of the batteries, the savings were lower than the ones from C.

The influence of SOC_i permitted to conclude that the absolute savings were different, but the savings per kWh were similar. Results show that this parameter did not influence the final result, only the allocation of the energy throughout the day. The influence of the season results showed that only for a summer weekday, the system presented a less than 100% usage of the energy from the PV system. In winter, it was always used 100% of the energy from PV system. This way, it is possible to conclude than the PV system is not oversized. In a typical summer day, the PV energy produced is much higher than in a winter day, and if the system produces more than it consumes.

The developed algorithm permitted to prove that a detailed model for the production can be effectively used in any energy management tool, with the integration of all the three radiation models and a PV production one. It is only necessary for the system to have access to trustworthy irradiation on a horizontal surface and temperature forecasts. Despite this, the algorithm has several limitations and most of the crucial parameters for a more rigorous energy management strategy implementation were simplified or neglected. What was gained in the detail of the production models was lost with these assumptions. But, the main difference between the usage of these models instead of a simple model on which the produced power is proportional to the radiation intensity is the insight of the problem. With a more detailed model it is possible to increase the intelligence and independence of the system. For instance, in the PV panels are movable, the system can provide an optimal hourly or daily orientation to maximize production. Or, if the production values are lower than the predictions, it can detect situations on which whether the panels need maintenance (electrical, cleaning, etc.) or if there are shading effects (*e.g.* a tree in front of the household that is shading the system).

The more intelligent a management algorithm is, the better are the optimization results. The algorithm relied on a linear programming tool, with only one decision variable. Besides the cost, it could be interesting for an algorithm like this to optimize other parameters like comfort or even the production. The orientation of the panels (for the case of production) or the regulation of temperature or humidity inside the house (a comfort objective) can enter the optimization. This

can be further developed with more complex machine learning tools, for which the energy production and consumption profiles can be modeled instead of assumed as a baseline. Also, it could easily manage the sale of exceeding produced energy to the grid.

No assessment of how long the system will be paid was made. The system was assumed to last 25 years and a total annual production of $E_t = 2208\ \mathrm{kWh}$, so the LCOE was calculated assuming this.

The more detailed analysis of the production of the PV system allows an energy management algorithm to make smarter decisions and predictions and to increase the number of decision variables to optimization process.

8. REFERENCES

[1] U.S. Energy Information Administration, “Annual Energy Outlook 2013.” p. 244, 2013.

[2] European Comission, “Climate Action,” 2017. [Online]. Available: https://ec.europa.eu/clima/policies/strategies/2020_pt. [Accessed: 05-May-2017].

[3] P. Bertoldi, B. Hirl, and N. Labanca, *Energy Efficiency Status Report 2012*. 2012.

[4] E. Bittenbender, “Genetic Algorithm-Based Optimization of Microgrids,” 2014.

[5] A. Luque and S. Hegedus, *Handbook of Photovoltaic Science and Engineering*, 1st ed. Chichester, West Sussex, United Kingdom: John Willey & Sons, Ltd., 2011.

[6] A. Joyce, L. Coelho, J. Martins, N. Tavares, R. Pereira, and P. Magalhães, “A PV / T and Heat Pump Based Trigeneration System Model for Residential Applications,” 2011, p. 13.

[7] O. Motlagh, T. Sai Hong, G. Grozev, P. Paevere, and F. Motlagh, “Neural Analysis of Residential Electricity Consumption Behaviours: Application in Modelling Impact of Domestic Electricity Generation.” 2014.

[8] J. A. Duffie and W. A. Beckman, *Solar Engineering of Thermal Processes*, 4th ed. New Jersey: John Wiley & Sons, Inc., 2013.

[9] J. P. Friedberg, *Plasma Physics and Fusion Energy*. Cambridge: Cambridge University Press, 2007.

[10] R. D’Inverno, *Introducing Einstein’s Relativity*, 5th ed. Oxford: Oxford University Press Inc., 1998.

[11] J. W. Spencer, “Fourier Series Representation of the Position of the Sun,” *Search 2*, vol. 2, p. 172, 1971.

[12] C. N. Rodrigues, “Centrais Solares Fotovoltaicas ligadas à rede eléctrica no Edifício Solar XXI,” 2008.

[13] P. I. Cooper and R. V. Dunkle, “A non-linear flat-plate collector model,” *Sol. Energy*, vol. 26, no. 2, pp. 133–140, 1981.

[14] F. Kasten and A. T. Young, “Revised optical air mass tables and approximation formula,” *Appl. Opt.*, vol. 28, no. 22, pp. 4735–4738, 1989.

[15] B. Y. H. Liu and R. C. Jordan, “The interrelationship and characteristic distribution of direct, diffuse and total solar radiation,” *Sol. Energy*, vol. 4, no. 3, pp. 1–19, 1960.

[16] D. G. Erbs, S. A. Klein, and J. A. Duffie, “Estimation of the diffuse radiation fraction for hourly, daily and monthly-average global radiation,” *Sol. Energy*, vol. 28, no. 4, pp. 293–302, 1982.

[17] K. L. Coulson, *Solar and Terrestrial Radiation*, 1st ed. New York: Academic Press, 1975.

[18] B. Y. H. Liu and R. C. Jordan, “The long-term average performance of flat-plate solar-energy collectors,” *Sol. Energy*, vol. 7, no. 2, pp. 53–74, 1963.

[19] J. A. Davies and J. E. Hay, “Calculation of the solar radiation incident on a horizontal surface,” in *Proceedings First Canadian Solar RAdiation Data Workshop*, 1980, p. 59.

[20] D. T. Reindl, W. A. Beckman, and J. A. Duffie, “Diffuse fraction correlations,” *Sol. Energy*, vol. 45, no. 1, pp. 1–7, 1990.

[21] T. M. Klucher, “Evaluation of models to predict insolation on tilted surfaces,” *Sol. Energy*, vol. 23, no. 2, pp. 111–114, 1979.

[22] R. Perez, P. Ineichen, R. Seals, J. Michalsky, and R. Stewart, “Modeling daylight availability and irradiance components from direct and global irradiance,” *Sol. Energy*, vol. 44, no. 5, pp. 271–289, 1990.

[23] R. M. G. Castro, “Energias Renováveis e Produção Descentralizada - INTRODUÇÃO À ENERGIA FOTOVOLTAICA,” Lisbon, 0, 2002.

[24] M. A. Green *et al.*, “Solar cell efficiency tables (version 49),” *Prog. Photovoltaics*, vol. 25, no. 4, pp. 333–334, 2017.

[25] D. Appleyard, “Utility-scale thin-film: three new plants in Germany total almost 50 MW,” *Renewable Energy World Magazine*, 2009.

[26] H. Bellia, R. Youcef, and M. Fatima, “A detailed modeling of photovoltaic module using MATLAB,” *NRIAG J. Astron. Geophys.*, vol. 3, no. 1, pp. 53–61, 2014.

[27] “Ideal Single Diode Model,” 2016. .

[28] A. F. Souka and S. H., “Determination of the optimum orientations for the double-exposure, flat-plate collector and its reflectors,” *Sol. Energy*, vol. 10, no. 4, pp. 170–174, 1966.

[29] E. McKenna, M. McManus, S. Cooper, and M. Thomson, “Economic and environmental impact of lead-acid batteries in grid-connected domestic PV systems,” *Appl. Energy*, vol. 104, pp. 239–249, 2013.

[30] S. Bloomfield, C. Roberts, and M. Cotterell, “Batteries and Solar Power: Guidance for domestic and small commercial consumers,” Garston, Watford, 2016.

[31] P. Torcellini, S. Pless, M. Deru, and D. Crawley, “Zero energy buildings: a critical look at the definition,” 2006.

[32] S. Pless and P. Torcellini, “Net-zero energy buildings: A classification system based on renewable energy supply options.,” 2010.

[33] F. S. Hillier and G. G. Lieberman, *INTRODUCTION TO OPERATIONS RESEARCH*, 6th ed. New York: ThomasCasson, 2001.

[34] R. E. Bellman and S. E. Dryfus, *Applied Dynamic Programming*, 1st ed. London: Princeton University Press, 1963.

[35] F. Garzia, F. Fiamingo, and G. M. Veca., “Energy management using genetic algorithms,” Rome, 2003.

[36] A. Arabali, M. Ghofrani, M. Etezadi-Amoli, M. S. Fadali, and Y. Baghzouz, “Genetic-Algorithm-Based Optimization Approach for Energy Management,” *Power Deliv. IEEE Trans.*, vol. 28, no. 1, pp. 162–170, 2012.

[37] P. Palensky, “A new Parallel Genetic Algorithm for Energy Management,” Vienna, 2001.

[38] S. Dragićević and M. Bojić, “Application of linear programming in energy management,” *Serbian J. Manag.*, vol. 4, no. 2, pp. 227–238, 2009.

[39] F. G. Üçtuğ and E. Yükseltan, “A linear programming approach to household energy conservation: Efficient allocation of budget,” *Energy Build.*, vol. 49, pp. 200–208, 2012.

[40] L. T. Youn and S. Cho., “Optimal operation of energy storage using linear programming technique,” in *Proceedings of the World Congress on Engineering and Computer Science*, 2009, pp. 480–485.

[41] A. J. Conejo, J. M. Morales, and L. Baringo, “Real-Time Demand Response Model,” *Smart Grid, IEEE Trans.*, vol. 1, no. 3, pp. 236–242, 2010.

[42] G. Lee, “How PV Grid-Tie Inverters Can Zap Utility Power Factor,” 2009. [Online]. Available: http://www.renewableenergyworld.com/articles/print/pvw/volume-1/issue-4/solar-energy/how-pv-grid-tie-inverters-can-zap-utility-power-factor.html. [Accessed: 28-Sep-2016].

[43] C. C. S. LLC, “Inverter Power Factor - What is the power factor of an PV or wind power inverter?,” 2016. [Online]. Available: https://ctlsys.com/inverter_power_factor/. [Accessed: 28-Sep-2016].

[44] D. Neves and C. Silva, “Modeling the impact of integrating solar thermal systems and heat pumps for domestic hot water in electric systems e The case study of Corvo Island,” *Renew. Energy*, vol. 72, pp. 113–124, 2014.

[45] “DL118/2013 de 20 de Agosto Regulamento de Desempenho Energético dos Edifícios de

Habitação (REH) Síntese da Regulamentação Aplicável (Decreto-Lei, Portaria e Despachos)," Coimbra, 2013.

[46] J. W. Stevens and G. P. Corey, "A Study of Lead-Acid Battery Efficiency Near Top-of-Charge and the Impact on PV System Design," in *Photovoltaic Specialists Conference, 1996., Conference Record of the Twenty Fifth IEEE*, 1996, pp. 1485–1488.

[47] EDP Energias de Portugal, "Horários Baixa Tensão Normal." .

[48] N. E. A. / I. A. / O. for E. C.-O. and Development, "Projected Costs of Generating Electricity (2005 Update)." p. 233, 2005.

[49] M. Analytics, "PV Price Forecast," 2015. .

[50] J. Rodriguez, "Levelised cost of storage: A better way to compare battery value," 2016. .

[51] "Battery Storage for Renewables: Market Status and Technology Outlook," Abu Dhabi, United Arab EMirates, 2015.

[52] C. Gorria, J. Jimeno, I. Laresgoiti, M. Lezaun, and N. Ruiz, "Forecasting flexibility in electricity demand with price/consumption volume signals," *Electr. Power Syst. Res.*, vol. 95, pp. 200–205, 2013.

[53] J. Y. Boivin, "Demand side management - The role of the power utility," *Pattern Recognit.*, vol. 28, no. 10, pp. 1493–1497, 1995.

[54] P. Palensky, "Demand Side Management: Demand Response, Intelligent Energy Systems, and Smart Loads," *Ind. Informatics, IEEE Trans.*, vol. 7, no. 3, pp. 381–388, 2011.

[55] A. Lopes, "O sobreaquecimento das cidades - causas e medidas para a mitigação da ilha de calor de Lisboa," *Territorium*, vol. 15, pp. 39–52, 2009.

9. APPENDIX

A.1. SOLAR EXTRATERRESTRIAL RADIATION AND GEOMETRY BASIC NOTIONS

It is possible to define the solar constant (G_{sc}) as the energy from the sun per unit time received on a unit area surface perpendicular to the radiation propagation direction at the mean Sun-Earth distance. The World Radiation Center (WRC) has adopted the value of 1367 W/m^2, with an uncertainty of 1% [8]. The Earth however, does not maintain the same distance to the sun throughout the year due to its elliptical trajectory [10], so the intensity of radiation that reaches the Earth's outer atmosphere changes in a range of ±3.3% [8]. As it would be expected, the maximum intensity occurs for the perihelion, which is the point in the Earth's elliptical trajectory closest to the sun, while the minimum occurs for the aphelion, which is the point in the trajectory further from the sun [8], [10], as it is possible to observe in Figure 8. Therefore, a new variable is needed to take into account this variation throughout the year, so it is possible to define, which is the extraterrestrial irradiance on the plane normal to the radiation on a given day n of the year (that ranges from 1 to 365) [8], [11]:

$$G_{on} = G_{sc}\left(1 + 0.033\cos\frac{360^{\circ}}{365}n\right) \tag{A.1.1}$$

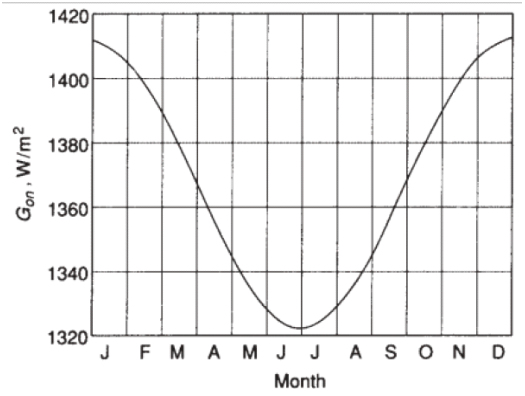

Figure 8 - Variation of G_{on} with the time of the year [8].

The radiation that reaches the outer atmosphere is, however, not the same that reaches the Earth's surface. By travelling through the atmosphere, the solar radiation interacts with its constituents (air molecules, clouds and dust) and consequently loses energy through processes of diffraction, reflection and absorption. It is necessary to define two types of radiation that reach the Earth's surface: beam and diffuse. Beam (or direct) radiation consists on the radiation that comes directly from the sun without having been scattered by the components of the atmosphere, while diffuse (or sky) radiation consists on the radiation that was scattered by the atmosphere's

components and, therefore, reaches the surface with different directions. So, it is possible to define as well the total radiation that reaches the surface, which is the sum of the beam and diffuse radiation [8].

A.1.1. GEOMETRY OF BEAM RADIATION

To have the best efficiency for collecting energy, it is necessary to know the best way of orientating a collector, so it is important to define the most relevant angles regarding a planar surface with a given orientation and the sun's direction. These angles are illustrated in Figure 9 and described summarily in Table 21 [12].

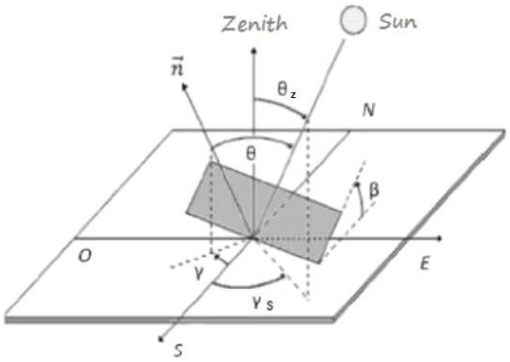

Figure 9 - Imported angles between the sun and a tilted surface (adapted from [12]).

Table 21- List and definition of the important angles between the sun and a tilted surface (adapted from [8]).

Angle	Denomination	Description
ϕ	Latitude	The angle between the location and the equator. It ranges from -90^o to 90^o (has negative values in the southern hemisphere and positive values in the northern hemisphere).
β	Collector's tilt or slope	The angle between the planar surface and the ground. It ranges from 0^o to 180^o (the first regards a horizontal to the place surface facing the sky and the second a horizontal to the place surface facing the ground).
δ	Declination	The angle between the position of the sun rays at solar noon *i.e.*, when the sun is on the local meridian and the plane of the equator. It ranges from -23.45^o to 23.45^o (negative in the southern hemisphere and positive in the northern hemisphere).
γ	Surface azimuth angle	The angle between the local meridian and the projection on a horizontal plane of the normal to the surface from the local meridian. It

		ranges from -180^{o} to 180^{o} (negative values for East, 0^{o} for South and positive values for West).
ω	Sun hour angle	The angular displacement of the sun's position to east (negative) or west (positive) of the local meridian due to Earth's rotation (per hour). It ranges from $\omega_{sunrise}$ to ω_{sunset}, which will be denoted as ω_s. NOTE: ω_s is not depicted in Figure 9.
ω_s	Sunset hour angle	Sun Hour Angle for the sunset.
θ	Incidence angle	The angle between the beam radiation direction and the normal to the surface direction.
θ_z	Zenith angle	The angle between the vertical to the place (zenith) and the line of the sun.
α_s	Solar altitude	The complement of the zenith angle *i.e.*, the angle between the horizon and the sun rays.
γ_s	Solar azimuth angle	Similar to the surface azimuth angle, but regarding the position of the sun.

The incidence angle is the most important one, since it will be the reference for the panel orientation. By geometry, it is possible to deduce its expression:

$$\cos\theta = \sin\delta\sin\phi\cos\beta - \sin\delta\cos\phi\sin\beta\cos\gamma + \cos\delta\cos\phi\cos\beta\cos\omega + \cos\delta\sin\phi\sin\beta\cos\gamma\cos\omega + \cos\delta\sin\beta\sin\gamma\sin\omega \quad \text{(A.1.1.1)}$$

To calculate this angle, it is necessary to know the expressions for other angles. ϕ is tabled for each place and β and γ can be measured directly from the orientation of the panel. According to the literature [8], [13], the declination is given by:

$$\delta = 23.45\sin\left(360\frac{284+n}{365}\right) \quad \text{(A.1.1.2)}$$

and the sun hour angle ω is given by:

$$\omega = 15^{o}t - 180^{o} \quad \text{(A.1.1.3)}$$

where t is the solar time, which satisfies the condition $t \in [0h, 24[$. It is also possible to find the relation between solar and standard time, which is given by the following expression:

$$t - standard\ time = 4(L_{st} - L_{loc}) + E \tag{A.1.1.4}$$

where the right-hand side is given in minutes, L_{st} is the standard meridian longitude for the local time zone, L_{loc} is the longitude of the given location and E is called the equation of time and it is given by:

$$E = 229.2(0{,}000075 + 0.001868\cos B - 0.032077\sin B - 0.014615\ \cos 2B - 0.04089\sin 2B) \tag{A.1.1.5}$$

where $B = (n-1)\frac{360^{\circ}}{365}$. The zenith angle corresponds to the incidence angle for a horizontal surface ($\beta = 0^{\circ}$), so its expression is given by:

$$\cos\theta_z = \cos\phi\cos\delta\cos\omega + \sin\phi\sin\delta \tag{A.1.1.6}$$

and by definition:

$$\alpha_s = 90^{\circ} - \theta_z \tag{A.1.2.7}$$

Once more, from geometrical considerations referred in [8], the solar azimuth angle is given by:

$$\gamma_s = \text{sign}(\omega)\left|\arccos\left(\frac{\cos\theta_z\sin\phi - \sin\delta}{\sin\theta_z\cos\phi}\right)\right| \tag{A.1.1.8}$$

where the $\text{sign}(\omega)$ function assumes the values of -1 or 1 if ω is either positive or negative respectively. Finally, according to [8], the sunset hour angle can be obtained for ω, which is the case when the sun is at the horizon ($\theta_z = 90^{\circ}$):

$$\cos\omega_s = -\tan\phi\tan\delta \tag{A.1.1.9}$$

and where can easily be defined the sunrise hour angle ω_{sr} as the symmetric of ω_s [8].

A.1.2. RATIO BETWEEN BEAM RADIATION ON A TILTED AND ON A HORIZONTAL SURFACE

Most of the world's available data for solar radiation is for horizontal surfaces and in most of the cases, the collector has a tilt, so it is necessary to convert these values for a surface at the plane of the collector. The geometric factor R_b represents the ratio between the beam radiation normal to a horizontal surface and the beam radiation normal to a tilted surface [8]. This ratio is given by:

$$R_b = \frac{G_{b,T}}{G_b} = \frac{\cos\theta}{\cos\theta_z} \tag{A.1.2.1}$$

In Figure 10, it is illustrated the beam radiation on a horizontal and a tilted surface.

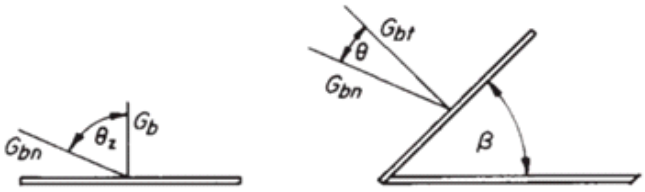

Figure 10 - Beam radiation and respective components on a horizontal (left) and a tilted (right) surface [8].

A.1.3. EXTRATERRESTRIAL RADIATION ON A HORIZONTAL SURFACE

To calculate or to predict the performance of a solar PV, it is necessary to know how solar radiation reaches the panel. But, since Earth's atmosphere scatters a significant amount of the radiation incident on the planet, it is logical to conclude that the radiation levels on the ground are not the same that on the outer atmosphere. Therefore, most of the models used for radiation calculations take into account normalized radiation levels, *i.e.*, the ratio between the radiation level (at ground) and the theoretically possible radiation that would be available if there were no atmosphere. So, it is necessary to know how to calculate extraterrestrial radiation.

After defining G_{on}, it is possible, to calculate G_o, which is the extraterrestrial irradiance on a horizontal surface. By making geometric considerations and by taking (A.1.1) and dividing it by (A.1.2.1) [8], the equation will take the form:

$$G_o = G_{sc}\left(1 + 0.033\cos\frac{360}{365}n\right)(\cos\phi\cos\delta\cos\omega + \sin\phi\sin\delta) \qquad \text{(A.1.3.1)}$$

The previous equation is valid for a given day n of the year from that day's sunrise to that day's sunset. G_o represents a power per unit of surface, but it is often necessary to calculate the daily or hourly total amount of energy per unit of surface. Integrating (A.1.3.1) over a period from sunrise to sunset, gives the daily extraterrestrial radiation on a horizontal surface [8]. But, if data is available, it is more useful to calculate the extraterrestrial irradiation on a horizontal surface for an hour period, which can be done by integrating it for a period between hour angles ω_1 and ω_2, which define an hour and where $\omega_1 < \omega_2$ [8]. The resulting expression becomes:

$$\begin{aligned} I_o = {} & \frac{12\times 3600}{\pi} G_{sc}\left(1 + 0.033\cos\frac{360}{365}n\right) \\ & \times\left(\cos\phi\cos\delta\,(\sin\omega_2 - \sin\omega_1) + \frac{\pi}{180}(\omega_2\right. \\ & \left. - \omega_1)\sin\phi\sin\delta\right) \end{aligned} \qquad \text{(A.1.3.2)}$$

Although (A.1.3.2) is defined for an hour, it is possible to have a period defined by ω_1 and ω_2 that does not correspond to this, without losing the generality of the previous expression.

B.1. PV PRODUCTION TOOLBOX TABLE

PV Production		
threep_pv	$T_{cell}, I_{sc}{}^{real}, V_{oc}{}^{real}, V_{max}, I_{max}, P_{max}, \eta$	G_{eff}, T_{amb}
Inverter_func	I_{AC}, V_{AC}, P_{AC}	I_{DC}, V_{DC}, P_{DC}
Solar radiation		
g_attenuation	G^{real}	$\theta, cleanness, G$

B.2. RADIATION TOOLBOX TABLE

Function Name	Output	Inputs
Solar Radiation Geometry		
delta	δ	n
omega	ω	t
omega_s	ω_s	δ, ϕ
theta	θ	$\delta, \phi, \beta, \gamma, \omega$
theta_z	θ_z	δ, ϕ, ω
gamma_s	γ_s	$\delta, \phi, \omega, \theta_z$
Time		
r_time	$standard\ time$	n, t, L_{st}, L_{loc}
Tilted/Horizontal Surface		
r_b	R_b	θ, θ_z
Extraterrestrial Radiation		
g_on	G_{on}	G_{sc}, n
g_o	G_o	$G_{on}, \delta, \phi, \omega$
h_o	H_o	$G_{on}, \delta, \phi, \omega_s$
i_o	I_o	$G_{on}, \delta, \phi, \omega_1, \omega_2$
Air Mass		
m	m	θ_z, h
Clearness Indexes		
clear_index	k_t	I_o, I
Terrestrial Radiation		
i_d	I_d	I, k_t
i_t_Liu_Jordan	I_T (Isotropic Model)	$I, I_d, R_b, \beta, \rho_g$
i_t_HDKR	I_T (HDKR Model)	$I, I_d, I_o, R_b, \beta, \rho_g$
i_t_Perez	I_T (Perez Model)	$I, I_d, \theta, \theta_z, G_{on}, m, R_b, \beta, \rho_g$

C.1. HOURLY IRRADIATION FUNCTION

```
%%% IMPORTANT INPUT PARAMETERS %%%

Phi = 38.77;
Phi = degtorad(Phi);
L_st = 0;
L_loc = 9.18;
rho_g = 0.2;
Gamma = 0;

% Maximum number of days in a year
year = 2015;
input_days = 24;

% Preallocating Varibles
Beta = zeros(input_days,1);
n =  zeros(input_days,1);
s_time = zeros(input_days,24);
Delta = zeros(input_days,1);
Omega = zeros(input_days,24);
Omega_mean = zeros(input_days,24);
Omega_s = zeros(input_days,1);
Omega_sr = zeros(input_days,1);
Sunset_s_t = zeros(input_days,1);
Sunset_r_t = zeros(input_days,1);
Sunrise_s_t = zeros(input_days,1);
Sunrise_r_t = zeros(input_days,1);
Theta = zeros(input_days,24);
Theta_z = zeros(input_days,24);
Alpha_z = zeros(input_days,24);
Gamma_s = zeros(input_days,24);
Air_mass = zeros(input_days,24);
G_on = zeros(input_days,1);
G_o = zeros(input_days,24);
I_o = zeros(input_days,24);
H_o = zeros(input_days,1);
H = zeros(input_days,1);
H_d = zeros(input_days,1);
R_b = zeros(input_days,24);
R_b_av = zeros(input_days,24);
H_t_HDKR = zeros(input_days,1);
H_t_Liu_Jordan = zeros(input_days,1);
I = zeros(input_days,24);
k_T = zeros(input_days,24);
I_d = zeros(input_days,24);
I_b = zeros(input_days,24);
I_T_Liu_Jordan = zeros(input_days,24);
I_T_HDKR = zeros(input_days,24);
I_T_Perez = zeros(input_days,24);
G_Liu_Jordan = zeros(input_days,24);
G_HDKR = zeros(input_days,24);
G_Perez = zeros(input_days,24);
H_T_Liu_Jordan = zeros(input_days,1);
H_T_HDKR = zeros(input_days,1);
H_T_Perez = zeros(input_days,1);
H_T_Liu_Jordan_av = zeros(12,1);
H_T_HDKR_av = zeros(12,1);
H_T_Perez_av = zeros(12,1);
e_I_T_Liu_Jordan = zeros(input_days,24);
e_I_T_HDKR = zeros(input_days,24);
e_I_T_Perez = zeros(input_days,24);
Number_of_month_days = zeros(1,12);

% Menu for the case of having input diffuse radiation data on the hori-
% zontal
disp('Do you have data for diffuse radiation on horizontal surface?')
disp('1 - Yes')
disp('2 - No')

lock = 0;
```

```
while lock == 0
    Switch = input(' ');
    if Switch == 1 || Switch == 2
        break;
    else
        disp('You must chose one of the options!')
    end
end

%%% CALCULATIONS %%%

%% Import Data from Excel Sheet

% Year Data
% Horizontal Data Input
filename1 = 'LNEG_hourly_radiation_input.xlsx';
Solar_Data_Hourly = xlsread(filename1,'Radiation_J_m2');
% Diffuse Data Input
Solar_Data_Hourly_Diffuse = xlsread(filename1,'Diffuse_J_m2');

%%% SOLAR TIME AND ANGLES

for N = 1:24

    % The inclination of the panels differs for different times of the year
    % January, February, November and December
    if (N >= 1 && N <= 4) || (N >= 21 && N <= 24)
        Beta(N) = 45;                                                  %[°]
        Beta(N) = degtorad(Beta(N));                                 %[rad]
    % March, 1st April, September, October
    elseif (N >= 5 && N <= 7)  || (N >= 17 && N <= 20)
        Beta(N) = 40;                                                  %[°]
        Beta(N) = degtorad(Beta(N));                                 %[rad]
    % 15th April, May, June, July, August
    elseif N >= 8 && N <= 16
        Beta(N) = 35;                                                  %[°]
        Beta(N) = degtorad(Beta(N));                                 %[rad]
    end

    n(N) = Solar_Data_Hourly(N + 1, 1);

    % Delta (Solar Declination)
    Delta(N) = delta(n(N));                                            %[°]
    Delta(N) = degtorad(Delta(N));                                   %[rad]

    % Omega_s (Sunset hour angle)
    Omega_s(N) = omega_s(Delta(N),Phi);                                %[°]
    Omega_s(N) = degtorad(Omega_s(N));                               %[rad]

    % Omega_sr (Sunrise hour angle)
    Omega_sr(N) = -omega_s(Delta(N),Phi);                              %[°]
    Omega_sr(N) = degtorad(Omega_sr(N));                             %[rad]

    % Sunset Solar Time
    Sunset_s_t(N) = (radtodeg(Omega_s(N))+180)/15;                     %[h]
    % Sunset Real Time
    Sunset_r_t(N) = real_time(Sunset_s_t(N),N,L_st,L_loc);             %[h]

    % Sunrise Solar Time
    Sunrise_s_t(N) = (radtodeg(Omega_sr(N))+180)/15;                   %[h]
    % Sunrise Real Time
    Sunrise_r_t(N) = real_time(Sunrise_s_t(N),N,L_st,L_loc);           %[h]

    for hour = 1:24
        % Solar Time
        s_time(N,hour) = solar_time(hour-0.5,n(N),L_st,L_loc);         %[h]

        % Omega (Sun hour angle)
        Omega(N,hour) = omega(s_time(N,hour));                         %[°]
        Omega(N,hour) = degtorad(Omega(N,hour));                     %[rad]

        % Mean Omega for each hour
        Omega_mean(N,hour) = (omega(solar_time(hour-1,n(N),L_st,L_loc))...
            + omega(solar_time(hour,n(N),L_st,L_loc)))/2;              %[°]
```

```
Omega_mean(N,hour) = degtorad(Omega_mean(N,hour));           %[rad]

% Theta (Incident angle)
Theta(N,hour) = theta(Delta(N),Phi,Beta(N),Gamma,...
    Omega_mean(N,hour));                                      %[°]
Theta(N,hour) = degtorad(Theta(N,hour));                     %[rad]

% Theta_z (Zenith angle)
Theta_z(N,hour) = theta_z(Delta(N),Omega_mean(N,hour),Phi);    %[°]
Theta_z(N,hour) = degtorad(Theta_z(N,hour));                 %[rad]

% Alpha_z (Altitude of the sun)
Alpha_z(N,hour) = alpha_z(Theta_z(N,hour));                   %[°]
Alpha_z(N,hour) = degtorad(Alpha_z(N,hour));                 %[rad]

% Gamma_s (Solar azimuth)
Gamma_s(N,hour) = gamma_s(s_time(N,hour),...
    Theta_z(N,hour), Phi, Delta(N));                          %[°]
Gamma_s(N,hour) = degtorad(Gamma_s(N,hour));                 %[rad]

%% R_b (Tilted / Horizontal Ratio)
R_b(N,hour) = r_b(Theta(N,hour),Theta_z(N,hour));
if hour == 1 || hour == 24
    R_b_av(N,hour) = 1;
else
    % Close to sunrise
    if Omega(N,hour) > Omega_sr(N) && Omega(N,hour-1) < Omega_sr(N)
    R_b_av(N,hour) = r_b_av(Delta(N), Phi, Beta(N), Gamma,...
        Omega_sr(N), Omega(N,hour));
    % Close to sunset
    elseif Omega(N,hour)>Omega_s(N) && Omega(N,hour-1)<Omega_s(N)
        R_b_av(N,hour) = r_b_av(Delta(N), Phi, Beta(N), Gamma,...
            Omega(N,hour-1), Omega_s(N));
    else
        R_b_av(N,hour) = r_b_av(Delta(N), Phi, Beta(N), Gamma,...
            Omega(N,hour-1), Omega(N,hour));
    end
end


%%% RADIATION

%% EXTRATERRESTRIAL RADIATION

% Solar constant
G_sc = 1367;                                                 %[W/m^2]

% G_on (Extraterrestrial Irradiance on a plane normal to the
%       surface)
G_on(N) = g_on(G_sc,n(N));                                   %[W/m^2]

% G_o (Extraterrestrial Irradiance on a horizontal plane)
G_o(N,hour) = g_o(G_on(N),Phi,Delta(N),Omega_mean(N,hour));
                                                             %[W/m^2]

if G_o(N,hour) < 0
    G_o(N,hour) = 0;                                         %[J/m^2]
end

% I_o (Hourly Extraterrestrial Irradiation)
if hour == 1 || hour == 24
    I_o(N,hour) = 0;
else
    % Close to sunrise
    if Omega(N,hour) > Omega_sr(N) && Omega(N,hour-1) < Omega_sr(N)
        I_o(N,hour) = i_o(G_on(N),Phi,Delta(N),...
            Omega_sr(N),Omega(N,hour));                      %[J/m^2]
    % Close to sunset
    elseif Omega(N,hour)>Omega_s(N) && Omega(N,hour-1)<Omega_s(N)
        I_o(N,hour) = i_o(G_on(N),Phi,Delta(N),...
            Omega(N,hour-1),Omega_s(N));                     %[J/m^2]
    else
        I_o(N,hour) = i_o(G_on(N),Phi,Delta(N),...
            Omega(N,hour-1),Omega(N,hour));                  %[J/m^2]
```

```
    end
end
if I_o(N,hour) < 0
    I_o(N,hour) = 0;                                        %[J/m^2]
end

% H_o (Daily Extraterrestrial Irradiation)
if hour == 1
    H_o(N) = I_o(N,hour);                                   %[J/m^2]
else
    H_o(N) = I_o(N,hour) + H_o(N);                          %[J/m^2]
end


%% TERRESTRIAL RADIATION

% Hourly Irradiation on an Horizontal Surface
% INPUT - The values from the data sheet must be in J/m^2
% Close to sunrise
  I(N,hour) = Solar_Data_Hourly(N + 1, hour + 1);           %[J/m^2]

% Clearness Index
if I_o(N,hour) == 0
    k_T(N,hour) = 0;
else
    k_T(N,hour) = clear_index(I(N,hour),I_o(N,hour));
end

% Diffuse Component of Hourly Irradiation
if I_o(N,hour) == 0
    I_d(N,hour) = 0;
else
    I_d(N,hour) = i_d(I(N,hour),k_T(N,hour));
end

%if Switch == 1
%    I_d(N,hour) = Solar_Data_Hourly_Diffuse(N + 1, hour + 1);
%end

% Beam Component of Hourly Irradiation
I_b(N,hour) = I(N,hour) - I_d(N,hour);

%% Radiation on Slopped Surfaces

% Isotropic Sky (Liu and Jordan)
% Hourly
I_T_Liu_Jordan(N,hour) = i_t_Liu_Jordan(I(N,hour), I_d(N,hour),...
    R_b(N,hour), Beta(N), rho_g);
if I_T_Liu_Jordan(N,hour) < 0 || I_o(N,hour) == 0
    I_T_Liu_Jordan(N,hour) = 0;
end

% Anisotropic Sky (HDKR model)
% Hourly
I_T_HDKR(N,hour) = i_t_HDKR(I(N,hour), I_d(N,hour), I_o(N,hour),...
    R_b(N,hour), Beta(N), rho_g);
if I_T_HDKR(N,hour) < 0 || I_o(N,hour) == 0
    I_T_HDKR(N,hour) = 0;
end

% air mass
Air_mass(N,hour) = air_mass(Theta_z(N,hour));

% Perez Model
% Hourly
I_T_Perez(N,hour) = real(i_t_Perez(I(N,hour), I_d(N,hour),...
    Theta(N,hour), Theta_z(N,hour), G_on(N), Air_mass(N,hour),...
    R_b(N,hour), Beta(N), rho_g));
if I_T_Perez(N,hour) < 0
    I_T_Perez(N,hour) = 0;
end

% G (Irradiance) <- INPUT FOR THE 3-P AND 5-P PV MODELS
% Close to sunrise
```

```
        if Omega(N,hour) > Omega_sr(N) && Omega(N,hour-1) < Omega_sr(N)
            period_length = (hour - Sunrise_r_t(N) - 1) * 3600;         %[s]
        % Close to sunset
        elseif Omega(N,hour) > Omega_s(N) && Omega(N,hour-1) < Omega_s(N)
            period_length = (Sunset_r_t(N) - (hour-2)) * 3600;          %[s]
        % Between sunrise and sunset
        else
            period_length = 3600;
        end
        G_Liu_Jordan(N,hour) = I_T_Liu_Jordan(N,hour) / period_length;
        G_HDKR(N,hour) = I_T_HDKR(N,hour) / period_length;
        G_Perez(N,hour) = I_T_Perez(N,hour) / period_length;

        [e_I_T_Liu_Jordan(N,hour), e_I_T_HDKR(N,hour), ...
            e_I_T_Perez(N,hour)] = ...
    radiation_models_errors(I(N,hour), I_o(N,hour), G_on(N), ...
    Air_mass(N,hour), k_T(N,hour), I_d(N,hour), I_b(N,hour), ...
    R_b(N,hour), Beta(N), Theta(N,hour), Theta_z(N,hour), rho_g);
    end
end

% Daily
H_T_Liu_Jordan = sum(I_T_Liu_Jordan,2);
H_T_HDKR = sum(I_T_HDKR,2);
H_T_Perez = sum(I_T_Perez,2);


%%% EXPORT DATA %%%

% Define Axis
Day = zeros(input_days,1);
for N = 1:24
    Day(N) = n(N);
end
Hour_of_the_day = zeros(1,24);
for hour = 1:24
    Hour_of_the_day(hour) = hour;
end
Month_of_the_year = zeros(12,1);
for month = 1:12
    Month_of_the_year(month) = month;
end


%% Writing on File 1 (Geometry)

file_export1 = 'Angles_Data_LNEG.xlsx';

% First Sheet
Title_sheet1 = {'N', 'Delta', 'Omega_s', 'Omega_sr', 'Sunset_s_t',...
    'Sunset_r_t', 'Sunrise_s_t', 'Sunrise_r_t'};
xlswrite(file_export1,Title_sheet1,1,'A1');
xlswrite(file_export1,Day,1,'A2');
xlswrite(file_export1,radtodeg(Delta),1,'B2');
xlswrite(file_export1,radtodeg(Omega_s),1,'C2');
xlswrite(file_export1,radtodeg(Omega_sr),1,'D2');
xlswrite(file_export1,Sunset_s_t,1,'E2');
xlswrite(file_export1,Sunset_r_t,1,'F2');
xlswrite(file_export1,Sunrise_s_t,1,'G2');
xlswrite(file_export1,Sunrise_r_t,1,'H2');

% Sheet Omega
Title_sheet2 = {'Day/hour'};
xlswrite(file_export1,Title_sheet2,'Omega','A1');
xlswrite(file_export1,Day,'Omega','A2');
xlswrite(file_export1,Hour_of_the_day,'Omega','B1');
xlswrite(file_export1,radtodeg(Omega),'Omega','B2');

% Sheet Theta
xlswrite(file_export1,Title_sheet2,'Theta','A1');
xlswrite(file_export1,Day,'Theta','A2');
xlswrite(file_export1,Hour_of_the_day,'Theta','B1');
xlswrite(file_export1,radtodeg(Theta),'Theta','B2');
```

```
% Sheet Theta_z
xlswrite(file_export1,Title_sheet2,'Theta_z','A1');
xlswrite(file_export1,Day,'Theta_z','A2');
xlswrite(file_export1,Hour_of_the_day,'Theta_z','B1');
xlswrite(file_export1,radtodeg(Theta_z),'Theta_z','B2');

% Sheet Alpha_z
xlswrite(file_export1,Title_sheet2,'Alpha_z','A1');
xlswrite(file_export1,Day,'Alpha_z','A2');
xlswrite(file_export1,Hour_of_the_day,'Alpha_z','B1');
xlswrite(file_export1,radtodeg(Alpha_z),'Alpha_z','B2');

% Sheet Gamma_s
xlswrite(file_export1,Title_sheet2,'Gamma_s','A1');
xlswrite(file_export1,Day,'Gamma_s','A2');
xlswrite(file_export1,Hour_of_the_day,'Gamma_s','B1');
xlswrite(file_export1,radtodeg(Gamma_s),'Gamma_s','B2');


%% Writing on File 2 (Radiation Calculations)

file_export2 = 'Radiation_Calculations_Hourly_LNEG.xlsx';

% First Sheet
Title_sheet3 = {'N', 'G_on', 'H_o'};
xlswrite(file_export2,Title_sheet3,1,'A1');
xlswrite(file_export2,Day,1,'A2');
xlswrite(file_export2,G_on,1,'B2');
xlswrite(file_export2,H_o,1,'C2');

% Sheet R_b
xlswrite(file_export2,Title_sheet2,'R_b','A1');
xlswrite(file_export2,Day,'R_b','A2');
xlswrite(file_export2,Hour_of_the_day,'R_b','B1');
xlswrite(file_export2,R_b,'R_b','B2');

% Sheet R_b_av
xlswrite(file_export2,Title_sheet2,'R_b_av','A1');
xlswrite(file_export2,Day,'R_b_av','A2');
xlswrite(file_export2,Hour_of_the_day,'R_b_av','B1');
xlswrite(file_export2,R_b_av,'R_b_av','B2');

% Sheet G_o
xlswrite(file_export2,Title_sheet2,'G_o','A1');
xlswrite(file_export2,Day,'G_o','A2');
xlswrite(file_export2,Hour_of_the_day,'G_o','B1');
xlswrite(file_export2,G_o,'G_o','B2');

% Sheet I_o
xlswrite(file_export2,Title_sheet2,'I_o','A1');
xlswrite(file_export2,Day,'I_o','A2');
xlswrite(file_export2,Hour_of_the_day,'I_o','B1');
xlswrite(file_export2,I_o,'I_o','B2');

% Sheet I
xlswrite(file_export2,Title_sheet2,'I','A1');
xlswrite(file_export2,Day,'I','A2');
xlswrite(file_export2,Hour_of_the_day,'I','B1');
xlswrite(file_export2,I,'I','B2');

% Sheet k_T
xlswrite(file_export2,Title_sheet2,'k_T','A1');
xlswrite(file_export2,Day,'k_T','A2');
xlswrite(file_export2,Hour_of_the_day,'k_T','B1');
xlswrite(file_export2,k_T,'k_T','B2');

% Sheet I
xlswrite(file_export2,Title_sheet2,'I','A1');
xlswrite(file_export2,Day,'I','A2');
xlswrite(file_export2,Hour_of_the_day,'I','B1');
xlswrite(file_export2,I,'I','B2');

% Sheet I_d
xlswrite(file_export2,Title_sheet2,'I_d','A1');
```

```
xlswrite(file_export2,Day,'I_d','A2');
xlswrite(file_export2,Hour_of_the_day,'I_d','B1');
xlswrite(file_export2,I_d,'I_d','B2');

% Sheet I_b
xlswrite(file_export2,Title_sheet2,'I_b','A1');
xlswrite(file_export2,Day,'I_b','A2');
xlswrite(file_export2,Hour_of_the_day,'I_b','B1');
xlswrite(file_export2,I_b,'I_b','B2');

% Sheet I_t_Liu_Jordan
xlswrite(file_export2,Title_sheet2,'I_t_Liu_Jordan','A1');
xlswrite(file_export2,Day,'I_t_Liu_Jordan','A2');
xlswrite(file_export2,Hour_of_the_day,'I_t_Liu_Jordan','B1');
xlswrite(file_export2,I_T_Liu_Jordan,'I_t_Liu_Jordan','B2');

% Sheet I_t_HDKR
xlswrite(file_export2,Title_sheet2,'I_t_HDKR','A1');
xlswrite(file_export2,Day,'I_t_HDKR','A2');
xlswrite(file_export2,Hour_of_the_day,'I_t_HDKR','B1');
xlswrite(file_export2,I_T_HDKR,'I_t_HDKR','B2');

% Sheet I_t_Perez
xlswrite(file_export2,Title_sheet2,'I_t_Perez','A1');
xlswrite(file_export2,Day,'I_t_Perez','A2');
xlswrite(file_export2,Hour_of_the_day,'I_t_Perez','B1');
xlswrite(file_export2,I_T_Perez,'I_t_Perez','B2');

% Sheet e_I_t_Liu_Jordan
xlswrite(file_export2,Title_sheet2,'e_I_t_Liu_Jordan','A1');
xlswrite(file_export2,Day,'e_I_t_Liu_Jordan','A2');
xlswrite(file_export2,Hour_of_the_day,'e_I_t_Liu_Jordan','B1');
xlswrite(file_export2,e_I_T_Liu_Jordan,'e_I_t_Liu_Jordan','B2');

% Sheet e_I_t_HDKR
xlswrite(file_export2,Title_sheet2,'e_I_t_HDKR','A1');
xlswrite(file_export2,Day,'e_I_t_HDKR','A2');
xlswrite(file_export2,Hour_of_the_day,'e_I_t_HDKR','B1');
xlswrite(file_export2,e_I_T_HDKR,'e_I_t_HDKR','B2');

% Sheet e_I_t_Perez
xlswrite(file_export2,Title_sheet2,'e_I_t_Perez','A1');
xlswrite(file_export2,Day,'e_I_t_Perez','A2');
xlswrite(file_export2,Hour_of_the_day,'e_I_t_Perez','B1');
xlswrite(file_export2,e_I_T_Perez,'e_I_t_Perez','B2');

% Sheet G_Liu_Jordan
xlswrite(file_export2,Title_sheet2,'G_Liu_Jordan','A1');
xlswrite(file_export2,Day,'G_Liu_Jordan','A2');
xlswrite(file_export2,Hour_of_the_day,'G_Liu_Jordan','B1');
xlswrite(file_export2,G_Liu_Jordan,'G_Liu_Jordan','B2');

% Sheet G_HDKR
xlswrite(file_export2,Title_sheet2,'G_HDKR','A1');
xlswrite(file_export2,Day,'G_HDKR','A2');
xlswrite(file_export2,Hour_of_the_day,'G_HDKR','B1');
xlswrite(file_export2,G_HDKR,'G_HDKR','B2');

% Sheet G_Perez
xlswrite(file_export2,Title_sheet2,'G_Perez','A1');
xlswrite(file_export2,Day,'G_Perez','A2');
xlswrite(file_export2,Hour_of_the_day,'G_Perez','B1');
xlswrite(file_export2,G_Perez,'G_Perez','B2');

% Daily Values
Title_sheet4 = {'Day', 'H_T_Liu_Jordan', 'H_T_HDKR', 'H_T_Perez'};
xlswrite(file_export2, Title_sheet4,'Daily_Values','A1');
xlswrite(file_export2,Day,'Daily_Values','A2');
xlswrite(file_export2,H_T_Liu_Jordan,'Daily_Values','B2');
xlswrite(file_export2,H_T_HDKR,'Daily_Values','C2');
xlswrite(file_export2,H_T_Perez,'Daily_Values','D2');

% Monthly Mean Values
Title_sheet5 = {'Month', 'H_T_Liu_Jordan_av', 'H_T_HDKR_av',...
```

```
    'H_T_Perez_av'};
xlswrite(file_export2, Title_sheet5,'Monthly_Mean_Values','A1');
xlswrite(file_export2,Month_of_the_year,'Monthly_Mean_Values','A2');
xlswrite(file_export2,H_T_Liu_Jordan_av,'Monthly_Mean_Values','B2');
xlswrite(file_export2,H_T_HDKR_av,'Monthly_Mean_Values','C2');
xlswrite(file_export2,H_T_Perez_av,'Monthly_Mean_Values','D2');
```

C.2. HOURLY PV PRODUCTION FUNCTION

```
%%% IMPORTANT INPUT PARAMETERS %%%

% Radiation Calculations Data
filename1 = 'PV_Validation_Input.xlsx';
% Irradiance Data
Radiation_Data_Hourly = xlsread(filename1,'Irradiance');
% Temperature Data
Temperature_Data_Hourly = xlsread(filename1,'Temperature');

% Preallocating Variables
G = zeros(24,1);                  % Irradiance incident on the panel [W/m^2]
T_amb = zeros(24,1);                              % Ambient Temperature [°C]
T_cell = zeros(24,1);                                % Cell Temperature [°C]
I_sc = zeros(24,1);                              % Short-Circuit Current [A]
V_oc = zeros(24,1);                               % Open-Circuit Voltage [V]
V_MP = zeros(24,1);                     % Voltage at Maximum Power Point [V]
I_MP = zeros(24,1);                     % Current at Maximum Power Point [A]
P_DC = zeros(24,1);              % Power DC at Maximum Power Point (MPP)  [W]
P_DC_max_real = zeros(24,1);                      % Real Maximum Power due to
                                                        % Temperature [W]
Ratio_P_DC = zeros(24,1);               % Ratio between P_DC and P_DC at MPP
eta = zeros(24,1);                                          % Efficiency
FF = zeros(24,1);                                          % Fill Factor


%%% CALCULATIONS %%%

%% Three P Model

for hour = 1:24

    % Irradiance
    G(hour) = Radiation_Data_Hourly(hour,2);                    %[W/m^2]

    % T_amb (INPUT)
    T_amb(hour) = Temperature_Data_Hourly(hour,2);               %[°C]

    % Parameters Calculation
    % When G = 0 (night)
    if G(hour) == 0
        I_sc(hour) = 0;
        V_oc(hour) = 0;
        V_MP(hour) = 0;
        I_MP(hour) = 0;
        P_DC(hour) = 0;
        eta(hour) = 0;
        FF(hour) = 0;
    % When G =/= 0 (day)
    else
    [T_cell(hour), I_sc(hour), V_oc(hour), V_MP(hour), I_MP(hour),...
        P_DC(hour), eta(hour),...
        FF(hour)] = threep_pv(G(hour),T_amb(hour));

    Ratio_P_DC(hour) = P_DC(hour) / P_DC_max_real(hour);
    end
end


%%% EXPORT DATA %%%
```

```
% Define Axis
Hour_of_the_day = zeros(24,1);
for hour = 1:24
    Hour_of_the_day(hour) = hour;
end

%% Writing on File 1 (Radiation Calculations)

file_export1 = 'PV_Validation_Output.xlsx';

% Sheet G
Title_sheet1 = {'hour','G','T_amb','I_sc','V_oc','V_MP','I_MP','P_DC',...
    'Ratio_P_DC','eta','FF'};
xlswrite(file_export1,Title_sheet1,'PV_Validation','A1');
xlswrite(file_export1,Hour_of_the_day,'PV_Validation','A2');
xlswrite(file_export1,G,'PV_Validation','B2');
xlswrite(file_export1,T_amb,'PV_Validation','C2');
xlswrite(file_export1,I_sc,'PV_Validation','D2');
xlswrite(file_export1,V_oc,'PV_Validation','E2');
xlswrite(file_export1,V_MP,'PV_Validation','F2');
xlswrite(file_export1,I_MP,'PV_Validation','G2');
xlswrite(file_export1,P_DC,'PV_Validation','H2');
xlswrite(file_export1,Ratio_P_DC,'PV_Validation','I2');
xlswrite(file_export1,eta,'PV_Validation','J2');
xlswrite(file_export1,FF,'PV_Validation','K2');
xlswrite(file_export1,T_cell,'PV_Validation','K2');
```

C.3. ENERGY MANAGEMENT ALGORITHM – CASE C

```
%%% IMPORTANT INPUT PARAMETERS %%%

%% Energy Costs

% Contracted Power
P_contract = 3.45;          %[kVA]

% Levelized Cost of Electricity of the PV System
LCOE_PV = 0.0330;              %[€/kWh]

% Levelized Cost of Electricity of the Battery
LCOE_batt = 0.3624;              %[€/kWh]

%% DHW
% Domestic Hot Water Temperature
T_DHW = 60;       %[°C]
% Water Tenperature at the beginning of the day
T_i = 20;         %[°C]

%% THERMAL ACCUMULATOR
% Maximum input power
P_therm_max = 2.0;          % [kWh]
% Total energy used for the Thermal accumulator
Q_therm_max = 5.58;


%% Battery
% SOC minimum
SOC_min = 0.4;
% SOC at the beggining of the day
SOC_i = 0.75;       %[%]
% Maximum input current from the grid
I_batt_max = 315;                  %[Ah]
% Voltage of the batteries
V_batt = 24;         %[V]
% Maximum Energy of the batteries
E_batt_max = I_batt_max * V_batt * 0.001;            %[kWh]
% Energy necessary to charge the battery at the beginning of the day
%E_charge_i = E_batt_max * (1 - SOC_i);     %[kWh]
% Available energy in the battery at the beginning of the day
```

```
%E_available_i = E_batt_max * (SOC_i - SOC_min);
[E_charge_i, E_available_i, SOC_test] = battery_state(SOC_i, 0, 0);

%%% PREALLOCATING VARIABLES %%%

G = zeros(24,1);                                        % Irradiance [W/m^2]
e_G = zeros(24,1);                          % Error of the Irradiance [W/m^2]
P_AC = zeros(24,1);                                     % Produced PV power [W]
e_P_AC = zeros(24,1);                  % Error of the produced PV power [W]
E_AC = zeros(24,1);                                % Produced PV energy [kWh]
e_E_AC = zeros(24,1);                % Error of the produced PV energy [kWh]
E_other_devices = zeros(24,1);     % Power consummed by other devices [kWh]
k = zeros(24,1);      % Hourly tariff for electricity from the grid [€/kWh]
E_therm = zeros(24,1);            % Maximum Energy consummed by the thermal
                                                        % accumulator [kWh]
E_used_therm = zeros(24,1);               % Energy consummed by the thermal
                                                        % accumulator [kWh]
Percentage_used = zeros(24,1);     % Percentage of the total PV energy that
                                                             % was used [%]
Energy_savings = zeros(24,1);                      % Total energy savings [€]
x = zeros(1,120);

%%% IMPORT DATA FROM EXCEL SHEET %%%

%% Irradiance and PV AC Production Data

% Day Choice
% Seasonal Approach
% filename1 = 'PV_Performance_Calculations_15_April.xlsx';
% filename1 = 'PV_Performance_Calculations_25_July.xlsx';
% filename1 = 'PV_Performance_Calculations_8_October.xlsx';
% filename1 = 'PV_Performance_Calculations_21_December.xlsx';
% Week or Weekend Day Approach
% filename1 = 'PV_Performance_Calculations_13_June.xlsx';
% filename1 = 'PV_Performance_Calculations_14_June.xlsx';
% filename1 = 'PV_Performance_Calculations_3_December.xlsx';
filename1 = 'PV_Performance_Calculations_13_December.xlsx';

% Irradiance
Irradiance_Hourly_Data = xlsread(filename1, 'Folha1');
% PV AC Production
PV_AC_Hourly_Data = xlsread(filename1, 'Folha3');


%% Energy Consumption Profiles Data
filename2 = 'Typical_Consumer_Profiles.xlsx';
Energy_Profiles_Hourly_Data = xlsread(filename2, 'Folha2');


%%% SYSTEM CALCULATIONS %%%

%% Day of the year
n = Irradiance_Hourly_Data(1,1);

%% Defining if wheter the Day is: Week, Weekend or Holiday
%% - Weekday -> Holiday = 0
%% - Weekend day and Holiday -> Holiday = 1
Holiday = 0;
for i = 1:54
    if n == 4 + (i - 1) * 7 || n == 5 + (i - 1) * 7
    Holiday = 1;
    end
end
if n == 1 || n == 108 || n == 115 || n == 121 || n == 161 || ...
    n == 170 || n == 227 || n == 278 || n == 305 || n == 335 || ...
    n == 342 || n == 359
    Holiday = 1;
end

for hour = 1:24

    %% Irradiance
    G(hour) = Irradiance_Hourly_Data(hour,3);                    %[W/m^2]
    e_G(hour) = Irradiance_Hourly_Data(hour,4);                  %[W/m^2]
```

```
    %% PV AC Production (Power)
    P_AC(hour) = PV_AC_Hourly_Data(hour,6);                              %[W]
    e_P_AC(hour) = PV_AC_Hourly_Data(hour,7);                            %[W]

    %% PV AC Production (Energy)
    E_AC(hour) = P_AC(hour) * 0.001;                                   %[kWh]
    e_E_AC(hour) = e_P_AC(hour) * 0.001;                               %[kWh]

    %% Energy Consumption Profile (Excluding the Thermal Accumulator)
    % Summer
    if n >= 106 && n < 289
        % Weekday
        if Holiday == 0
            E_other_devices(hour) = Energy_Profiles_Hourly_Data(hour, 4);
            h_down = 7;
            h_up = 9;
        % Weekend day or Holiday
        elseif Holiday == 1
            E_other_devices(hour) = Energy_Profiles_Hourly_Data(hour, 5);
            h_down = 9;
            h_up = 11;
        end
    end
    % Winter
    if (n >= 1 && n < 106) || (n >= 289 || n < 366)
        % Weekday
        if Holiday == 0
            E_other_devices(hour) = Energy_Profiles_Hourly_Data(hour, 2);
            h_down = 7;
            h_up = 9;
        % Weekend day or Holiday
        elseif Holiday == 1
            E_other_devices(hour) = Energy_Profiles_Hourly_Data(hour, 3);
            h_down = 9;
            h_up = 11;
        end
    end

    %% Defining the Tariffs from the Grid (k)
    % Empty Hours
    if (hour > 0 && hour <= 8) || (hour > 22 && hour <= 24)
        k(hour) = 0.1002;          %[€/kWh]
    % Full Hours
    else
        k(hour) = 0.1909;          %[€/kWh]
    end

end



%%% OPTIMIZATION CALCULATIONS %%%

% Inequality Constraints
A = zeros(73,120);
b = zeros(73,1);
for i = 1:24
    A(i, (2 + 5 * (i - 1))) = 1;
    A(i, (4 + 5 * (i - 1))) = 1;
    A(i + 24, (1 + 5 * (i - 1))) = 1;
    A(i + 24, (3 + 5 * (i - 1))) = 1;
    A(i + 48, (3 + 5 * (i - 1))) = 1;
    A(i + 48, (4 + 5 * (i - 1))) = 1;
    A(i + 48, (5 + 5 * (i - 1))) = 1;
    A(73,(5 + 5 * (i - 1))) = 1;
    b(i) = E_AC(i);
    b(i + 24) = P_contract - E_other_devices(i);
    b(i + 48) = P_therm_max;
    b(73) = E_available_i;
end

% Bound Constraints
% Lower Bound Constraints
```

```
lb = zeros(1, 120);
% Upper Bound Constraints
ub = zeros(1, 120);
for i = 1:120
    for j = 1:24
        if i == (1 + (j - 1) * 5) || i == (3 + (j - 1) * 5)
            ub(i) = P_contract - E_other_devices(j);
        elseif i == (2 + (j - 1) * 5) || i == (4 + (j - 1) * 5)
            ub(i) = E_AC(j);
        elseif i == (5 + (j - 1) * 5)
            ub(i) = E_available_i;
        end
    end
end

% Equality Constraints
Aeq = zeros(3,120);
for i = 1:h_down
    Aeq(1,(3 + 5 * (i - 1))) = 1;
    Aeq(1,(4 + 5 * (i - 1))) = 1;
    Aeq(1,(5 + 5 * (i - 1))) = 1;
end
for i = 22:24
    Aeq(1,(3 + 5 * (i - 1))) = 1;
    Aeq(1,(4 + 5 * (i - 1))) = 1;
    Aeq(1,(5 + 5 * (i - 1))) = 1;
end
for i = h_up:20
    Aeq(2,(3 + 5 * (i - 1))) = 1;
    Aeq(2,(4 + 5 * (i - 1))) = 1;
    Aeq(2,(5 + 5 * (i - 1))) = 1;
end
for i = 1:24
    Aeq(3,(1 + 5 * (i - 1))) = 1;
    Aeq(3,(2 + 5 * (i - 1))) = 1;
end
for i = 1:h_down
    Aeq(3, (5 + 5 * (i - 1))) = -1;
end
for i = h_up:20
    Aeq(3, (5 + 5 * (i - 1))) = -1;
end
for i = 22:24
    Aeq(3, (5 + 5 * (i - 1))) = -1;
end
beq = [Q_therm_max
       Q_therm_max
       E_charge_i];

%% Objective Function

f = zeros(1,120);
for i = 1:120
    for j = 1:24
        if i == (1 + (j - 1) * 5) || i == (3 + (j - 1) * 5)
            f(i) = k(j);
        elseif i == (2 + (j - 1) * 5) || i == (4 + (j - 1) * 5)
            f(i) = LCOE_PV;
        elseif i == (5 + (j - 1) * 5)
            f(i) = LCOE_batt;
        end
    end
end

%% Optimization

x(:) = linprog(f, A, b, Aeq, beq, lb, ub);
for i = 1:120
    if x(i) < 10^-4
        x(i) = 0;
    end
end

%%% EVALUATION
```

```
for j = 1:24
   if E_AC(j) == 0
       Percentage_used(j) = 0;
   else
       Percentage_used(j) = (x((2 + (j - 1) * 5)) + x((4 + (j - 1) * 5))) / E_AC(j) *
100;
   end
   Energy_savings(j) = ...
       x((2 + (j - 1) * 5)) * k(j) - x((2 + (j - 1) * 5)) * LCOE_PV + ...
       x((4 + (j - 1) * 5)) * k(j) - x((4 + (j - 1) * 5)) * LCOE_PV + ...
       x((5 + (j - 1) * 5)) * k(j) - x((5 + (j - 1) * 5)) * LCOE_batt;
   if j == 1
       Daily_savings = Energy_savings(j);
   else
       Daily_savings = Daily_savings + Energy_savings(j);
   end
end


%%% ADDING SOLUTIONS TO A NEW VECTOR
for j = 1:24
    x_batt_1(j) = x(1 + (j - 1) * 5);
    x_batt_2(j) = x(2 + (j - 1) * 5);
    x_therm_1(j) = x(3 + (j - 1) * 5);
    x_therm_2(j) = x(4 + (j - 1) * 5);
    x_therm_3(j) = x(5 + (j - 1) * 5);
end


%%% EXPORT DATA %%%

% Defining the Axis
Hour_of_the_day = zeros(24,1);
for hour = 1:24
    Hour_of_the_day(hour) = hour;
end

%% Writing on the File (Irradiance on a Tilted Surface Calculations)
file_export = 'Energetic_Daily_Optimization_F.xlsx';

% First Sheet
Title_sheet1 = {'N', 'Hour', 'Energy_Grid_Battery (kWh)', ...
    'Energy_PV_Battery (kWh)', 'Energy_Grid_Thermal_Accumulator (kWh)', ...
    'Energy_PV_Thermal_Accumulator (kWh)', ...
    'Energy_Battery_Thermal_Accumulator (kWh)', ...
    'Percentage_Used', 'Energy_Savings', 'Total_Energy_Savings'};
xlswrite(file_export,Title_sheet1,'Optimization','A1');
xlswrite(file_export,n,'Optimization','A2');
xlswrite(file_export,Hour_of_the_day,'Optimization','B2');
xlswrite(file_export,x_batt_1.','Optimization','C2');
xlswrite(file_export,x_batt_2.','Optimization','D2');
xlswrite(file_export,x_therm_1.','Optimization','E2');
xlswrite(file_export,x_therm_2.','Optimization','F2');
xlswrite(file_export,x_therm_3.','Optimization','G2');
xlswrite(file_export,Percentage_used,'Optimization','H2');
xlswrite(file_export,Energy_savings,'Optimization','I2');
xlswrite(file_export,Daily_savings,'Optimization','J2');
```